We thank all three anonymous referees, Quentin Simon and Richard Staff as editor for the valuable comments which have improved the manuscript and the age model. Please find our responses here (in blue) with new page and line numbers of applied changes followed by the manuscript with tracked changes.

Editor

Minor comments/suggestions:

L45 (of original submission): "…at the top of…" – do you mean "…towards the north of…"?
changed to "towards the north of" P2 L41.

L55: This could be a lengthy discussion(!), but is "tephrochronology" itself an "absolute dating technique"? It is if "absolute" ages are associated with the "tephrostratigraphy"… But those ages come from other "absolute" chronological techniques don't they (e.g., 40Ar/39Ar on the volcanic material itself, or 14C or luminescence from previously dated sedimentary archives containing the tephras in question)?
We agree, this is somewhat "in between". We changed this from "absolute" to "numerical" as this should highlight the difference between the techniques we use here. P2 L53.

L58: "Taupo Volcanic Zone (TVZ)" abbreviation already introduced on L50.
Changed to "TVZ" only (note this section has been moved to the methods (3.1)). P3 L98.

L77: invert "…may which disturb…".
This half-sentence has been removed during restructuring (moving this from the introduction to section 3.5).

L82: re-word as (something like) "In comparison to this earlier model, the present study…" (for clarification).
Changed as suggested. P2 L58.

L94-95: is there a way to avoid repetition of "crater rim"?
replaced the second "crater rim" with "the tuff ring surrounding the maar lake" P2 L7.

Section 3.1: Personally, I would like the inclusion at this stage of how many tephra layers were analysed, and also a note that these were all visible (rather than crypto-) tephra layers. (This would be consistent with following sections that note, e.g., how many plant macros were collected for 14C dating.)
extended to "Tephra identification of eight visible layers" P3 L102.

L134 & 139: change "anomalous" to "anomalously".
changed accordingly. P4 L121 & 125.

L236: change "were performed" to "was "performed" (or "measurement" to "measurements").
changed to "measurements". P7 L240.

L260: is there a reason that "Virtual" is capitalised but not "…axial dipole moment"?
removed the capitalisation of Virtual. P7 L262.

L265: Presumably, "strata" (plural) should be "stratum" (singular)?
True. Changed accordingly. P7 L265.

L314: insert "…[a] similar depth…".
Changed accordingly. P9 L329.

L374: should this be "…of Earth's magnetic field"?
This part of the sentence has been removed as part of restructuring the sentence.

L408: change to "These facies unit[s]…".
changed accordingly. P12 L447.

L438: delete "a".
Deleted. P13 L491.

L564: insert "…through [the] chosen mean…"
Added accordingly. P16 L623.

L583: "…unrealistically low confidence ranges…" – this is unclear. Do you instead mean "…unrealistically precise confidence ranges…"?
Yes. As in "small" or "narrow". Changed to "precise". P16 L645.

Response to Reviewer 3 (RC3-C1): "In order to avoid inflating the current manuscript even more, we decided to use the investigation of the resulting sedimentation rates in comparison with the lithology as the test for the age model's reliability." I think that Reviewer 3 was not asking for an (e.g.) pollen record to precisely align (climatically wiggle-match) your record to others, as this would prevent the assessment of environmental synchrony/asynchrony as you say. Rather, I think that the comment was saying that if such an environmental record were also presented, then this would allow "rough" assessment of the reliability of the chronology (e.g., is the Last Interglacial approximately "in the right place"). Anyway, I fully accept that the present manuscript if focussing solely on chronology (rather than palaeoenvironment), and that no such comparison data are therefore included. However, the current wording of the sedimentological argument (L594-596: "The slowest sedimentation rate of the entire sequence is observed in an interval of very fine laminations (facies unit 10; Fig. 9), which is consistent with slow sedimentation. Fine laminations generally indicate slower accumulation rates because only small amounts of sediment are slowly deposited at the lake bottom." seems circular as written. Please could you clarify this line of argument.
Updated to "The slowest sedimentation rate of the entire sequence is observed in an interval of very fine laminations (facies unit 10; Fig. 11), which is consistent with slow sedimentation in a quiet depositional environment dominated by in-lake production of biological particles and characterised by the absence of mass movement deposits indicative of instantaneous deposition." P17 L657-660.

Referee#1

We thank Referee #1 for their constructive and helpful review and address the raised below. RC1 = reviewer comment from reviewer 1. C1-C9 = comments 1 to 9 followed by our response.

Specific comments

(RC1-C1) The abstract is very long (spanning two paragraphs). I would suggest to remove the discussion of the Be-10 from the abstract - better to focus on the chronological methods that were incorporated into the final age model.

Response to (RC1-C1): We have removed the Be-10 part from the abstract and reduced it to one paragraph as suggested.

(RC1-C2) With SHCal20 now out I leave it up to the authors whether they choose to update their chronology. I would certainly encourage this, since presumably the next step will be palaeoclimate interpretations.
Response to (RC1-C2): The age model has been updated with SHCal20.

(RC1-C3) Discussion of reservoir corrections for radiocarbon dating is brief, and slightly conflates the 'hardwater effect' with the marine reservoir effect, which arise due to separate processes. I wouldn't have thought that there would be much of a hardwater effect as the catchment is presumably basaltic rather than carbonate?
Response to (RC1-C3): Surprisingly we have observed higher $CaCO_3$ contents than expected in places within the sequence. We have removed the sentence on marine reservoir corrections to eliminate the confusion.

(RC1-C4) For the tuning of the palaeomagnetic RPI curve, why were the tuning points selected randomly? It would seem better to select parts where there is more confidence in the alignment? Or, perhaps at least explain why a random approach is used for the DTW algorithm.
Response to (RC1-C4): To explain this, we have added: "We chose to select these tuning points randomly (apart from the basal point) in order to prevent any bias that involved selecting points to arrive at a favoured solution" P7 L281 – P8 283.

(RC1-C5) Is the geomagnetic excursion at _62 ka the Greenland-Norwegion Sea excursion? Was this considered to be used in the chronology development? It seems quite well defined in the Orakei RPI (though perhaps the trough is not clear).
Response to (RC1-C5): Maybe, given that Quentin Simon has raised the same observation we added a whole paragraph on this possibility: "The short-duration RPI trough around 52 m aligns with a very shallow inclination of +0.4° at 51.2 m (Fig. 6). The combination of inclination, low RPI and its depth (inferring an age of ca. 61,000 yr) suggests that this may be the Norwegian-Greenland Sea Excursion (Bleil and Gard, 1989; Løvlie, 1989). This probable reversal of the geomagnetic field was considered to be restricted to high latitudes accompanied by a global low in geomagnetic field intensity and has been confirmed in various northern high-latitude sites (Channell et al., 1997; Nowaczyk et al., 1994, 2003; Nowaczyk and Baumann, 1992; Nowaczyk and Frederichs, 1999; Simon et al., 2012; Xuan et al., 2012). However, low field strength and potentially excursional directions have also been interpreted as the Norwegian-Greenland Sea Excursion in Black Sea sediments (Liu et al., 2020; Nowaczyk et al., 2013) and the Western Equatorial Pacific (Lund et al., 2017). The occurrence of the Norwegian-Greenland Sea Excursion in the Orakei maar lake record would thus constitute its first observation this far south although additional samples are needed to confirm its occurrence in the Orakei record." P12 L461-470.

Technical corrections
(RC1-C6) Line 50-52: 'Orakei maar paleolake is of unprecedented quality...' Please quantify this statement.
Response to (RC1-C6): We are not sure how this is supposed to be quantified but we updated the sentence to "The sediment record from the Orakei maar paleolake is unprecedented in its combination of length, resolution, and completeness in the context of the terrestrial south-west (SW) Pacific." P2 L48-50.

(RC1-C7) Line 85: 'improve temporal constraints on regional of palaeoclimatic...' Please

rephrase.
Response to (RC1-C7): Deleted “of”, see comment (RC3-C11). P2 L61.

(RC1-C8) Fig 6 and 7: I believe these will need to be reformatted into a portrait format.
Response to (RC1-C8): Figures are reformatted (and updated) into portrait format.

(RC1-C9) Line 151: There is no section 3.6.1?
Response to (RC1-C9): Corrected to “section 3.7”. P4 L136.

Referee#2

We thank Referee #2 for their constructive and helpful review and address the raised points below. RC2 = reviewer comment from reviewer 2. C1-C12 = comments 1 to 12 followed by our response.

General Comments

(RC2-C1) Radiocarbon:
I feel that, while not perfect data (e.g., age reversals, unknown reservoir effects), the treatment of the radiocarbon data is fair and the authors are honest about their uncertainties. I would recommend the authors update the calibration to the SHCal20, now that it is available, and present (and make available) both the SHCal13 and SHCal20 based age models (so that other authors can make direct comparisons to either). Otherwise, the next study that presents Orakei maar lake data on age will need to re-do the age model and this age model will be dated.
Response to (RC2-C1): The age model has now been updated to use SHCal20. The difference to the earlier version using SHCal13 is max. 200 yr, usually less than 100 yr. No work from this record using the earlier age model (with SHCal13) has been published yet so that we refrain from a comparison between both age models and urge all co-workers to use the updated age model for future work.

(RC2-C2) Tephra Stratigraphy:
Obviously, the author’s identification of the “unidentified” basaltic tephra layer T66 is central to the older part of this age model and the only real constraint beyond the RPI correlation (as the uncertainties in the luminescence data prevent those data from providing strong constraint at the temporal resolution of the final age-depth model). The authors propose that this a newly recognized tephra for the AVF, AVFaa, as it cannot be correlated to previously identified tephra layers. They use the Ar/Ar constraints from their proposed eruptive center, Mt. Albert, to assign an age to this layer. I think this assumption is reasonable, and while it is better explained in the appendix, I think it deserves a little more attention in the main text (and perhaps the abstract) because of how important this interpretation/assumption it is to the final age model. This should maybe include the data needed to identify the tephra in the main text, as the authors do for their other tephra in Figure 3. The way the treatment of T66 is presented in the results section 4.1 makes it seem like the age of this tephra layer is well known, the eruptive history of Mt. Albert is well known, and the tephra identification has no ambiguity. This new AVFaa tephra may also be important for future studies. See below, but I also am curious if there is an RPI DTW solution that independently supports this age assignment.

Response to (RC2-C2): We have moved the text from the appendix to a new section "4.1.2 Basaltic tephra sample T66" (P9 L346 – P10 L364) and added a new figure 4 summarising the relevant figures from the appendix (A4-A6). See comment below (RC2-C4) regarding the RPI DTW solution for AVFaa.

(RC2-C3) I am assuming that AVF1 was not used in the age model because it has two possible ages _106 vs _83 ka. It seems like the author's age model, while not using the tephra as a constrain, is more consistent with the older of these two ages. I think it would be worthwhile to add a paragraph in the main text to discuss the AVF1 tephra, how the previously published age constraints were derived and how the new age model compares. Does the new age agree with either of the older ages? Why or why not do you think that is the case? Does it provide an addition independent support for the RPI based correlation?

Response (RC2-C3): AVF1 was not used in the age model because it has not been identified via EMPA in the new Orakei 2016 cores that are mostly used in the composite stratigraphy and age model. Its depth is correlated from the core presented in Molloy et al 2009 and could be used but its investigation (along with the same question for all other tephra layers) is part of a separate study in review (with minor revision requested) in New Zealand Journal of Geology and Geophysics. Actually, the updated age model produces an age for AVF1 of ca. 90.4 ka falling somewhat between both ages. As this is discussed in the upcoming NZJGG paper we chose not to discuss it here.

(RC2-C4) Paleomagnetism:
I liked the authors use and application of DTW in their correlation of the RPI data. We all know that wiggle stratigraphic correlations can be non-unique, so while not always perfect, at least DTW is objective. However, to get a perfect DTW solution requires perfect data (which is never the case and cannot be expected in paleomagnetism). Thus, the result of the DTW solution when using a general DTW algorithm (like the one used in this study) for geologic data is often a stair-step pattern, implying sediment delivery in pulses separated by periods of no deposition. However, we often assume that sedimentary records like these accumulate gradually over time. The authors in a way deal with this by randomly sampling tuning points from the DTW solution and setting hard start/end tie points. However, this is problem that Hay et al, which the authors cite, also address through their development of a DTW algorithm. In this algorithm, users can work with imperfect data by varying assumptions relevant to geologic data (such as how variable sediment accumulations are) to explore various possible DTW solutions that can be evaluated against independent constraints and/or expert knowledge.
Do the authors think it would be worth trying the Hay et al. DTW approach to explore other possible DTW solutions that may be more reasonable for imperfect geologic data? Why or why not? Can you treat the AVFaa tephra age independent of the RPI DTW solution and find a solution that independently supports the age the authors assign to the AVFaa tephra?

Response to (RC2-C4): Obtaining various possible DTW solutions and evaluating them might become an interesting exercise once we have a better understanding of the depositional environment of the sediments. We are expecting ongoing multi-proxy environmental reconstructions and high-resolution micro-facies work to shed light in this matter. A future study may find a better DTW solution but this goes beyond the scope of the current paper.
It is true that the alignment path looks very "staircase"-like which is not expected for the mode of sediment delivery (at least on the resolution we can study it here) but is necessary to allow enough stretching and compressing between the PISO and Orakei RPI to happen in the alignment. For this

reason, we do not use the alignment path itself as an age model but allow for smoothness again by integrating the tuning points into Bacon.

As for the AVFaa tephra age. We have now updated the DTW procedure (section 3.6) and removed the split at the level of the AVFaa tephra. Thus we're treating the tephra age independently and note that it agrees with the DTW solution within +/- 2 sd.

(RC2-C5) Sedimentation Rates:
It makes me nervous when I see a major change in sedimentation rates at a depth where the main chronometer for the age model changes. In the case of this study the authors find a switch from lower to higher sedimentation rates at around the same depth that the age model changes from being primarily constrained by RPI correlation to radiocarbon. I think this observation should be included in the main text. Why should I, the reader, be convinced that this accumulation rate change is the real signal and not an artifact of a non-unique or problematic RPI correlation? It doesn't appear to exactly line up with the facies unit changes or the lithologic log, but maybe there are other data that show a sedimentological change around the same time?
Response to (RC2-C5): We have added the following paragraph to section 4.8 "The stepwise increase in sedimentation rate at ~45 m nearly coincides with the change in chronometer from RPI tuning points to tephra and 14C ages. Whilst we cannot entirely disprove an influence of the chronometer change on the increase in sedimentation rate, we do note several observations that support this sedimentation rate change to be method-independent: (1) It is a stepwise change not a sudden change at the exact change point in chronometer. (2) In the interval where both chronometers overlap, albeit very short, the Rotoehu tephra and the uppermost RPI running point agree well (Fig. 10). (3) The increase in sedimentation rate does occur at the transition from facies unit 8b to 8a. These sub-facies differ in their colour contrasts between the laminations potentially indicating slightly different chemical composition, thus a slightly different depositional context which may well agree with a different sedimentation rate. (4) Further changes in sedimentation rate, even larger in magnitude than at ~45 m occur at other positions in the sediment sequence independent of strong lithological/facies changes (and independent of chronometer changes) such as at ~39 m and within facies unit 4 (Fig. 11)." P15 L596-605.

(RC2-C6) Data Availability:
Thanks for posting your data to Pangea. I would also recommend including the actual age-depth relationship with uncertainty as an independent contribution.
Response to (RC2-C6): Thank you for this suggestion. We post the updated age-depth relationship (on a cm-resolution) as a supplementary to this publication.

Specific Comments:

(RC2-C7) Line 263: Hay et al. aligned chemostratigraphic data, not paleomagnetic data. Their algorithm was modified to work with paleomagnetic vector data by Hagen at al. But, the Hay et al. algorithm would be the appropriate choice for RPI correlations.
Response to (RC2-C7): Corrected the sentence to "Dynamic time warping (DTW) aligns time series datasets through generalized dynamic programming (Hay et al., 2019) and has been adapted for paleomagnetic vector data by Hagen et al. (2020)." P7 L263-265.

(RC2-C8) Lines 495-515: There is information in this section that seems like it would fit better in the methods section, particularly the choice of DTW algorithm.
Response to (RC2-C8): We moved most of section 4.6 into the methods section 3.6 and extended the

results section on the aligned curves to better focus on the match between RPI from Orakei and PISO-1500.

(RC2-C9) Figure 2: Would it be helpful to indicate the stratigraphic position/labels of the tephra layers?
Response to (RC2-C9): We have added the tephra layers to this figure.

(RC2-C10) Figure 6: It is difficult to read the small text in this figure. Please make the text larger.
Response to (RC2-C10): We have made the text larger (now Fig. 8).

(RC2-C11) Figure 7: It might help the clarity of the figure to decrease the symbol size so that it is easier to see how the age control points compare to each other.
Response to (RC2-C11): We have decreased the symbol size (now Fig. 9).

(RC2-C12) Figures B1-B2, B4, C4: All of these figures would benefit from increasing the font size of the smaller fonts to make them more legible.
Response to (RC2-C12): We have increased the font size in all mentioned figures.

Referee#3

We thank Referee #3 for their constructive and helpful review and address the raised points below. RC3 = reviewer comment from reviewer 3. C1-C16 = comments 1 to 16 followed by our response.

General comments
(RC3-C1) Test of the model: The authors do an admirable job of stitching together the various chronological threads. However, I would like to have seen a test of the age-depth model. If this were published with a pollen record, for instance, we could see if the appearance of critical taxa corresponds with other records from the northern North Island. As is, the reliability of the reconstruction is hard to gauge. One option could be to remove a tephra, run the model, and compare the model's estimated age of the tephra to the tephra's actual age, then repeat.
Response to (RC3-C1): Unfortunately, publishing a pollen record alongside the age model is beyond the scope of this paper. However, this is also somewhat circular since if we were to only trust the age model if it matches the ages inferred from expected ages of changes in proxies (i.e., MIS stages) we would fail to recognise local variability so that the inferred model age-proxy correlations are in error.
The test via removing tephra ages and comparing the modelled age to the published age is part of a paper currently in review in New Zealand Journal of Geology and Geophysics (alongside resulting new tephra ages for previously undated tephra layers) but gives a high degree of confidence in the age model. It also doesn't work for a long section of the record where no (previously dated) tephra layers were found. In order to avoid inflating the current manuscript even more, we decided to use the investigation of the resulting sedimentation rates in comparison with the lithology as the test for the age model's reliability.

(RC3-C2) Dynamic time warping: This is an interesting technique that I have not seen applied to matching proxy records. While creative, I wonder about the heavy-handedness of the warping function on the original data. The stepwise pattern in the RPI data implies the algorithm expands and compresses the record quite regularly. Further, the VADM reference curve is interpolated from a data point every 1000 yr to 200-yr resolution.

All of this results in an uncertainty that is seemingly not transferred to the age-depth model. The stock +/- 1000 years does not seem realistic given the uncertainty of the Rotoehu. The authors should consider a meaningful exercise in quantifying this error. Perhaps randomly sampling 13 data points could be repeated multiple times to estimate uncertainty? From a different angle, are there RPI measurements from the top 40 m? If so, the DTW technique could be compared to the chronology established with radiocarbon and tephrochronology.

Response to (RC3-C2): The manuscript urges the need for more realistic errors already in point 2 of section 6 (conclusions) but we expand on this in section 5.1 (as a weakness of the age model). We have updated the errors on the tuning points to reflect the match from the DTW alignment (compare new Fig. 8; Tab. 5) such that points that are matched to more than one age have a higher uncertainty spanning the range of ages that they are matched to.

Repeated sampling of the points will result in various points over the same curve but not produce different age estimates for the same depth point (which would be necessary for the uncertainty).

As stated in section 3.4 there are no RPI measurements above 40 m depth as the sequence contains frequent basaltic tephra layers that obviate development of a reliable paleomagnetic signal from this section of the sequence.

(RC3-C3) Changing sedimentation rate: I think strong caveats need to be stated when highlighting the major trends in sedimentation rate. The authors rightly point out that the changes are not strongly related to stratigraphy. However, change in sedimentation rate is related to a change in dating technique (from RPI matching to radiocarbon and tephrochronology).

Response to (RC3-C3): We have added the following paragraph to section 4.8 “The stepwise increase in sedimentation rate at ~ 45 m nearly coincides with the change in chronometer from RPI tuning points to tephra and 14C ages. Whilst we cannot entirely disprove an influence of the chronometer change on the increase in sedimentation rate, we do note several observations that support this sedimentation rate change to be method-independent: (1) It is a stepwise change not a sudden change at the exact change point in chronometer. (2) In the interval where both chronometers overlap, albeit very short, the Rotoehu tephra and the uppermost RPI running point agree well (Fig. 10). (3) The increase in sedimentation rate does occur at the transition from facies unit 8b to 8a. These sub-facies differ in their colour contrasts between the laminations potentially indicating slightly different chemical composition, thus a slightly different depositional context which may well agree with a different sedimentation rate. (4) Further changes in sedimentation rate, even larger in magnitude than at ~45 m occur at other positions in the sediment sequence independent of strong lithological/facies changes (and independent of chronometer changes) such as at ~39 m and within facies unit 4 (Fig. 11).” P15 L596-605

(RC3-C4) Reservoir effect: If this was a known problem, then why only have two couplets of macrofossil/tephra and bulk sediment? It is beyond the scope to resample in the current paper, but perhaps more extensive comparisons between macrofossil and bulk sediment ages would be worth investigating in a future publication.

Response to (RC3-C4): This was, unfortunately, not known beforehand. The couplets of dates were intended to show that this is no/a minor problem but gave a larger difference than expected. More couplets however are very difficult to achieve (over the entire sequence/in representative places) as no macrofossils were found in long parts of the record within the limit of radiocarbon dating.

(RC3-C5) SHCal20: Given this will be the age-depth model for many proxy records to come, along with associated inter-hemispheric comparisons, I reluctantly suggest the authors recalibrate their age-depth models with this new curve.

Response to (RC3-C5): The age model has been updated using SHCal20.

Specific comments

(RC3-C6) Define “high resolution”
Response to (RC3-C6): (sedimentation rate above ~1m/ka) added to abstract. P1 L17.

(RC3-C7) Typically, errors are reported as 2 sigma, but here they are reported as 1 sigma. Please explain why this is the case or change to 2 sigma.
Response to (RC3-C7): Thank you for catching this, they were actually reported as a mix of both depending on how the respective literature reported them and because input values to Bacon are required to be 1 sigma. We have now changed them all to 2 sigma (or 95% confidence ranges).

(RC3-C8) Hyphenate units and value when acting as adjective. E.g., change, “: : :using wireline drilling in 1 m-length sections” to “: : :using wireline drilling in 1-m sections”.
Response to (RC3-C8): Changed. P3 L90.

(RC3-C9) P1L30: Change “spall” to “span”
Response to (RC3-C9): Changed. P1 L26.

(RC3-C10) P2L45: New Zealand does not need to be possessive
Response to (RC3-C10): Removed possessive “ ‘s ”. P2 L41.

(RC3-C11) P3L85: Delete “of” before “paleoclimatic”
Response to (RC3-C11): Deleted “of”. P2 L61.

(RC3-C12) P3 Regional setting: Influx of erosional material is often invoked as a confounding factor throughout the manuscript. However, the catchment of Orakei is very small and crater wall slumps were presumably removed from the stratigraphy. Please explain potential sources of the erosional influx.
Response to (RC3-C12): The crater is the catchment but undetected (small) debris flows from the crater wall were invoked as a reason for potentially problematic data whilst larger flows have been removed from the stratigraphy.

(RC3-C13) P7L274: Add “)” after “Accumulation model”
Response to (RC3-C13): Added “)” P8 L288.

(RC3-C14) P8L316: Change “: : :as identified by (Molloy et al., 2009): to “: : :as identified by Molloy et al. (2009)”
Response to (RC3-C14): Changed as suggested. P9 L331.

(RC3-C15) P16L648: Delete second “associated”
Response to (RC3-C15): deleted first “associated” as it preserves the flow of the sentence better. P18 L716.

(RC3-C16) Figure 8: Interestingly, the age-depth model underestimates most radiocarbon dates between the Rotorua and Okareka tephras and overestimates most ages between the Okareka and Rotoehu tephras. Any thoughts on this?
Response to (RC3-C16): See discussion of the outliers in the manuscript. The interval between Rotorua and Okareka is dominated by fluvial inwash following a crater rim breach by a stream which has likely transported macrofossils of an older age into the lake basin. The younger-than-the-model

ages between the Okareka and Rotoehu tephras may have to do with small sample masses as larger macrofossils could not be found and thus smaller samples had to be used and/or with not fully captured reservoir corrections.
The Okareka age is not as well constrained as the KOT age, an adjustment of the Okareka age would potentially allow the model to include more of the older-than-the-model ages but 1) at this stage we have no indication that the used Okareka tephra age is in error and 2) it would still mean that several clearly too old outliers remain in the fluvial facies.

Quentin Simon

We thank Quentin Simon for his detailed comments from the attached pdf which we address in table form.

Line number	Comment QS	Comment by authors	New page/ line
13	location (?)	changed accordingly	P1 L13
14-15	strikethrough “of associated changes”	deleted “of associated changes”	P1 L14
14-15	I understand what you mean, but I'm not sure about the sentence.	changed as suggested in line 15	P1 L15-16
15	Why not something like this? "Sediments from the Auckland Volcanic Field maar lakes preserve records of such large-scale climatic influences on regional paleoenvironment changes, as well as past volcanic eruptions."	changed accordingly as suggested	P1 L15-16
17	rapidly deposited	changed accordingly	P1 L17
17	high-resolution	changed accordingly	P1 L17
19	highlighted “combining” and “combined”	replaced the first “combining” with “using”	P1 L19
23-24	results suggest major influences of unaccounted catchment processes, preventing straightforward geomagnetic interpretations,	this section (on Be in the abstract) was now removed following comment (RC1-C1)	
25	can you really confirm the presence of the Laschamp based only on 10Be? I'm not sure.	this section (on Be in the abstract) was now removed following comment (RC1-C1)	
25-27	highlighted “We have integrated our absolute chronology with tuning of the relative paleointensity record of the Earth’s magnetic field to a global reference curve (PISO-1500).”	not changed as it is unclear why this sentence was highlighted	P1 L22
35	strikethrough “events”	deleted “events”	P1 L31
36-37	Convoluted sentence. (...) uncertainties prevent	changed to “… uncertainties prevent accurate	P1 L32-33

	understanding accurately the generation (...)?	understanding of the generation…"	
41	of	changed accordingly	P1 L37
41	available	added "available"	P1 L37
41	spanning	changed accordingly	P1 L37
42-43	Convoluted sentence. Why not something like: "In this context, the laminated sediment sequences from maar lakes of the Auckland Volcanic Field (AVF) provide key paleoclimate records for the LGI and beyond."	changed as suggested	P2 L38-40
50	How does it change through time?	extended the sentence to "This study focuses on the lacustrine sediment sequence contained in Orakei Basin, deposited following the phreatomagmatic eruption forming the maar crater until the post-glacial sea-level rise breached the crater rim and led to the current connection between Orakei Basin and the sea (Fig. 1; Peti and Augustinus, 2019)."	P2 L45-48.
55-57	In this study, we integrate absolute dating techniques (tephrochronology, radiocarbon, luminescence) and correlative dating (tuning of paleomagnetic field variations established by the relative paleointensity and meteoric 10Be) to develop an original age-depth model of the Orakei maar lake sediments.	changed as suggested	P2 L53-55
55-57	The following paragraph (or most of it) could be move in the method section.	The segments of the two following paragraphs (with respective edits) have now been moved to the beginning of the respective methods sections.	
62-63	strikethrough "since it is a well-established technique for dating organic macrofossil samples younger than ca. 50,000 years (Bronk Ramsey, 2008)."	deleted "since it is a well-established technique for dating organic macrofossil samples younger than ca. 50,000 years (Bronk Ramsey, 2008)."	P4 L119
71-72	Do you mean by wiggle-matching of climatic records?	deleted "environmental" in "synchronous changes" given caveats of circularity when	P5 L183

		wiggle-matching climatic records	
72-75	I don't think this is a good exemple to illustrate previous sentence. Geomagnetic changes are independant of environmental variations (idealy). I'm not sure to understand properly these two highlighted sentences. You could also add another reference dealing with 10Be (the one cited is about RPI)	See above comment. Removed 10Be part of this sentence to solely focus on paleomagnetic data here, and on 10Be in the following sentence.	
78	Carcaillet et al do not used 10Be for dating terrestrial sediments. Simon et al. (2020 QGeo, 10.1016/j.quageo.2020.101081) do such a thing, but not by correlating with paleointensity changes (rather using 10Be radioactive decay). To my knowledge your paper and the one submitted by Lisé-Pronovost et al. (in revision in QGeo) are the first ones to try using 10Be as a relative dating tool by comparing with RPI references. Despite poor results, you could mention this here ;)	We moved this part to section 3.5 (Be methods) and removed the caveat in terrestrial settings and reference to Carcaillet et al as the same statement is repeated in this section. We added "Though the radioactive decay of ^{10}Be has been used to date sediment much older than the Orakei sequence (e.g., Frank et al., 2008; Simon et al., 2020a), no study has been published yet applying 10Be variations in sediment cores as a relative dating tool by comparison to RPI reference data beyond the Laschamp Excursion (Nilsson et al., 2011)." to section 3.5.	P6 L213-216
83	because you most likely do not retrieved a 10Be production signal, I agree with your interpretation.	see more detailed comments in results and discussion sections	
83	deposition	changed accordingly	P2 L59
83, 84	highlighted "robust" twice	changed second instance of "A robust independent chronology" to "This detailed independent chronology"	P2 L61
85	highlighted "significantly"	deleted "significantly"	P2 L61
118	strikethrough "visible", added "identified"	changed accordingly	P3 L95
132	strikethrough "carefully"	deleted "carefully"	P4 L120
135-13	strikethrough "Marine reservoir age corrections are routinely addressed	deleted entire sentence	

	in the marine realm but more difficult to assess in lake basins due to their different sizes, variable regional lithologies, depths and movement of water masses (Philippsen, 2013)."		
138-139	strikethrough "to increase the age resolution"	deleted "to increase the age resolution"	P4 L124
150-151	I understand it is annoying, but could you calibrate using the new SHCal20 curve? At least, look at the difference obtained between the ages after using both references.	The age model has been updated using SHCal20 now.	
192	I'm not sure paleomagneticians will like this explanation, but I do understand the following argument ;)	The problem has been observed in nearby Lake Pupuke (Nilsson et al., 2011) so that we assume this to be a real problem…	
194-195	strikethrough "This is a problem especially around the age of the Mono Lake Excursion, which correlates with a flare-up of the basaltic volcanoes of the AVF around 30,000 cal yr BP (Molloy et al., 2009)."	Not adjusted, this sentence is needed to explain why no paleomagnetic data is available above ca. 40,000 cal yr BP which would have been great for a comparison of 14C/tephra derived chronology and RPI DTW based chronology (see later part of comment (RC3-C2)).	P5 L191
195	strikethrough "Orakei maar sediment"	deleted "Orakei maar sediment"	P5 L192
209-210	To my opinion, this is very light and you'll need to explain a bit more why you are confident in this RPI proxy if you want to correlate it with references to help building the age model. See for instance the recent paper by Hatfield et al. (2020, Frontiers). What is your magnetic mineralogy? It is very likely that rock mag properties changes through core considering lithological and grain-size changes. It is important to discuss this since you use later RPI to build the age model. Moreover, ARM is also very dependent on grain size at constant magnetic mineralogy.	We added a reference for details to section 4.4 where the more detailed discussion of the NRM/ARM ratio is now placed. See also later comments.	P6 L210

211	6	sentence deleted	
213-215	I would rephrase.	Split into two sentences "Meteoric cosmogenic ^{10}Be is produced in the atmosphere via nuclear reactions of cosmic ray particles with nuclei such as nitrogen and oxygen. ^{10}Be readily attaches to aerosols and dust, and with a short residence time of ~1 yr, is deposited on the Earth surface mainly via precipitation (Willenbring and von Blanckenburg, 2010)."	P6 L216-219
217	You could also mention here that you still need to normalized 10Be if you want to obtain records of geomagnetic field strength variations. The two cited references use different approaches, i.e. 230Thxs and flux. Most papers reconstructing past geomagnetic dipole moment from deep marine sediments use the 9Be normalisation.	adapted to "variability in (normalised) ^{10}Be concentrations" added the "(normalised)" as the specific normalisation with 9Be is mentioned further below we chose not to expand further on this here	P6 L219
216	strikethrough "to a first order"	deleted "to a first order"	P6 L218
218	These processes essentially complicate the identification of a 10Be production signal (see also recent papers by Czymzik et al.).	adapted to "complicate ^{10}Be provenance, delivery and accumulation and hence the identification of a ^{10}Be production signal (e.g., Czymzik et al., 2015; Nilsson et al., 2011)."	P6 L221-223
224	es	changed accordingly	P6 L228
224	were	changed accordingly	P6 L228
225	strikethrough "down-core"	deleted "down-core"	P6 L229
225	strikethrough "the"	deleted "the"	P6 L229
226	strikethrough "in the Orakei sediment sequence, which cannot be dated with radiocarbon,"	deleted "in the Orakei sediment sequence, which cannot be dated with radiocarbon,"	P6 L230-231
231	measure	changed accordingly	P6 L235
232	using	changed accordingly	P6 L236
240	to increase the 10Be resolution	changed accordingly	P7 L244
245-246	strikethrough "Authigenic 9Be was not analysed for these ten samples and was considered negligible compared to the 9Be spike mass following	not changed as we consider this statement crucial to justify why 10Be/9Be is not presented for the Lund/ETH samples	P7 L249-250

	measurements at UoA and ANSTO (see above)."		
252	strikethrough "Orakei maar lake"	deleted "Orakei maar lake"	P7 L255
253-256	I agree with this, but you might synthesis this part.	Slightly shortened to "It is crucial to avoid circularity in tuning climate proxies based on assumed synchroneity, when the presence or absence of this possible synchroneity is actually an overarching study objective (Blaauw, 2012)."	P7 L256-258
256	"relative paleointensity of the Earth magnetic field strength" is strange. Rephrase.	changed to "relative intensity of the Earth's magnetic field (RPI)"	P7 L258-259
257-258	strikethrough "unlike climate signals"	deleted "unlike climate signals"	P7 L259
259	You could add the new study by Hatfield et al. (2020)	reference to Hatfield et al., 2020 added	P7 L261
261-262	strikethrough "uses generalized dynamic programming, in which a complex problem is divided into smaller problems and their solutions are stored for later use. DTW"	deleted "uses generalized dynamic programming, in which a complex problem is divided into smaller problems and their solutions are stored for later use. DTW"	P7 L263-265
278-279	Identified by which proxy in your sediments? PMAG intensity or direction? 10Be? You should say that you applied the age from Lascu to the identified Laschamp interval in your sediments.	sentence extended to "the U/Th-age of the Laschamp Excursion as identified by paleomagnetic direction and intensity using the age of 41,100 ± 350 (2 σ) years BP from Lascu et al. (2016)"	P8 L292-293
280	RPI	changed accordingly	P8 L295
281	strikethrough "reference curve"	deleted "reference curve"	P8 L295
281	strikethrough "with"	deleted "with"	P8 L296
281	stack	added "stack"	P8 L295
281	of radiocarbon ages using	added "of radiocarbon ages using"	P8 L296
282	strikethrough "of radiocarbon ages"	deleted "of radiocarbon ages"	P8 L296
282	strikethrough "conducted by"	deleted "conducted by"	P8 L296
282	done by	added "done by"	P8 L296
298-299	highlighted "and substantial thickness (>30 cm) suggest that this layer is the Rotoehu tephra."	Not clear why this was highlighted?	P9 L312
338	These outliers were not incorporated in the age-model.	Not added, sentence from next comment moved here instead (slightly adapted to "Since the model recognises these outliers there was no	P10 L310

		need to remove them manually."). We like to make the difference clear between removing sample ages by the operator ("manually") vs. adding them to the Bacon input and the age model not passing through them at all and thus the model recognising them as outliers.	
345-346	strikethrough "The Bacon age model recognises all 13 outliers and hence there was no need to remove them manually."	see comment above	P10 L310
356	strikethrough "The remaining six samples provided ages, and these results"	deleted "The remaining six samples provided ages, and these results"	P10 L387
356	of the remaining six samples	added "of the remaining six samples"	P10 L387
356	They are	changed to "They conform"	P10 L387
374-375	strikethrough "of magnetic field inclination and reduced intensity of the Earth magnetic field."	deleted "of magnetic field inclination and reduced intensity of the Earth magnetic field."	P11 L404
374	geomagnetic	added "geomagnetic"	P11 L404
382	Some of the Figure in Appendix C should appear in the main text and be discussed more thoroughly here. This is very important to allow the use of RPI record. An easy way is to discuss if your data respect the Tauxe's criteria. Also, did you removed part of your record due to identified problematic layers?	Problematic layers were removed as part of the construction of the event corrected depth scale removing most problematic paleomagnetic data as well as samples with MAD > 15 as stated in section 3.4. We have now moved Figure C5 (and parts of its caption) to the main text (section 4.4) and extend the text by the following discussion regarding Tauxe's criteria: "The magnetic data partially fulfils the loosely defined criteria to assess the reliability of paleointensity data from sediments (Tauxe, 1993). It appears that magnetic concentration variations exceed one order of magnitude at times and the magnetic grain size is likely not confined to a very	P11 L414-417

		narrow range, but all other criteria are generally fulfilled.	
389	You should probably add other references presenting the Laschamp excursion from sediments or lava flows.	changed to "Laschamp Excursion (e.g., Cassata et al., 2008; Ingham et al., 2017; Laj et al., 2014; Laj and Channell, 2015; Mochizuki et al., 2006; Roperch et al., 1988) dated to 41,400 ± 350 yr by Lascu et al. (2016)."	P11 L424-426
393-394	could...	changed to "could correspond to"	P11 L430
394	Similarly to previous comment, they are numerous (although less numerous than for the Laschamp) papers dealing with the Blake from sediments, cite some of them. Why only referencing results from speleothems?	extended to "Blake Excursion (Smith and Foster, 1969; Thouveny et al., 2004; Tric et al., 1991; Zhu et al., 1994) dated to 116,500 ± 700 to 112,000 ± 1,900 years by Osete et al. (2012)."	P11 L430-431
404	Use the slope to calculate RPI. The slope method should give high correlation coefficients if demagnetisation steps look alike, this is good to reinforce trust on your RPI record.	We choose not to apply the slope method as we already provide the information of different demagnetisation steps which all give very similar data. Following Valet and Meynadier (1998) it is mostly not significant which approach is used.	
406	e.g.	added "e.g.,"	P12 L445
408	add also references from lava flows. Some measurements exist from nearby lava flows. See introduction in my recent paper for exemples and a discussion of such low intensity during the Laschamp (10.1016/j.epsl.2020.116547).	adapted to "the Laschamp Excursion as measured in sediments (e.g., Channell et al., 2009) as well as in lava flows from France (e.g., Laj et al., 2014; Roperch et al., 1988) and New Zealand (Cassata et al., 2008; Ingham et al., 2017; Mochizuki et al., 2006)"	P12 L445-446
410	not removed by normalization procedure then...	added ", which was not fully removed by the NRM/ARM normalisation procedure"	P12 L451
412-413	Is any rock mag or environmental proxy correlate with the RPI? If yes, say it and discuss. If no, say it since it strengthen your interpretation.	sentence above extended to "NRM recording in a higher energy depositional environment (compare Fig. 2) and observed in a minor anti-correlation between dry bulk density (not shown) and RPI."	P12 L448-450
416	Norwegian Greenland Sea Excursion? The RPI low	The following paragraph has been added:	P12 L461-470

	corresponds to a slight shift in inclination. Is it reliable? If yes, say it and discuss. It would be the first NGS-Exc. identified in this area.	"The short-duration RPI trough around 52 m aligns with a very shallow inclination of +0.4° at 51.2 m (Fig. 6). The combination of inclination, low RPI and its depth (inferring an age of ca. 61,000 yr) suggests that this may be the Norwegian-Greenland Sea Excursion (Bleil and Gard, 1989; Løvlie, 1989). This probable reversal of the geomagnetic field was considered to be restricted to high latitudes accompanied by a global low in geomagnetic field intensity and has been confirmed in various northern high-latitude sites (Channell et al., 1997; Nowaczyk et al., 1994, 2003; Nowaczyk and Baumann, 1992; Nowaczyk and Frederichs, 1999; Simon et al., 2012; Xuan et al., 2012). However, low field strength and potentially excursional directions have also been interpreted as the Norwegian-Greenland Sea Excursion in Black Sea sediments (Liu et al., 2020; Nowaczyk et al., 2013) and the Western Equatorial Pacific (Lund et al., 2017). The occurrence of the Norwegian-Greenland Sea Excursion in the Orakei maar lake record would thus constitute its first observation this far south although additional samples are needed to confirm its occurrence in the Orakei record."	
422	+ ref	changed to "inverse record to the relative paleointensity time-series (Elsasser et al., 1956; Ménabréaz et al., 2011)."	P12 L475-476
423	strikethrough "may have"	deleted "may have"	P12 L476

423	contains	added “contains”	P12 L476
425	strikethrough “geochemistry”	deleted “geochemistry”	P12 L478
426	+ ref. Please be more specific!	extended by “as ^{9}Be is commonly released by weathering (Wittmann et al., 2015).”	P12 L479-480
432	Please look at fig. 3 from Simon et al., 2017 (10.1016/j.epsl.2016.11.052). In that paper, we identified two huge 9Be peaks within tephra layers. More interestingly, an other tephra layer does not bear similar large 9Be signature. Likely influenced by the nature of the eruption. In your study, there is only one 9Be peak while you have other tephra layers, why? Any idea.	Interesting. Contrary to your study we find the large peak below the position of the Rotoehu tephra layer (quite sharp base of the tephra but some cracks extend material below its base). Note that no samples were taken in the tephra layer and the actual layer itself has been excluded from the event corrected depth scale too. In this record, the Rotoehu tephra layer is clearly the thickest and from a very large eruption which may explain why the same or similar 9Be peaks have not been observed at other tephra layers.	
437	Why so? Induced by very heterogenic lithologies and a sampling artefact? Normalising by 9Be would have likely reduce these deviations (if of lithological origins).	Added the sentence “The reason for this discrepancy is unclear but may be due to very heterogenic lithologies or represent a sampling/analytical artefact.”	P13 L491-492
447	Bourlès et al., 1989	reference changed to Bourlès et al., 1989	P13 L502
460	The reason why the Be ratio likely does not work is because it does not respect the homogeneous mixing of both isotopes prior to scavenging.	added “as the ratio does not respect the homogeneous mixing of both isotopes prior to scavenging.”	P13 L514-515
462-464	Please consider rewriting this sentence. What is enhanced? "galactic cosmic-ray production of 10Be" looks weird.	Changed to “Elevated ^{10}Be deposition…”	P13 L518
473	Don't look further, this is explaining data deviation in some intervals.	see below	
475-476	It seems very unlikely that you sediments could bear a 11 year solar modulation signal and not a	We agree, we corrected this to “Again, we have no clear explanation of this	P14 L530-531

	large-scale event associated with the Laschamp.	discrepancy but it likely is due to heterogenic lithologies and/or represents a sampling/analytical artefact."	
479	Does it compare favorably with records from the Pupuke Lake by Nilsson et al. (2011)?	added ", as also observed at nearby Lake Pupuke (Nilsson et al., 2011),"	P14 L533-534
481	Most importantly I think is: does your record show coherent features with available 10Be (Be ratio) records? Compare with records presented in Figs. 5 & 6 of Simon et al. (2016; 10.1002/2016JB013335).	we added "– a pattern not observed in the previous ^{10}Be records (Simon et al., 2016)."	P14 L536-537
483	What did you expected? directional deviation or RPI low? I guess the second which presents a long duration... say it.	added "as an RPI low, hence a peak in ^{10}Be"	P14 L540
484	Is it significant? It looks to me the Be ratio show the same pattern.	revised to "Two small peaks in 10Be at 73.6 m and 74.6 m may correspond to the inferred level of the Blake Excursion". As we cannot be sure whether it is significant or not, we do not use the Blake Excursion age in the age model.	P14 L540-541
490	and marine sediments (e.g. Simon et al., 2020, EPSL).	added accordingly	P14 L548-549
497	strikethrough "s"	deleted "s"	P7 L274
497	These similarities	"This correlation" changed to "these similarities"	P7 L274
501	Why not the opposite? It looks more correct to me since you don't gain anything to sample PISO at 200 year and, at the opposite, you might smooth unreliable RPI feature doing the opposite (Orakei RPI sample to 1 ka). Considering DRM it looks more correct to me.	Thank you for this observation, this indeed also improves the fit. We have updated the DTW application with the Orakei RPI smoothed to match the 1000 yr resolution of PISO and hence updated the age model as well as all related text.	
502	strikethrough "between the equivalent ages"	deleted "between the equivalent ages"	
512	What is the age uncertainty of PISO?	No age uncertainty is given in Channell et al., 2009. We use ±1000 years given the temporal resolution of PISO-1500.	P7 L276

514	Carcaillet is dealing with marine sediments, not lacustrine catchment problem.	reference deleted	
528	You mentioned just above that the chronology for the lower part of the Orakei sequence is mainly guided by the "AVFAA" tephra... I hope your age model agrees with this age then. It seems very circular to me.	we clarified the above statement to “the “AVFaa” tephra provides an age for the chronology development close to the position of the possible Blake Excursion.”	P15 L565
538	I don't get it.	This sentence refers to fig 9. The following description follows the mean line and ignores the related uncertainties presented in the figure. We conclude that this is too confusing to state and potentially self-exploratory so we deleted this.	
552	strikethrough “VADM”	deleted “VADM”	P16 L611
575-577	PISO has a resolution of 1 ka because it's a global stack, not because of measurements resolution. The huge advantage is that PISO mainly extracts a dipole variations proxy, useful for global correlation. Orakei RPI can averages a theoretical average resolution of 168 years, but this is likely smoothed by magnetisation acquisition in the sediments.	changed to “Orakei RPI record has a theoretical average resolution one measurement per 168 years although it is likely smoothed by magnetisation acquisition in the sediments”	P16 L637-638

Development of a multi-method chronology spanning the Last Glacial Interval from Orakei maar lake, Auckland, New Zealand

Leonie Peti[1], Kathryn E. Fitzsimmons[2], Jenni L. Hopkins[3], Andreas Nilsson[4], Toshiyuki Fujioka[5,^], David Fink[5], Charles Mifsud[5], Marcus Christl[6], Raimund Muscheler[42], Paul C. Augustinus[1]

1 School of Environment, The University of Auckland, New Zealand

2 Research Group for Terrestrial Palaeoclimates, Max Planck Institute for Chemistry, Mainz, Germany

3 School of Geography, Environment and Earth Sciences, Victoria University of Wellington, New Zealand

4 Department of Geology, Lund University, Lund, Sweden

5 Australian Nuclear Science and Technology Organisation (ANSTO), Lucas Heights, Australia

6 Laboratory of Ion Beam Physics, ETH Zurich, Switzerland

^ current address: Centro Nacional de Investigación sobre la Evolución Humana, Burgos, Spain

Correspondence to: Leonie Peti (lpet986@aucklanduni.ac.nz)

Abstract. Northern New Zealand is an important ~~site~~ location for understanding Last Glacial Interval (LGI) paleoclimate dynamics, since it is influenced by both tropical and polar climate systems which have varied in relative strength and timing ~~of associated changes~~. Sediments from the Auckland Volcanic Field maar lakes preserve records of such large-scale climatic influences on regional paleoenvironment changes, as well as past volcanic eruptions. ~~The Auckland Volcanic Field maar lakes preserve these climatic influences on the regional paleoenvironment, as well as past volcanic eruptions, in their sedimentary infill.~~ The sediment sequence infilling Orakei maar lake is continuous, laminated, rapidly deposited ~~high resolution~~ and provides a ~~robust~~high-resolution (sedimentation rate above ~1m/ka) archive from which to investigate the dynamic nature of the northern New Zealand climate system over the LGI. Here we present the chronological framework for the Orakei maar sediment sequence. Our chronology was developed ~~combining~~ using Bayesian age modelling of combined radiocarbon ages, tephrochronology of known-age rhyolitic tephra marker layers, $^{40}Ar/^{39}Ar$-dated eruption age of a local basaltic volcano, luminescence dating (using post infrared-infrared stimulated luminescence, or pIR-IRSL), and the timing of the Laschamp paleomagnetic excursion. ~~We also investigated the application of meteoric (cosmogenic) Beryllium-10 variability to improve the age-depth model by complementing relative paleointensity measurements. However, the results were apparently influenced by some unaccounted catchment process and unable to reach satisfactory interpretation, apart from confirming the presence of the Laschamp excursion, and therefore the ^{10}Be data are not used in the production of the final age model.~~ We have integrated our absolute chronology with tuning of the relative paleointensity record of the Earth's magnetic field to a global reference curve (PISO-1500).

The maar-forming phreatomagmatic eruption of the Orakei maar is now dated to >~~130~~132,~~120~~ 305 yr (95% confidence range ~~128~~131,~~665~~ 430 to ~~131~~133,~~560~~ 180 yr). Our new chronology facilitates high-resolution paleoenvironmental reconstruction for northern New Zealand spanning the last ca. 130,000 years for the first time as most NZ records that ~~spall~~ span all or parts of the LGI are fragmentary, low-resolution and poorly dated. Providing this chronological framework for LGI climate events inferred from the Orakei sequence is of paramount importance in the context of identification of leads and lags in different components of the Southern Hemisphere climate system as well as identification of Northern Hemisphere climate signals.

1 Introduction

A better understanding of past climatic change ~~events~~, and coeval responses of the terrestrial ecosystems, is fundamental for quantifying the nature, magnitude, rates and drivers of these changes. However, temporal and spatial uncertainties prevent ~~remain in our~~accurate understanding of the generation and transmission of climate events in a global context (Alley et al., 2003; Broecker, 2003; NGRIP Members, 2004; Seelos et al., 2009; Shanahan et al., 2009; Vandergoes et al., 2005). The incomplete picture of the spatial and temporal variability of terrestrial responses to climatic forcing globally is partly due to two factors: 1) a paucity of complete, long and high-resolution terrestrial records of past climatic change in the Southern Hemisphere mid-latitudes, and 2) large chronological uncertainties ~~associated with~~ of the few available records ~~that~~ spanning the Last Glacial Interval (LGI; 115,000 – 12,000 BP). ~~It is in these contexts~~In this context, ~~that~~ the laminated sediment sequences from maar lakes in the Auckland Volcanic Field (AVF) ~~are significant as several of them contain laminated sediment sequences that span~~provide key paleoclimate records for the LGI and beyond (e.g., Augustinus et al., 2012; Augustinus, 2007; Pepper et al., 2004; Stephens et al., 2012).

The ~~Auckland Volcanic Field (~~AVF~~)~~ is located in the City of Auckland ~~at the top~~towards the north of the North Island of New Zealand~~'s~~ (Fig. 1) and consists of 53 basaltic volcanic centres that erupted since ca. 200,000 yr ago (e.g., Lindsay et al., 2011; Leonard et al., 2017). Of these 53 AVF volcanoes, 13 centres are extant or paleo maar crater lakes, ranging from ca. 200,000 yr to ca. 100,000 yr in age (Augustinus, 2007, 2016). Seven of the maar lake sequences have been drilled to date and all contain well-laminated lacustrine sediment intercalated with tephra from a range of AVF and other volcanic centres in the Taupo Volcanic Zone (TVZ). This study focuses on the lacustrine sediment sequence contained in Orakei Basin, deposited following the phreatomagmatic eruption forming the maar crater until the post-glacial sea-level rise breached the crater rim and led to the current connection between Orakei Basin and the sea~~an AVF paleo maar crater lake currently connected to the sea~~ (Fig. 1; ~~(~~Peti and Augustinus, 2019~~)~~). The sediment record from the Orakei maar paleolake is ~~of~~ unprecedented in its combination of ~~quality,~~ length, resolution, and completeness in the context of the terrestrial south-west (SW) Pacific. The Orakei archive has the potential to facilitate reconstruction of the most detailed picture yet of past climatic changes in this part of the Southern Hemisphere, a region bridging the westerly-dominated mid-latitudes and the subtropics (Peti and Augustinus, 2019).

~~This study focusses~~In this study, we ~~on the integration~~ integrate of a range of absolutenumerical dating techniques (tephrochronology, radiocarbon, luminescence) ~~with~~ and correlative dating (tuning of paleomagnetic field variations established by the relative paleointensity and meteoric ^{10}Be) ~~for the~~to develop an original age-depth model ~~ment~~ of the Orakei maar lake sediments ~~sequence age-depth model~~.

~~Detailed tephrochronology is possible since several volcanic centres from the Taupo Volcanic Zone (TVZ), North Island, New Zealand, frequently ejected large volumes of rhyolitic material throughout the late Quaternary, repeatedly mantling the Auckland region with volcanic ash providing isochronous tephra marker layers (e.g., Shane and Hoverd, 2002a; Molloy et al., 2009; Zawalna-Geer et al., 2016) in the AVF maar lake sequences (Fig. 1). Radiocarbon dating was used to refine the tephrochronology based age estimates of the Orakei sequence, since it is a well established technique for dating organic macrofossil samples younger than ca. 50,000 years (Bronk Ramsey, 2008). Luminescence dating, a technique which determines the time elapsed since crystalline minerals such as quartz and feldspar were last exposed to sunlight (Aitken, 1990), was also applied. In this case, feldspar was used for luminescence dating, since New Zealand's relatively young geological history precludes effective dating of quartz due to reduced sensitisation of the luminescence signal (Almond et al., 2007). Feldspar is common in the Orakei sediments, its comparatively brighter infrared stimulated luminescence (IRSL) signal was used to date deposition of the lake sediment. The most stable known signal from feldspar, known as post infrared infrared stimulated luminescence (pIR IRSL), was used for the Orakei sediments >50,000 yr since it was recently demonstrated to be effective for dating lacustrine feldspars (Roberts et al., 2018).~~

~~Synchronous environmental changes observed in multiple proxies allow the transfer of chronological information from one record to another. For example, correlation of changes preserved in polar ice cores and sediment archives can be made on the~~

basis of fluctuations in geomagnetic field intensity (reconstructed from paleomagnetic measurements such as the ratio of natural to anhysteretic remanent magnetisation; relative paleointensity) and cosmogenic ^{10}Be atmospheric nuclide production (Stockhecke et al., 2014). With regard to terrestrial sediment archives, ^{10}Be-inferred dating is a relatively recent approach and its utility for chronology development for sediment records beyond ca. 50,000 years (limit of radiocarbon dating) remains challenging due to overprinting by local catchment processes may which disturb the ^{10}Be inventory based solely on paleointensity changes (Carcaillet et al., 2004). Paleomagnetic measurements down core can also be used to identify magnetic excursions of known age, for integration into an absolute age model. Here we apply and assess the utility of each of these approaches in the context of the development of the Orakei maar lake sediment sequence chronology.

A preliminary age model had been presented based on rhyolitic tephra marker layers in Peti and Augustinus (2019). In comparison to the this earlier model, this present study re-evaluates the tephra identification and adds radiocarbon and luminescence dates, as well as paleomagnetic measurements and variations in ^{10}Be productiondeposition. This study develops a robust chronological framework for the long lacustrine sediment sequence retrieved from Orakei maar (Peti and Augustinus, 2019). A robustThis independent chronology for this record will significantly improve temporal constraints on regional of paleoclimatic and –environmental reconstructions from the New Zealand sector of the SW Pacific, thereby enhancing our ability to identify leads and lags in climate teleconnections between the poles and tropics.

2 Regional setting

Orakei maar lies adjacent to the sea at the mouth of the Waitematā Harbour where it joins the Hauraki Gulf through the Tamaki Strait (Fig. 1). The Orakei maar was formed as the result of a highly explosive, phreatomagmatic eruption (126,150 ± 3,320 yr (2 σ); Hopkins et al. (2017)). Since then it has hosted a lake that persisted for most of its history protected by a ca. 50 m-high tuff ring from which material has slumped into the lake basin at various times and at various magnitudes (Peti and Augustinus, 2019).

Sedimentation in the Orakei maar lake was dominated by autochthonous biogenic processes with contributions from distal aeolian transport and mass flows from erosion of the steep crater rim (Fig. 1d), since the catchment was mostly constrained by the crater rimtuff ring surrounding the maar lake (Fig. 1d). A short period of fluvial sedimentation interrupted endorheic lacustrine conditions (Peti and Augustinus, 2019). Postglacial sea level rise breached the crater rim abruptly at ca. 9,000 cal yr BP, after which 18.6 m of estuarine muds were rapidly deposited, controlled by tidal inflow given Orakei Basin's proximity to the sea (Fig. 1; Hayward et al., 2008; Peti and Augustinus, 2019). Orakei Basin is presently connected to the sea by artificially-controlled inflow and outflow following the construction of a railway embankment in the 1920s (Hayward and Hayward, 1999) and is surrounded by residential areas (Fig. 1c, d).

Orakei maar and the Auckland area is dominated by a warm temperate to subtropical climate (Hessell, 1988) with a mean annual temperature of 15°C. The mean annual rainfall is 1000-1400 mm, with drier summers and wetter winters (Hessell, 1988; Hurnard, 1979). On a larger scale, New Zealand experiences a spatially variable climate dependent on synoptic-scale pressure systems, wind regimes, latitude, topography and marine proximity. These dynamic climate subsystems likely have expanded and contracted through time, so influencing the long-term climate of the Orakei area. Kidson (2000) described six regional climate zones in New Zealand from north to south, which experience very different climate parameters. Persistent mid-latitude westerly circulation brings moisture laden air masses to much of New Zealand (Hessell, 1988), although the northern parts of the archipelago, including the Orakei area, are also seasonally-influenced by the subtropical anticyclonic belt (Alloway et al., 2007; Barrell et al., 2013). The modern landscape and vegetation of Auckland have been heavily modified by human activity (Shane and Sandiford, 2003) following Maori arrival in the late 13th century (Newnham et al., 2018).

3 Material and Methods

The Orakei sediment sequence is a composite of several overlapping cores (Peti and Augustinus, 2019). Two overlapping cores with 50 cm vertical offset were retrieved from Orakei Basin in 2016 using wireline drilling in 1-~~-~~m ~~length~~ sections. The sediment sections collected in 2016 were combined with a shorter core collected in 2007 to produce a complete composite stratigraphy as described in Peti and Augustinus (2019). The Orakei sediment sequence consists of 14 sediment facies units overlying the Waitemata sandstone basement and basaltic volcanic ejecta from the maar-forming eruption, and is summarised in Fig. 2 (Peti and Augustinus, 2019). The Orakei maar core chronology presented here was established based on the event-corrected depth (ECD; Peti and Augustinus, 2019), in which all ~~visible~~ identified events of instantaneous deposition (tephra layers and mass movement deposits) have been removed.

3.1 Tephrochronology

Detailed tephrochronology is possible since several volcanic centres from the TVZ, North Island, New Zealand, frequently ejected large volumes of rhyolitic material throughout the late Quaternary, repeatedly mantling the Auckland region with volcanic ash providing isochronous tephra marker layers (e.g., Shane and Hoverd, 2002a; Molloy et al., 2009; Zawalna-Geer et al., 2016) in the AVF maar lake sequences (Fig. 1).

Tephra identification of eight visible layers was undertaken by major element analysis of glass shards via electron microprobe analyses (EMPA) following standard protocols as described in Peti et al. (2019). EMPA were performed by a JEOL JXA 8230 Superprobe at Victoria University of Wellington. A minimum of 10 individual glass shards in carbon-coated epoxy mounts were analysed using wavelength diffraction spectroscopy (WDS) with a static defocused beam at 10 µm and 8 nA. Major element oxide concentrations were determined using the ZAF[1] correction method and normalised to 100% to account for variable degrees of post-eruption hydration (Shane, 2000). Compositional data, such as major element percentages, are non-normally distributed and highly constrained by the closed-sum-effect (Aitchison, 1986). For this reason, we transformed the major element oxide concentrations using the centralised-log-ratio transformation (clr in the R package "compositions 1.40-2"; van den Boogaart et al. (2018)) prior to principal component analysis (PCA) using the prcomp command in the "stats" package as part of R version 3.5.3 (R Core Team, 2020).

-The age for the Okareka tephra layer was re-calculated using ^{14}C ages from (Molloy et al., 2009) as follows: Only ^{14}C ages from leaf fragments were accepted for the age determination of the Okareka tephra layer from the Molloy et al. (2009) ^{14}C-dataset. The ^{14}C ages OZK262 and OZK263 were combined in OxCal 4.3 (Bronk Ramsey, 2009) with the "R_combine" command to obtain a combined conventional radiocarbon age for the Okareka tephra (used in section 3.2 for reservoir-correction determination), which was then calibrated with SHCal20 (Hogg et al., 2020).

~~Additional details are included in Appendix A.~~

3.2 Radiocarbon dating

Radiocarbon dating was used to refine the tephrochronology-based age estimates of the Orakei sequence. 25 macrofossils (twigs and bark) were ~~carefully~~ extracted for radiocarbon dating, rinsed with de-ionized water and dried at 40°C. 28 bulk sediment samples were also extracted from 1 cm-thick slices, dried at 40°C and thoroughly homogenised. Anomalously old radiocarbon ages in lacustrine sediment samples can arise due to a freshwater reservoir effect, resulting from water rich in dissolved ancient calcium carbonates (Philippsen, 2013). ~~Marine reservoir age corrections are routinely addressed in the marine realm but more difficult to assess in lake basins due to their different sizes, variable regional lithologies, depths and movement of water masses (Philippsen, 2013).~~ We made efforts to restrict radiocarbon dating to short-lived terrestrial material, but the

[1] The ZAF correction method refers to the consideration of the atomic number (Z), absorption of X-rays (A), and the fluorescence (F).

scarcity of macrofossils often obviated this approach so that we also used bulk sediment ^{14}C dates ~~to increase the age resolution~~ at the risk of obtaining anomalously old ages via incorporating old carbon. To determine facies-dependent freshwater reservoir-effect corrections, we compared paired radiocarbon ages from terrestrial macrofossils and bulk sediment taken from the same depth. For facies unit 4, we selected the age of the Okareka tephra layer instead of a macrofossil and sediment sample OZX348, and samples OZX341 (wood) and OZX347 (bulk sediment) for facies 8 following the recommendations of Philippsen (2013). Radiocarbon dating of organic macrofossils and bulk sediment was conducted at the Australian Nuclear Science and Technology Organisation (ANSTO) (Fink et al., 2004), apart from one macrofossil sample at the Radiocarbon Dating Laboratory (Department of Geology, Lund University) and one published date (NZA28865) from the Rafter Radiocarbon Laboratory (GNS, New Zealand). Samples for Accelerator Mass Spectrometry (AMS) measurement were pre-treated with 2M HCl to remove carbonate, 0.5-4% NaOH to remove humic and fulvic acids, followed by 2M HCl to remove absorbed CO_2 from the atmosphere during the preparation process. After drying, the samples were combusted, graphitised and analysed at the respective AMS-facilities. Ages were reservoir corrected and calibrated using the ~~SHCal13~~ SHCal20 calibration curve (Hogg et al., 2020) ~~(Hogg et al., 2013)~~ as part of the age-depth modelling process (see section 3.~~7~~6.1).

3.3 Luminescence dating

Luminescence dating, a technique which determines the time elapsed since crystalline minerals such as quartz and feldspar were last exposed to sunlight (Aitken, 1990), was also applied. In this case, feldspar was used for luminescence dating, since New Zealand's relatively young geological history precludes effective dating of quartz due to reduced sensitisation of the luminescence signal (Almond et al., 2007). Feldspar is common in the Orakei sediments, its comparatively brighter infrared-stimulated luminescence (IRSL) signal was used to date deposition of the lake sediment. The most stable known signal from feldspar, known as post-infrared infrared-stimulated luminescence (pIR-IRSL), was used for the Orakei sediments >50,000 yr since it was recently demonstrated to be effective for dating lacustrine feldspars (Roberts et al., 2018). Luminescence dating of feldspar from ten samples was undertaken for the Orakei core. The fine-grained fraction was targeted in order to maximize the percentage component of non-volcanic, distally-sourced dust, which is more likely to yield a reliable luminescence signal. The sediment cores were stored wrapped in light-proof plastic at 4˚C until opened and subsampled for luminescence dating under subdued orange light at the University of Auckland (New Zealand), taking care to only sample the innermost parts of the core for dating. Samples were taken to ensure maximal spread over the >45,000 year interval of the Orakei sequence, based on a preliminary age model which extrapolates the sedimentation rate between the two oldest tephra layers of known age (Tahuna and Rotoehu).

Luminescence dating sample pre-treatment for polymineral fine grains (4-11 μm) was undertaken at the Max Planck Institute for Chemistry (Mainz, Germany) following published methods (Mauz and Lang, 2004) and involved HCl and H_2O_2 digestion, sieving and settling. Additionally, coarse-grained K-feldspar (90-115 μm) was extracted from sample L20 (A0113) by density separation using lithium heterotungstate for comparison with the fine-grained signal. The other samples yielded insufficient coarse-grained material for dating. Samples were loaded using a pipette onto 10-15, 1 cm diameter stainless steel discs depending on the amount of material remaining after chemical preparation. Additional details are included in Appendix B.

The equivalent dose (D_e) was measured using the post-infrared infrared ($pIR\text{-}IRSL_{290}$) protocol, stimulated at 290˚C to minimize the potential for feldspar signal fading (Buylaert et al., 2012; Thiel et al., 2011, 2014). Measurements were undertaken using an automated Risø TL-DA-20 reader using infrared (IR) LEDs for illumination, with the resulting signal detected by an EMI 0235QA photomultiplier tube with a D410 filter for feldspar (Bøtter-Jensen, 1997; Bøtter-Jensen et al., 1999). Irradiation was provided by a calibrated $^{90}Sr/^{90}Y$ beta source (Bøtter-Jensen et al., 2000). An internal alpha contribution of 0.12 was assumed for the samples, in order to account for the lower luminescence efficiency of alpha radiation relative to the beta and gamma components (Rees-Jones, 1995; Rees-Jones and Tite, 1997). A higher stimulation temperature was chosen based on equivocal results of the preheat plateau test which showed substantial inter-aliquot scatter irrespective of

measurement temperature (Fig. B1). The accepted aliquots of all samples yielded either normal distributions, which were typically very wide, or skewed distributions indicative of incomplete bleaching. In the first case, equivalent dose values were calculated using the Central Age Model (CAM) (Galbraith et al., 1999). In the latter, equivalent dose was calculated using the Minimum Age Model (MAM~~;~~) ~~(~~Olley et al., 2004~~)~~; ~~(Figure~~ Fig. B2). Further details can be found in Appendix B.

Sub-samples were collected for dose rate analysis from the same depth in the core as each dating sample. These were dried and homogenised. A weighed part of this sample was ashed at 950°C and K concentrations were obtained by XRF at the University of Waikato, Hamilton (New Zealand, see Appendix B for further details). The other weighed part was treated with HNO_3 and HF at ANSTO, from which U and Th concentrations were obtained by inductively-coupled plasma mass spectrometry (ICP-MS) at the University of Auckland (see Appendix B for further details). The measured activities of the radioactive elements K, Th, and U were converted to dose rates using published factors (Adamiec and Aitken, 1998; Guerin et al., 2011). Dose-rate attenuation was estimated using published values (Mejdahl, 1979) and the sediment moisture content. Water content was estimated assuming saturation of the lacustrine sediments, taking into account water loss in the laboratory subsequent to core extraction (Lowick and Preusser, 2009). Substantial uncertainties in water content of 20 ± 10% were included in order to mitigate potential inaccuracies in the dose rate calculations due to desiccation. Cosmic-ray dose rates were calculated based on sediment density estimates, altitude, latitude, longitude, and depth, following Prescott and Hutton (1994). Cosmic-ray dose rate values were negligible (<0.01 Gy/ka) due to the depths of the samples within the lake sediments.

3.4 Paleomagnetism

Synchronous changes observed in multiple proxies allow the transfer of chronological information from one record to another. For example, correlation of changes preserved in polar ice cores and sediment archives can be made on the basis of fluctuations in geomagnetic field intensity (reconstructed from paleomagnetic measurements such as the ratio of natural to anhysteretic remanent magnetisation; relative paleointensity; Stockhecke et al., 2014). Paleomagnetic measurements down core can also be used to identify magnetic excursions of known age, for integration into an absolute age model.

Sediments below ~40 m depth (representing ages > ca. ~~35~~36,000 cal yr BP) were used for paleomagnetic measurements. The upper (younger) interval of the Orakei sequence was not used for paleomagnetism as it can be reliably dated with radiocarbon and we note that the presence of numerous basaltic tephra layers can obscure a reliable paleomagnetic signal (Nilsson et al., 2011). This is a problem especially around the age of the Mono Lake Excursion, which correlates with a flare-up of the basaltic volcanoes of the AVF around 30,000 cal yr BP (Molloy et al., 2009). Measurements of the ~~Orakei maar sediment~~ Natural Remanent Magnetisation (NRM), Anhysteretic Remanent Magnetisation (ARM) and Saturation isothermal remanent magnetisation (SIRM) were conducted using a 2G-Enterprises model 760-R SQUID magnetometer equipped with an automatic three-axis alternating field (AF) demagnetisation system at Lund University (Sweden). Oriented standard (volume = 7 cm^3) plastic paleomagnetic sampling cubes were used, with 48 samples treated as pilot samples and progressively demagnetised in 5 mT increments from 0 to 40 mT, and in 10 mT increments up to a maximum AF of 80 mT. The remaining samples were demagnetised in increments of 5 mT up to 30 mT, and in increments of 20 mT from 40 mT to a maximum AF field of 80 mT. Preliminary analyses on the pilot samples indicated that a stable single component magnetisation, demagnetising towards the origin, could usually be isolated between 15 mT and 80 mT (see Appendix C). This interval was therefore used to isolate the characteristic remanent magnetisation (ChRM) using principal component analysis (Kirschvink, 1980). Samples with Maximum Angular Deviations MAD >15, mostly associated with weak NRMs, were rejected.

ARMs were induced in a peak AF of 80 mT with a DC bias field of 0.05 mT. The ARMs were measured and AF demagnetised in increments of 5 mT from 0 to 30 mT and in increments of 20 mT from 40 to 80 mT in the pilot samples and in increments of 10 mT from 20 to 40 mT in all remaining samples. SIRMs were induced with a DC field of 1 T using a Redcliffe 700 BSM pulse magnetizer. Volume specific magnetic susceptibility (κ) was measured using a AGICO MFK1-FA Kappabridge. ~~Relative~~

~~paleointensities (RPIs) were estimated by normalising the NRM_{20mT} with the magnetic concentration dependent ARM_{20mT}.~~ ~~The application of the Orakei RPI for chronology development is described in section 4.7.~~

Relative paleointensities (RPIs) were estimated by normalising the NRM_{20mT} with the magnetic concentration dependent ARM_{20mT}. There remains a possibility for some minor RPI variations induced by changes in lithology and indirectly by magnetic grain size and concentration which we attempt to correct with a facies-dependent correction factor in coarser sediments (see details in section 4.4).~~.~~

3.5 Beryllium-10

With regard to terrestrial sediment archives, ^{10}Be-inferred dating is a relatively recent approach and its utility for chronology development for sediment records beyond ca. 50,000 years (limit of radiocarbon dating). Though the radioactive decay of ^{10}Be has been ~~-~~used to date sediment much older than the Orakei sequence (e.g., Frank et al., 2008; Simon et al., 2020a), no study has been published yet applying ^{10}Be variations in sediment cores as a relative dating tool by comparison to RPI reference data beyond the Laschamp Excursion (Nilsson et al., 2011). ~~remains challenging due to overprinting by local catchment processes may which disturb the ^{10}Be inventory based solely on paleointensity changes (Carcaillet et al., 2004).~~ Meteoric ~~(i.e., atmospheric),~~ cosmogenic ^{10}Be~~,~~ ~~once~~ is produced in the atmosphere via nuclear reactions of cosmic ray particles with nuclei such as nitrogen and oxygen. ^{10}Be~~,~~ readily attaches to aerosols and dust, and with a short residence~~y~~ time of ~1 yr, is deposited on the Earth surface mainly via precipitation (Willenbring and von Blanckenburg, 2010). In open depositional environments (i.e., deep-sea and polar-ice cores), ~~to a first order,~~ variability in (normalised) ^{10}Be concentration~~s~~ can be used as a proxy of past geomagnetic field variation (e.g., Frank et al., 1997; Muscheler et al., 2005). In terrestrial settings, such as lakes, catchment processes and lithology (i.e., erosion, soil geochemistry, aeolian input, grain size) complicate ^{10}Be provenance, delivery and accumulation and hence the identification of a ^{10}Be production signal (e.g., Czymzik et al., 2015; Nilsson et al., 2011). To overcome such complexity, one approach is to normalise ^{10}Be measurements to an element or isotope with similar geochemical properties, such as ^{9}Be, where it has been demonstrated that authigenic ^{10}Be/^{9}Be ratio can compensate effects of catchment processes and grain size variations (e.g., Bourles et al., 1989; Wittmann et al., 2012). Although the Orakei catchment is small, grain size and lithology variability throughout the core is problematic due to in-wash events of clastic grains. In this study, we extract both authigenic ^{10}Be and ^{9}Be to compensate the effect of grain size and possible catchment process~~es~~ variation. Meteoric ^{10}Be and authigenic ^{9}Be w~~as~~ere measured in order to detect variations in cosmogenic nuclide production rates ~~down-core~~ to supplement ~~the~~ paleomagnetic measurements (section 3.4).

Laminated sediment intervals below ~40 m-depth ~~in the Orakei sediment sequence, which cannot be dated with radiocarbon,~~ were targeted for cosmogenic ^{10}Be measurements with a focus on the lower half of the sequence.

59 samples were processed for AMS measurements at ANSTO. Sample preparation (detailed in Appendix D) followed White et al. (2019) and involved 1-cm thick core slices (representing ca. 25-year duration; average sedimentation accumulation rate (SAR) of 0.04 cm/yr) from which 0.5 to 1 g of dried, homogenised sediment was treated with 6M HCl for 2 hours to leach out the authigenic ^{10}Be and ^{9}Be. A sub-sample of each leachate was extracted to ~~provide a HCl extractable~~measure ^{9}Be concentration (White et al., 2019) ~~as measured on~~using an Agilent 7700 ICP-MS at the Mass Spectrometry Equipment Centre (University of Auckland (UoA), New Zealand). ^{9}Be spike, derived from ^{10}Be-free beryl mineral, was added to the remainder of the leachate prior to treatment with HF, $HClO_4$ to remove silicon and boron complexes. Beryllium was separated from other cations by passage through anion and cation exchange columns, converted to $Be(OH)_2$, oxidised to BeO at 800˚C and finally mixed with Nb powder. AMS ^{10}Be/^{9}Be measurement~~s~~ of these 59 samples were performed at the Centre for Accelerator Science, ANSTO (Australia) on the 6MV SIRIUS accelerator (Wilcken et al., 2019). The measured ^{10}Be/^{9}Be values were normalised to either the 2007-KN5-2 (nominal ratio of 8.558×10^{-12}) or the 2007-KN5-3 (6.320×10^{-12}) standard (Nishiizumi et al., 2007). Full chemistry procedural blank ^{10}Be/^{9}Be ratios range from 1.1-13.7 x 10^{-15} and are ≤~1% of the measured sample ratios.

Ten additional samples were prepared at Lund University ~~for a high-resolution study of cosmogenic ^{10}Be variation~~to increase the ^{10}Be resolution during the Laschamp Excursion. Each sample consists of a 10-cm interval, representing ca. 250-year duration (SAR = ~0.04 cm/yr). Samples were weighed, homogenised, spiked with ^{9}Be and leached with H_2O_2, HCl, and HNO_3. Separation and precipitation of $Be(OH)_2$ was achieved by treatment with ammonia solution and NaOH for pH adjustment and followed by oxidation to BeO at 600°C (See details in Appendix D). AMS ^{10}Be/^{9}Be measurements of these 10 samples were performed at ETH (Eidgenössische Technische Hochschule) Zurich. Authigenic ^{9}Be was not analysed for these ten samples and was considered negligible compared to the ^{9}Be spike mass following measurements at UoA and ANSTO (see above). The measured ^{10}Be/^{9}Be ratios were normalised to the ETH Zurich in-house standard material S2007N, which has a nominal ^{10}Be/^{9}Be ratio of 28.1 x 10^{-12} (Christl et al., 2013) and is consistent with the 2007-KN^{10}Be/^{9}Be standards used at ANSTO. All measured ^{10}Be concentrations were several orders of magnitude higher than the background of full chemistry procedural blanks, so that blank corrections were negligible.

3.6 Correlation of magnetic relative paleointensity for relative dating

We applied relative dating using magnetic relative paleointensity (RPI) to ~~Orakei maar lake~~ sediments older than ca. 45,000 years to supplement the absolute age information provided by luminescence (pIR-IRSL) dating (see section 4.3). ~~As highlighted by Blaauw (2012), I~~it is crucial to avoid circularity in tuning climate proxies ~~(such as pollen percentages, isotopes or elemental compositions)~~ based on assumed synchroneity, when the presence or absence of this possible synchroneity is actually an overarching study objective (Blaauw, 2012). Hence, we make use of the ~~RPI~~relative intensity of the Earth's magnetic field (RPI) ~~strength~~ which is considered to be a globally synchronous signal over millennial timescales (e.g., Channell et al., 2000; Laj et al., 2004) ~~unlike climate signals~~. This approach was successful in Lake Van (Turkey) where several RPI minima were aligned to provide a chronologic framework (Hatfield et al., 2020; Stockhecke et al., 2014).

We use a dynamic programming algorithm to align the Orakei RPI with the ~~Virtual~~ virtual axial dipole moment (VADM) reference curve from the marine PISO-1500 stack (Channell et al., 2009). Dynamic time warping (DTW) ~~uses generalized dynamic programming, in which a complex problem is divided into smaller problems and their solutions are stored for later use. DTW~~ aligns time series datasets through generalized dynamic programming (Hay et al., 2019) and has been ~~used~~ adapted for paleomagnetic vector data by ~~Hay et al. (2019) and~~ Hagen et al. (2020). The DTW algorithm calculates every possible match between the reference and query time series at every ~~strata~~stratum (data point), producing a cost matrix. This cost matrix quantifies the Euclidean distance between each point in the query time series and each point in the reference time series. Under step-pattern constraints, an optimal alignment path is then found through the cost matrix which represents the optimal alignment path between both time series (Hagen et al., 2020). The step pattern only allows two directions in the path. This prevents the creation of age inversions, and heavily penalises alignments between points with very different indices, so that major jumps and/or hiatuses are very unlikely. The DTW approach relies on (mostly) complete time series with a substantial component that overlaps between the reference and query time series (Hay et al., 2019).

Visual inspection of the Orakei RPI and the variation of the PISO-1500 VADM (Channell et al., 2009) over the period ca. 30,000 – 140,000 years suggests strong similarities between both curves (see section 4.6). These similarities facilitate an improvement of the absolute age model by tuning the Orakei RPI to the PISO chronology. The PISO-1500 stack has a temporal resolution of one datapoint per 1000 years. To reach a similar resolution in both time series, the Orakei RPI was interpolated to match the resolution of the PISO-1500 stack and at the same time to smooth possibly unreliable features in the Orakei RPI record. Records were scaled by subtracting the mean of the time-series and dividing by its standard deviation. DTW was then performed in R (package dtw (Giorgino, 2009)) with closed start and open end points on the two time-series, and using a Euclidean distance-based cost matrix and symmetric step pattern. We integrated 13 tuning points from the resulting alignment path into a Bacon age model. We selected 12 random tuning points supplemented by the basal tuning point. We chose to select these tuning points randomly (apart from the basal point) in order to prevent any bias that involved selecting points to arrive

at a favoured solution. The depth and age values of these 13 tuning points were incorporated into the Bacon age modelling process (see section 3.7). The standard deviation for these tuning points reflects the match between the RPI and PISO so that a point matched to several ages has a larger standard deviation spanning the entire range of matched ages.

3.7 Bacon age model development

The final age-depth model for the entire Orakei sediment sequence was produced using the Bacon package (Bayesian Accumulation model), using rbacon 2.4.~~2~~ 3 (Blaauw and Christen, 2011, 2020) with a prior accumulation rate of 15 yr/cm (assumed from a maximum core age of ca. 130,000 yr and a core length of 8000 cm, i.e., ~16.25 yr/cm). Prior accumulation shape, memory strength and memory mean were suggested by the Bacon package following Blaauw and Christen (2011) based on the age data provided (see Table 1). The age-depth model is further constrained by the provided rhyolitic tephra, radiocarbon and luminescence ages from the core (Tables 2, 3 and 4 respectively), the U/Th-age of the Laschamp Excursion as identified by paleomagnetic direction and intensity using the age of 41,100 ± 350 (2 σ) yr BP from (Lascu et al.~~,~~ (2016) ~~(41,100 ± 350 (1 σ) years BP; Lascu et al., 2016)~~, the Ar/Ar-age of the locally-sourced basaltic Mt Albert eruption (119,200 ± ~~2~~5,~~800~~ 600 (~~1~~ 2 σ) ~~years~~yr; Leonard et al., 2017), and the dated tuning points obtained from matching the Orakei ~~paleomagnetic data~~RPI to the PISO-1500 global ~~reference curve~~stack (see section 3.6, Table 5). Reservoir correction and calibration of radiocarbon ages using ~~with~~ the Southern Hemisphere calibration curve SHCal~~13~~20 (Hogg et al., 2020) ~~(Hogg et al., 2013) of radiocarbon ages~~ was ~~conducted~~ done by Bacon as part of the age modelling procedure (Blaauw and Christen, 2020). A Student's t-distribution, essentially a symmetric distribution with longer tails than a typical Gaussian distribution, was used for the radiocarbon ages since it is more robust against outliers (Blaauw, 2010; Blaauw and Christen, 2011; Christen and Pérez E, 2009). Gaussian distributions were assumed for tephra and pIR-IRSL ages, the Laschamp Excursion age and tuning point ages.

4 Results

4.1 Tephrochronology

4.1.1 Rhyolitic tephra layers

The identification of the rhyolitic tephra layers follows Peti et al. (2019) with the addition of the Rotorua tephra and is demonstrated in Figure 3 using multivariate statistics. PCA was first performed on published tephra EMPA data (black and grey symbols in Fig. 3), which serve as reference tephra in this study. The same scaling and rotation of the reference PCA were then applied to the unknown compositional data and the tephra layers were thus assigned to their source eruptive events through multivariate similarity (Fig. 3). The identification of tephra layers and the correlation to their eruption events is supported by the geochemical composition of the glass shards and stratigraphic position in relation to the AVF framework (Hopkins et al., 2015; Molloy et al., 2009). The resulting identifications then allowed the direct transfer of published ages (or adjusted ages in this study) onto the Orakei sediment sequence. ~~Further details can be found Appendix A.~~

Tephra sample T-74 could not be clearly identified solely from its major oxide geochemistry (Fig. 3, A1), since many layers show similar geochemical composition. However, its stratigraphic position and substantial thickness (>30 cm) suggest that this layer is the Rotoehu tephra. Tephra sample T-73 displays the same geochemistry as the Tahuna tephra, an interpretation supported by its stratigraphic position (Figs. 3, A1). Tephra sample T-71 can confidently be assigned to the eruption pair of Hauparu and Maketu (both from Okataina Volcanic Centre (OVC)), which occurred within 300 years of each other (Molloy et al., 2009) and show similar major oxide compositions (Fig. 3). Given the similarity between Hauparu and Maketu reference major oxide data (Fig. 3), we cannot confirm from the tephra geochemistry whether T-71 represents the Maketu or Hauparu eruptions. Since only one layer has been found, we assign sample T-71 to Maketu given that this was the larger eruption with more widespread and voluminous ashfall (estimated to be 15 km^3 for Maketu compared to 10 km^3 for Hauparu by (Froggatt

and Lowe, 1990)). From a chronological perspective, this uncertainty in identification is irrelevant, since the two tephra are essentially the same age (Hauparu dates to 36,000 ± 1,000 – 2,000 years and Maketu to 36,300 ± 1,000 – 2,000 years; ages and generic error ranges of 1,000 to 2,000 years for rhyolitic tephra older than 21,000 years from Molloy et al. (2009)).

The geochemical compositions of tephra T-02 (25 mm-thick) and T-04 (5 mm-thick) are very similar (Fig. 3, A1). They are positioned between the Okareka and Maketu tephras (above T-02 and below T-04). Stratigraphically-feasible candidates include the Te Rere, Kawakawa/Oruanui tephra (KOT), Poihipi, and Okaia tephra (Lowe et al., 2013). Te Rere and Poihipi can be rejected, since neither T-02 or T-04 show geochemical overlap with reference data for the products of these two eruptions (Fig. 3, A1). Stratigraphic ordering suggests that T-02 may be the younger KOT, whilst T-04 may correlate to the older Okaia tephra. However, a similar depth in the stratigraphic framework developed for the Orakei sequence (Peti and Augustinus, 2019) and the position of T-04 between several basaltic AVF tephra layers (Peti et al., 2019) suggests an identification of sample T-04 as the KOT as identified by ~~(~~Molloy et al.~~,~~ (2009). This would imply a previously unknown eruption as the source of the thicker T-02 layer (25 mm thick), which is unlikely ~~-~~given the well-studied eruptive history of the Taupo Volcanic Zone (e.g., Lowe et al., 2013). Layer T-02 is well preserved, fining upwards and shows no signs of reworking (Peti et al., 2019). Its thickness supports identification as KOT, since the Kawakawa/Oruanui eruption was much larger than Okaia (Froggatt and Lowe, 1990) and thus a thicker deposit would be expected in the sediment sequence. Most importantly, the glass shards of both samples show very different morphology in backscatter images (Fig. A2). Shards in T-02 are very large, cuspate, and bubbly with preserved thin bubble walls signifying a very large, explosive eruption. On the other hand, small, blocky shards in T-04, suggest a smaller, less explosive eruption (Heiken, 1972; Liu et al., 2015). This observation links sample T-02 to the Kawakawa/Oruanui super-eruption and out of stratigraphic necessity T-04 to the smaller Okaia eruption. It follows that Molloy et al. (2009) may have mis-correlated the apparent KOT in light of very similar geochemical compositions between sample and reference data and following the same assumption that the larger eruption should have been more easily preserved over the smaller eruption. The true KOT had been missed in a core break in the 2007 Orakei sequence. Other known major tephra, including Rerewhakaaitu, Te Rere and Poihipi, were not observed as macroscopic event layers within the Orakei sediment sequence in this study, although they may be present as cryptotephra. Samples T-01 and T-15 can be clearly identified as the Okareka and Rotorua tephras based on geochemistry (Fig. 3) and stratigraphic position.

4.1.2 ~~ID of s~~Basaltic tephra sample T66

An unidentified basaltic tephra layer, sample~~s~~ ~~"~~T66 ~~"~~ could not be matched stratigraphically or geochemically to any other Auckland Volcanic Field (AVF) tephra layer previously documented in Molloy et al. (2009) or Hopkins et al. (2015; 2017). Its occurrence between the layer AVF1 and the basal eruptive material sourced from the Orakei Volcanic Centre (Fig. A3) suggests that it is a new, previously undocumented tephra layer from a different AVF source. ~~In order to test this hypothesis, electron microprobe analyses (EMPA) were conducted on sample T66 glass shards at Victoria University of Wellington following the method outlined in section 3.1. The results are presented in figures A3–A5.~~ We confirmed that T66 is not a correlative to the Orakei Volcanic Centre and/or AVFa tephra layer (Fig. ~~A3~~4A). Furthermore, glass shard geochemistry also obviates correlation to the AVF1 tephra layer (Fig. ~~A4~~4B). We consider that T66 constitutes a basaltic tephra that has not so far been encountered in any AVF maar cores (Hopkins et al., 2015, 2017).

Based on the position of T66 between AVF1 (correlated to Domain/Grafton eruption) and AVFa (correlated to Orakei eruption; Hopkins et al. (2017)), several AVF volcanoes are potential sources for the T66 tephra (Hopkins et al., 2017; Leonard et al., 2017). Despite the difficulties in comparing whole rock and tephra material based on major element oxides, we compare data from sample T66 to the potential AVF source centres (Fig. ~~A5~~4C): Grafton Park, Mt Albert, Mt Roskill, as well as the correlatives for AVF1 and AVFa, Domain and Orakei, respectively. Low FeO and SiO_2% in Mt Albert whole rock composition as well as in sample T66 suggests strongly that Mt Albert is the source of the T66 tephra layer (Fig. ~~A5~~4C). The formative eruption of Mt Albert has been Ar-Ar dated to 119,~~-~~200 ± ~~2~~5,600~~.8~~ (~~1~~2 σ~~sd~~) yr~~ka~~ by (Leonard et al., 2017) which falls between

the ages obtained for AVFa (126,150 ± 3,320 (2 σsd) yr, Hopkins et al., 2017) and AVF1 (106,170 ± 4,300 (2 σsd) kayr (Hopkins et al., 2017); 83,100 kayr (Molloy et al., 2009)) giving further support for this identification. Hence, we conclude that sample T66 is sourced from Mt Albert with an eruptive age of 119,000 ± 25,8600 (2 σ) yrka. In order to maintain nomenclature consistency, we assign the name "AVFaa" to this tephra layer.

~~Basaltic tephra T66 was sourced from Mt Albert (119,200 ± 2,800 (1 σ) years; Leonard et al., 2017). This tephra was documented here for the first time in the AVF tephra framework (Hopkins et al., 2015, 2017; Molloy et al., 2009). We have termed it "AVFaa" (see Appendix A for details).~~

4.2 Radiocarbon dating

All 54 radiocarbon dates from the Orakei core (53 new and the NZA28865 date previously published in Hayward et al. (2008)) are summarised in Table 3.

The Bacon age model recognises 13 ages as outliers (24%), which is in agreement with visual identifications in comparison to the model ~~(Fig. 6)~~. Since the model recognises these outliers there was no need to remove them manually. The four wood sample ages OZW884-887, and 3 bulk sediment sample ages OZX869, OZX888 and OZX889 are considered outliers being much older than bracketing ages and thus the age-depth model. ~~(Fig. 6).~~ These outliers, all between 12.5 and 16.5 m-depth, are interpreted as representing fluvial in-wash containing reworked organic matter and, in the case of bulk sediment ages, carry additional uncertainties from necessary reservoir corrections. The ages for OZX873 and OZX882 are also older than anticipated. This is most likely due to the unknown reservoir correction, since no double-dating of these facies units (5-7) was possible due to an absence of plant macrofossils. The ages OZW874, OZX340, OZX343 and OZX878 are too young and probably explained by the first three yielding very small masses of organic carbon, whereas the reason for the latter age is unclear. ~~The Bacon age model recognises all 13 outliers and hence there was no need to remove them manually.~~

The facies-dependent reservoir effect in facies 4 is 1,026 ± 117 yr and 410 ± 170 yr in facies 8. Where the reservoir correction is stated with a question mark in Table 3, no reservoir correction for these specific facies could be calculated. In that case we used the reservoir correction from the stratigraphically closest facies (i.e., reservoir correction from facies 4 also applied to facies 3 and 5, marked with a question mark in Table 3).

4.3 Luminescence Dating

Luminescence data were obtained for six of the ten fine-grained samples measured from the Orakei series, and for one coarse-grained sample, L20. Samples L18, L20 and L29 yielded insufficient natural signal for equivalent dose estimation. These are also the youngest luminescence samples according to depth and therefore had accumulated less charge during burial. The sensitivity of the Orakei samples was low for feldspars and may suggest a primary igneous origin.

~~The~~ Results of the remaining six samples ~~provided ages, and these results~~ are summarised in Table 4. They ~~results broadly~~ econform (within 2 σ error) to the expected ages based on the other approaches presented here but suffer from limitations as described below and in Appendix B.

The luminescence characteristics of the Orakei samples were not optimal for age determination. Ages could only be calculated by relaxing the acceptance criteria for analysis. The samples are typically very dim, yielding generally low signal counts (Fig. B4a) and low sensitivity. Late background subtraction was used to optimize the signal measured. The sensitivity to test dose over the regenerative cycles of the pIR-IRSL$_{290}$ protocol typically decreased to 20-30% of the test dose sensitivity following the natural signal measurements and remained fairly constant over subsequent cycles (Fig. B4b). Dose-response curves could often, but not always, be fitted to an exponential or exponential-plus-linear function, but rarely passed through the origin due to the high degree of thermal transfer (Fig. B4c). Recuperation was very high, yielding values of up to 50%, and recycling ratios were variable but often exceeding 20% divergence from unity (Table B1). In order to obtain results, aliquots were

accepted if dose-response curves could be reasonably fitted; threshold criteria for other quality control measurements such as recycling ratios and recuperation were relaxed such that values of 1.0 ± 0.4 and <67% (mostly <25%) were accepted for analysis respectively. The residual dose test run on sample L15/A0111 provided usable signals only in 1/3 aliquots, and so the residual correction was made on the basis of that lone aliquot. Despite these limitations, the residual-corrected ages yield results more closely fitting with the age predicted by the matching of the paleomagnetic RPI to the PISO-1500 stack.

4.4 Paleomagnetism

Down core paleomagnetic measurements of the Orakei sediment sequence were undertaken to support the development of the chronology with the identification of known-age geomagnetic excursions ~~of magnetic field inclination and reduced intensity of the Earth magnetic field~~. Additionally, relative changes in the strength of the Earth's magnetic field were estimated to allow the transfer of chronological information from dated sediment sequences showing corresponding variations in the relative paleointensity.

Mineral magnetic data (~~see Appendix C~~Fig. 5) of the Orakei sediment sequence is consistent with the detrital magnetite as the main magnetic carrier. Following Peters and Thompson (1998) we classify the magnetic assemblage of the Orakei samples as magnetite/titanomagnetite (Fig. ~~C~~5a). We identify both detrital and extracellular magnetite components based on the definition of Egli (2004; Fig. ~~C~~5b), with the latter mostly found in facies 10. Variations in magnetic grain size, estimated following Thompson and Oldfield (1986), suggest that most Orakei sediment samples used for paleomagnetic measurements fall in the pseudo-single domain range of magnetite (0.1 – 20 µm; Fig. ~~C~~5c), consistent with a detrital origin although the increased scatter in the lower left half of Fig. 5c, suggesting increasing magnetic grain size, may partly reflect the importance of superparamagnetic (e.g., facies 10) and/or paramagnetic effects in samples with low magnetite concentration. The magnetic data partially fulfils the loosely defined criteria to assess the reliability of paleointensity data from sediments (Tauxe, 1993). It appears that magnetic concentration variations exceed one order of magnitude at times and the magnetic grain size is likely not confined to a very narrow range, but all other criteria are generally fulfilled.

The coring procedure at Orakei prevented useful declination determination. The 1 m-long core sections were not oriented with respect to magnetic north/south and several segments were further rotated as they broke along coarser clastic layers such as tephra.

The ChRM inclination in the lower ~40 m of the Orakei sediment sequence mostly varies from -50 to -60°, which is consistent with the geocentric axial dipole (GAD) prediction of -56° for the site latitude. A reversed polarity direction with inclination reaching +66° is observed at 43.24 m (Fig. ~~4A~~6A). Its position between the Tahuna and Rotoehu tephra layers (see section 4.1) implies that this short-lived reversal can be assigned to the Laschamp Excursion ~~ion~~(e.g., Cassata et al., 2008; Ingham et al., 2017; Laj et al., 2014; Laj and Channell, 2015; Mochizuki et al., 2006; Roperch et al., 1988) ~~(~~dated to 41,1~~4~~00 ± 350 (2 σ) yr by~~;~~ Lascu et al.~~,~~ (2016). Significantly shallower inclinations are recorded between ~63 and 68 m, as well as around the facies unit boundary 13/12 at ~73 m (Fig. 4). The inclination flattens to -4.1° at 73.42 m, 10 cm below the tephra "AVFaa" from the Mt Albert eruption (119,200 ± ~~2~~5,~~800~~ 600 (2 σ) yr; Leonard et al., 2017; Fig. 6~~4~~)). This age constraint in proximity of this near-reversed inclination, along with pronounced and sustained decrease in RPI starting at the time of deposition of "AVFaa", suggests that it could correspond~~s~~ to the Blake Excursion (Smith and Foster, 1969; Thouveny et al., 2004; Tric et al., 1991; Zhu et al., 1994) ~~(~~dated to 116,500 ± 700 to 112,000 ± 1,900 (2 σ) y~~rears~~ by~~,~~ ~~(~~Osete et al.~~,~~ (2012)~~)~~. Other occurrences of reversed/transitional (positive or near-zero) inclinations at 49.77 m, ~~51.23 m,~~ 63.38 m, and shallower inclinations between ~63 and 68 m, occur in intervals of coarser grain size ~~more likely~~possibly indicating previously unidentified thin mass movement deposits (King, 1955). No data was obtained between 65.8 and 67.78 m due to sand bands preventing sampling of the intercalated laminated sediment as the sample cubes are larger (2.2 cm) than samples taken for other techniques (e.g., 1-cm slices for Beryllium, see below).

The NRM and ARM variation of the Orakei sediment sequence show the same broad pattern in each demagnetisation step (Fig. ~~4B~~6B, C). Very low NRM and ARM in facies unit 14 are followed by a sudden increase at ~76 m (Fig. ~~4B~~6B, C), then decreasing stepwise until very low values are reached again at ~60 m. Up to 40 m, NRM and ARM values remain very low, although the ARM curve is interrupted by slightly elevated values in facies unit 9 (~55-50 m; Fig. ~~4C~~6C).

To calculate the relative paleointensity - expressed by the NRM/ARM ratio - we used the NRM and ARM after 20 mT AF demagnetisation, as a similar pattern was obtained from all demagnetisation steps (different colours in Fig. ~~4D~~6D). ~~(~~Valet and Meynadier~~,~~ (1998) and ~~(~~Stanton et al.~~,~~ (2011) show that differences between different methods to obtain the RPI values are minor. Very low values are associated with the ~~partially reversed~~partially reversed polarity direction tentatively identified as the Laschamp Excursion (Fig. ~~4~~6). The strength of the global magnetic field is known to have been exceptionally low during the Laschamp Excursion as measured in sediments (e.g., Channell et al., 2009) as well as in lava flows from France (e.g., Laj et al., 2014; Roperch et al., 1988) and New Zealand (Cassata et al., 2008; Ingham et al., 2017; Mochizuki et al., 2006), supporting this interpretation. Equally low RPI values are also observed in facies unit 9 and facies unit 11 (Fig. ~~4~~6). These facies units represent coarser grain size facies, suggesting that the low RPI values could be artefacts associated with less efficient NRM recording in a higher energy depositional environment (compare Fig. 2) and observed in a minor anti-correlation between dry bulk density (not shown) and RPI. This may indicate a possible link between sedimentary facies and the efficiency to acquire ~~a~~an NRM signal, which was not fully removed by the NRM/ARM normalisation procedure. The down-core variation in NRM/ARM (Fig. 4D) is assumed to be proportional to the scatter around a linear trend-line in a scatterplot (Fig. ~~C6~~C5). ~~However, t~~The offset between the linear trend-lines fitted to the data points of the coarse and the fine-grained facies units indicates only a very small difference in efficiency of NRM acquisition. Nevertheless, we correct this difference with a ~~Hence, no~~ facies-dependent correction factor ~~is~~ applied to the paleomagnetic intensities of facies 9 and 11 to match the slope of the fine-grained facies. The facies-corrected RPI (shown in Fig. 6E) strongly resembles the raw RPI and henceforth, RPI refers to this facies-corrected RPI.

The Orakei RPI shows marked variation with a short-lived peak at 78.35 m (Fig. ~~4D~~6D) and troughs around 70, 73, and 76 m. Pronounced low RPI values between ca. 65 and 61 m are followed by high-frequency variability up to ~55 m, then a pronounced decrease to reach a short-duration trough around 52 m. RPI values then increase toward a maximum around 49 m, followed by a step-wise decrease to a RPI minimum coincident with the Laschamp Excursion (Fig. ~~4D~~6D).

The short-duration RPI trough around 52 m aligns with a very shallow inclination of +0.4° at 51.2 m (Fig. 6). The combination of inclination, low RPI and its depth (inferring an age of ca. 61,000 yr) suggests that this may be the Norwegian-Greenland Sea Excursion (Bleil and Gard, 1989; Løvlie, 1989). This probable reversal of the geomagnetic field was considered to be restricted to high latitudes accompanied by a global low in geomagnetic field intensity and has been confirmed in various northern high-latitude sites (Channell et al., 1997; Nowaczyk et al., 1994, 2003; Nowaczyk and Baumann, 1992; Nowaczyk and Frederichs, 1999; Simon et al., 2012; Xuan et al., 2012). However, low field strength and potentially excursional directions have also been interpreted as the Norwegian-Greenland Sea Excursion in Black Sea sediments (Liu et al., 2020; Nowaczyk et al., 2013) and the Western Equatorial Pacific (Lund et al., 2017). The occurrence of the Norwegian-Greenland Sea Excursion in the Orakei maar lake record would thus constitute its first observation this far south although additional samples are needed to confirm its occurrence in the Orakei record.

4.5 Beryllium

Relative changes in the ^{10}Be production rate in the atmosphere, at first order, should reflect fluctuations in the relative strength of the Earth's magnetic field, whilst on shorter time scales, it should reflect solar magnetic shielding assuming a constant galactic cosmic ray flux (e.g., Frank et al., 1997; Muscheler et al., 2005). As such, the direct-fallout meteoric ^{10}Be record can be expected to provide an inverse record to the relative paleointensity time-series ~~described in section 4.4~~(Elsasser et al., 1956; Ménabréaz et al., 2011). However, in this case, the authigenic ^{10}Be signal ~~may have~~contains contributions from non-direct-

fallout component(s) such as associated with catchment-derived erosional influx and material of aeolian origin, and thus may be modulated by associated grain size variability. Authigenic (HCl-extracted) ^{9}Be serves as the normalizing factor for ^{10}Be ~~geochemistry~~ to compensate such effects but may also indicate shifts in the sedimentary regime on its own as ^{9}Be is commonly released by weathering (Wittmann et al., 2015).~~.~~

4.5.1 Beryllium-9

^{9}Be shows nearly constant, long-term increasing values from the core base up to large step-wise increase between 50 and 45 m reaching its maximum of ~6 x 10^{17} atoms/g just below the Rotoehu tephra layer, then returning to constant (near pre-peak) values up core (Fig. ~~5A~~7A). The large peak between 47 and 45 m may reflect accelerated weathering and erosion in the catchment and/or wind-blown deposits with a different ^{9}Be inventory although the catchment is confined to the crater rim environment and enhanced weathering and erosion are not apparent at this depth in the Orakei core.

4.5.2 Beryllium-10

The ^{10}Be record (from ANSTO, black in Fig. ~~5B~~7B, D) increases up-core, peaking at the top of unit 10 (~57 m), interrupted by a prominent trough in facies unit 9 and followed by relatively constant values across facies unit 8, punctuated by discernible peaks at ~44 and ~42 m. The Lund-ETH ^{10}Be data largely follows the ANSTO ^{10}Be but deviates considerably for three of its deepest four samples (i.e., ~~a~~ below ~44 m (Fig. ~~5B~~7B, ~~5D~~7D)). The reason for this discrepancy is unclear but may be due to very heterogenic lithologies or represent a sampling/analytical artefact.

The trough in ^{10}Be in the coarser facies unit 9 (50 – 55 m depth) is interpreted to be caused by a higher proportion of coarser (sandy) grains and hence, reduced surface density of ^{10}Be/g, reflecting apparent reduction of surface area per unit of mass in coarser grains. The same behaviour of the ^{10}Be profile is observed in facies unit 11 (~64 – 69 m depth, sand and silt dominated) but the trough is not as distinct as in facies unit 9 (Fig. ~~5B~~7B). This is likely a response to the more effective separation between distinct coarse-grained sand bands, which have been removed on the ECD, and intercalated finer silt from which the Beryllium samples originate. On the other hand, in facies unit 9, the sand bands are less distinct, and the Beryllium sample material likely originates from a multi-modal grain size distribution in which particles of different grain sizes (clay, silt, sand) are mixed.

4.5.3 Beryllium-10/ Beryllium-9 ratio

In order to correct for catchment processes that modulate the ^{10}Be concentration (e.g., sediment influx variability, grain size variation and geochemical variation in Beryllium transport and deposition) the ^{10}Be/^{9}Be ratio (Bourlès et al., 1989) is plotted in Fig. ~~5C~~7C. The data incur high analytical uncertainties originating from low level ^{9}Be ICP-MS measurements near detection limits (ranging from <1 to 13 ppb, with most data <2 ppb to which we assigned 30% errors). Very low ratios in facies unit 14 are followed by elevated ratios in unit 13, which are largely maintained to ~48 m-depth (Fig. ~~5C~~7C). The uppermost studied interval is characterised by a pronounced ^{10}Be/^{9}Be trough (due to the strong ^{9}Be peak at 45.5 m) followed by an abrupt increase near coincident with facies unit boundary 8b/8a (dashed grey line in Fig. ~~5C~~7C) and associated with elevated values up to ~40 m-depth (Fig. 5C).

The conspicuous saw tooth profile in the ^{10}Be/^{9}Be ratio in facies unit 9 originates from ^{9}Be measurement uncertainties (Fig. ~~5A~~7A, C) rather than from the bimodal grain size distribution of sand and silt, which we avoided. Samples were measured for ^{10}Be and ^{9}Be in two campaigns in 2018 and 2019 with the former having larger uncertainties. Thus, we attribute the scatter mostly to measurement uncertainties rather than a true signal of the geomagnetic field strength, cosmogenic nuclide production or sediment influx. In summary, ^{10}Be/^{9}Be ratios are associated with large uncertainties preventing any correlation to paleomagnetic variations with high confidence as the ratio does not respect the homogeneous mixing of both isotopes prior to scavenging. On the other hand, ^{10}Be data, except for unit 9 where effects of larger grain size cannot be ruled out, are probably more reliable and discussed further below.

4.5.4 Paleomagnetic Excursions in the Beryllium record

Elevated~~nhanced galactic cosmic ray production of~~ ^{10}Be deposition during a paleomagnetic excursion, such as the Laschamp Excursion (McHargue et al., 1995) enables the use of peaks in the ^{10}Be concentration record to identify dated excursions and hence to include them in the age modelling process. Based on the estimated age range covered by the lower ~40 m of the Orakei sediment sequence, for which we have obtained a Beryllium isotope record, we expected to see elevated ^{10}Be (and/or ^{10}Be/^{9}Be) during the Laschamp and Blake Excursions. The magnitude of the peak above baseline would depend on the magnitude of the decrease in paleomagnetic field intensity and the impact of competing terrestrial processes which can also alter Beryllium delivery and deposition.

The Tahuna (~~37~~38,~~800~~ 400 ± ~~900~~ 1,700 (2 σ) cal yr BP) and Rotoehu (45,100 ± 3,300 (2 σ) yr BP) tephra layers serve as upper and lower age markers, respectively, for the Laschamp excursion in the Orakei sediment sequence. For a detailed, ~~high~~ high-resolution study of this interval, we use ^{10}Be data from ANSTO and Lund/ETH (Fig. ~~5D~~7D). Aside from one data point at ~44.5 m and two data points below 46 m-depth, the two curves overlap well despite the Lund/ETH samples above 46 m representing mixed sediment from 10-cm intervals (i.e., ~250 yr) and the ANSTO samples representing 1-cm sediment slices (i.e., ~25 yr) of sediment only. Three Lund/ETH samples below 46 m, which deviate the most from ANSTO data, represent mixed material from 2-cm intervals (~50 yr). Again, we have no clear explanation of this discrepancy but it likely is due to heterogenic lithologies and/or represents a sampling/analytical artefact.~~Hence, the short term field intensity fluctuations (e.g., 11 yr solar cycles; (Beer et al., 1990))ANSTO and Lund/ETH ^{10}Be data may reflect short term field intensity fluctuations (e.g., 11 yr solar cycles; (Beer et al., 1990)) resulting in the inconsistency between both datasets (Fig. 5D).~~

^{10}Be shows increasing values from ~44 to 42 m with a distinct peak at 42.5 m and return to lower ^{10}Be at 41 m-depth (Fig. ~~5D~~7D). This peak may represent the Laschamp Excursion at Orakei, as also observed at nearby Lake Pupuke (Nilsson et al., 2011), and the onset may be placed at 43.3 m-depth which aligns well with the sharp reversal in paleomagnetic inclination (Fig. ~~4A~~6A) and RPI minimum (Fig. ~~4D~~6D; see section 4.4).

The ^{10}Be increase in the lower part of the section (facies unit 13) is interrupted by smaller peaks – a pattern not observed in the previous ^{10}Be records (Simon et al., 2016). Furthermore, n~~N~~one of these peaks stand out above background level as would be expected for the Blake Excursion (116,500 ± 700 to 112,000 ± 1,900 (2 σ) ~~years~~ yr (Osete et al., 2012)). However, the "AVFaa" tephra (119,200 ± ~~5~~2,~~800~~ 600 (2 σ) ~~years~~ yr (Leonard et al., 2017)) provides a suitable time marker in proximity to where the Blake Excursion i~~wa~~s expected as an RPI low, hence a peak in ^{10}Be (Fig. ~~5~~7). Two ~~S~~small peaks in ^{10}Be ~~-~~at 73.6 m ~~-~~and ~~75~~ 74.6 m may ~~depth~~ correspond to the inferred level of the Blake Excursion (Fig. ~~5C~~7C). However, the Blake Excursion is not independently identifiable in the Orakei sediment sequence, neither in the paleomagnetic inclination or intensity (RPI) records (see section 4.4, Fig. ~~4~~6) nor in the cosmogenic ^{10}Be record. Consequently, the Blake Excursion is not used to inform the chronology development.

In the present study, the ^{10}Be data, although showing trends and variability correlated with different facies units, is limited in its ability to directly reflect geomagnetic field variations, whilst the ^{10}Be/^{9}Be data suffered from large analytical uncertainties. For example, the Laschamp reduction in geomagnetic field strength approximately doubled the globally-averaged atmospheric production rate of ^{10}Be as observed in polar ice core (e.g., Wagner et al., (2000)) and marine sediment (e.g., Simon et al., 2020) ^{10}Be records ~~(e.g., Wagner et al., (2000))~~. In this study, the inferred Laschamp ^{10}Be is no larger than x1.3 above adjacent base level ^{10}Be and the Blake Excursion barely stands out. Variations in the ^{10}Be/^{9}Be data suggest strong catchment and/or regional influences on isotopic Beryllium records that may not easily be compensated via normalisation with ^{9}Be. Therefore, the interpretation of ^{10}Be in terms of geomagnetic field changes and its utility for dating appears to be rather limited in the context of the Orakei maar sediment sequence.

4.6 Tuned Paleomagnetic RPI curve

Initial visual inspection highlighted the similarities between the Orakei RPI curve and the PISO-1500 stack (Fig. 8A, B).~~Visual inspection of the Orakei RPI and the variation of the PISO-1500 VADM (Channell et al., 2009) over the period ca. 30,000 - 140,000 years suggests strong similarities between both curves (Fig. 6A, B). This correlation facilitates an improvement of the absolute age model by tuning the Orakei RPI to the PISO chronology. Records were scaled by subtracting the mean of the RPI time-series and dividing by its standard deviation. The PISO-1500 stack has a temporal resolution of one datapoint per 1000 years. To reach a similar resolution in both time series, the PISO-1500 stack was linearly interpolated to a 200 year resolution. The interval between the Laschamp Excursion (ca. 41,100 yr) and the 'AVFaa' tephra (ca. 119,200 yr) was extracted from the Orakei RPI record and compared to the PISO-1500 stack between the equivalent ages. DTW was then performed in R (package dtw (Giorgino, 2009)) with closed start and end points on the two time-series, and using a Euclidean distance-based cost matrix and symmetric step pattern. The remainder of the Orakei RPI curve was then matched from the 'AVFaa' tephra to its base with an open end to the PISO-1500 stack up to 140,000 years (estimated maximum age of the sequence by extrapolating the sedimentation rate). We integrated 13 tuning points into a Bacon age model. We selected 10 random tuning points (TuP in Table 5) from the alignment path (solid line in middle panel of Fig. 6C, D) over the interval between the Laschamp Excursion and the 'AVFaa' tephra. Two additional tuning points (TuPex) from the alignment path over the interval from the 'AVFaa' tephra to the Orakei core base were extracted randomly and supplemented by the basal tuning point (TuPex115 in Table 5). The depth and age values of these 13 tuning points were incorporated into the Bacon age modelling process (see section 3.7 and Table 5). A standard deviation of ±1000 years is assumed for all tuning points which equals the temporal resolution of the PISO-1500 stack.~~

The fit of ~~both~~ both curves~~curves~~ following DTW alignment (Fig. 8C) is presented in Fig. ~~6E~~8D. The stretching and compressing by the DTW alignment become visible in the aligned RPI curve which shows strong agreement with the PISO-1500 stack although some minor fluctuations between ca. 80,000 and 95,000 yr appear only in the PISO-1500 stack (Fig. 8D). Neither ^{10}Be concentration nor ^{10}Be/^{9}Be curves display a comparable pattern, likely due to an unidentified catchment-influx overprint ~~(Carcaillet et al., 2004)~~. We therefore do not incorporate the Beryllium results into the tuned chronology.

4.7 Integration of multiple chronologies: The Orakei age model

All ages from radiocarbon dating, tephrochronology, the Laschamp Excursion, luminescence dating and the RPI tuning points obtained in the Orakei sediment core are presented in Fig. 9~~7~~. The age of the Blake Excursion has not been used for the chronology development, since its identification in the Orakei sequence is equivocal in both the paleomagnetic and ^{10}Be data, and the "AVFaa" tephra provides an age for the chronology development close to the position of the possible Blake Excursion.~~and the chronology for the lower part of the Orakei sequence is mainly guided by the "AVFaa" tephra.~~ The age model obtained using Bacon is shown in Fig. 8. The mean 95% confidence age range is 1,~~599~~431 years, with a minimum of ~~227~~220 years at 2.~~58~~57 m ECD and a maximum of 3,~~084~~231 years ~~between 69.65 and~~at ~~69~~59.~~68~~23 m ECD. Only ~~65~~68% of all ages overlap with the 95% range of the age-depth model.

The Orakei age-depth model defines the age of onset of lacustrine sedimentation (at 79.24 m ECD) as ~~130~~132,~~120~~305 yr (95% confidence range ~~128~~131,~~665~~430 - ~~131~~133,~~560~~180 yr). Following that, the age-depth model is predominantly guided by the RPI tuning points (Fig. ~~8~~10) despite not always passing through or near the mean. This occurs as the modelling process is designed to avoid strong or abrupt changes in the accumulation rate unless supported by a hiatus (which has not been observed). Nevertheless, a notable inflection of the age model occurs at ca. 59 m caused by nearby tuning points of different ages which represent the interval ca. 80,000 to 95,000 yr in which two RPI minima are matched by the DTW algorithm but the intermittent variations are not captured in the Orakei RPI (Fig. 8D). Whilst this inflection is not supported by any noticeable sedimentological change in the facies model, the strong match between Orakei RPI and PISO after the age modelling process (Fig. C6) gives credibility to this behaviour of the age model although it might be slightly overexaggerating the change given

the new for more robust uncertainty estimations of the tuning points. The Orakei age model agrees well with the "AVFaa" tephra age (Fig. 8<u>10</u>). Except for sample L32, the Orakei age model lies well within the error ranges of the accepted luminescence ages (L15, L14, L35, L65; Fig. 8), despite their limitations. Aside from the outliers (see section 4.2), most radiocarbon ages, all known-age rhyolitic marker tephras and the Laschamp Excursion age agree well with the Orakei age-depth model in its upper half (Fig. 8<u>10</u>). The facies units 6 and 7, as well as (parts of) 2 and 3, are however, much less well constrained. The radiocarbon dating density is less than ideal given the lack of *in-situ*, datable terrestrial macrofossils in these facies units. —Furthermore, the absence of macrofossils adds uncertainty to the freshwater reservoir/input of old carbon correction estimates and potentially introduces additional error in the bulk sediment radiocarbon ages of the bulk sediment (Fig. 10<u>8</u>). The shape of the age-depth model (steepness, inflection points, angles) represents changes in the sedimentation rate which are described in section 4.8 and shown in Fig. 9<u>11</u>.

4.8 Sedimentation rate variability

~~Our description and interpretation of the sedimentation rate follows its mean (red line in Fig. 9).~~ At the Orakei core base the sedimentation rate is ~ 0.2 cm/yr and maintaining a fairly constant rate, ex<u>c</u>p<u>e</u>~~e~~<u>p</u>t a short-term drop within the finely laminated facies unit 10 <u>caused by the inflection in the age model described in section 4.7</u> to ~45 m ~~ECD~~ in facies unit 8 (Fig. 9<u>11</u>). Stepwise accelerations in sedimentation rate follow and reach ~0.6 cm/yr around the boundary between the facies units 8 and 7. An interval with slightly decreased sedimentation rates in facies unit 4 is followed by a jump to maximum sedimentation rate of ~ 0.9 cm/yr at ~20 m ~~ECD~~ (Fig. 9<u>11</u>). High but slowly decreasing sedimentation rate towards the Orakei core top follows in facies units 3 and 2 with an abrupt drop to ~0.4 cm/yr at 8 m ~~ECD~~ (Fig. 9<u>11</u>). Another strong decrease in sedimentation rate occurs at the onset of the peat interval (facies unit 1) which records values below 0.2 cm/yr (Fig. 9<u>11</u>).

<u>The stepwise increase in sedimentation rate at ~45 m nearly coincides with the change in chronometer from RPI tuning points to tephra and ^{14}C ages. Whilst we cannot entirely disprove an influence of the chronometer change on the increase in sedimentation rate, we do note several observations that support this sedimentation rate change to be method-independent: (1) It is a stepwise change not a sudden change at the exact change point in chronometer. (2) In the interval where both chronometers overlap, albeit very short, the Rotoehu tephra and the uppermost RPI running point agree well (Fig. 10). (3) The increase in sedimentation rate does occur at the transition from facies unit 8b to 8a. These sub-facies differ in their colour contrasts between the laminations potentially indicating slightly different chemical composition, thus a slightly different depositional context which may well agree with a different sedimentation rate. (4) Further changes in sedimentation rate, even larger in magnitude than at ~45 m occur at other positions in the sediment sequence independent of strong lithological/facies changes (and independent of chronometer changes) such as at ~39 m and within facies unit 4 (Fig. 11).</u>

5 Discussion

5.1 Strengths and weaknesses of the Orakei age-depth model

A strength of the Orakei chronology lies in its multi-method approach and high dating density and resolution in the post-45,000 yr BP range using Bayesian age-depth modelling. The Orakei age model agrees with the well-constrained ages of all rhyolitic tephra markers layers found in the sequence highlighting another strength of the presented chronology. The fit between the reference PISO-1500 stack ~~VADM~~ (Channell et al., 2009) and the Orakei RPI is robust for the pre-45,000 yr BP section of the record (see Fig. ~~C7~~<u>C6</u>). Using the Earth's magnetic field strength for relative dating, the Orakei age-depth model is independent of presumptions of climate event synchroneity which is one of the central questions of studies using this tuning approach to chronology development (Blaauw, 2012). Avoiding this circularity allows reliable intra- and inter-hemispheric comparison of the Orakei sequence to independently-dated proxy records of environmental, climatic and oceanographic change, for example Greenland and Antarctic ice cores (EPICA Community Members, 2006; NGRIP Members, 2004;

Rasmussen et al., 2014), marine sediment cores (Carolin et al., 2013) and terrestrial records from Australia (Kemp et al., 2020), South America (Zolitschka et al., 2013) and central and eastern Europe (Lézine et al., 2010; Pickarski et al., 2015; Seelos et al., 2009).

Relative dating using DTW alignment and absolute age control does not require any correction for down core compaction, which is notoriously difficult to estimate and would have been necessary if the basal age was primarily derived from sedimentation rate extrapolation (Allen, 2000; Bird et al., 2004; Stanley and Hait, 2000). The integration of the DTW-derived tuning points into the Bayesian Bacon age model allows for some flexibility, since the age model does not have to pass directly through the chosen mean of the tuning point if this does not agree with other calculated ages and/or violates the assumptions of smoothness.

The weaknesses of the Orakei chronology include difficulty in assessing the sedimentological context of facies units 5 to 7, and the unknown freshwater reservoir correction for ^{14}C measurements due to an absence of datable macrofossils. This results in higher age uncertainty, complicating the validation of sedimentation rates for this interval. Luminescence dating and the ^{10}Be variation were not as robust as hoped, most likely due to the inferred detrital volcanic source of the pIR-IRSL samples and unaccounted for variability in catchment sediment processes impacting the Beryllium isotope influx.

The DTW tuning approach only works successfully if a long overlap between the reference and query time series is present and is dependent on the absence of (large) gaps in the query record. The Orakei core is characterized by continuous sedimentation since ca. 130,000 years ago. However, the Orakei RPI record shows a gap between 65.8 – 67.89 m ECD where no samples could be collected. This has potential implications for the alignment of the RPI to the PISO- stack, since it is not known how much of the RPI record is missing. The resolution (and quality) of the alignment achieved through DTW is restricted by the resolution (and quality) of the reference and original data sets. Whilst well-suited to the task thanks to continuous sedimentation, the PISO-1500 stack has a resolution of 1,000 years per measurement (Channell et al., 2009), whereas the Orakei RPI record has a theoretical ~~averages~~ average resolution one measurement per 168 years although it is likely smoothed by magnetisation acquisition in the sediments. Even though our approach of assigning errors to the ages of the tuning points considers the fit between the tuned curves, a more rigorous procedure to error estimation is desired for future applications. Furthermore, our approach relies on an approximate age at or near the core base, which is necessary to estimate the total time interval contained in the record and thus to select the corresponding section in the reference data for reliable tuning of both curves. In our study, this is achieved by the "AVFaa" tephra for most of the Orakei sediment sequence and allows a fairly well constrained basal age by extrapolation. Our random selection of a finite number of DTW tuning points may influence the resulting age model. However, additional tuning points reduce the flexibility of the Bacon age modelling process, which may result in overfitting of the age-depth model and unrealistically ~~low~~ precise confidence ranges for the final model.

5.2 Validation of the final age model

In order to assess the validity of the Orakei sediment core chronology, we expect variability in sedimentation rate to be in agreement with the observed lithological changes. The major difference in sedimentation rate between the upper ~40 m of the core, which has higher rates than the lower ~40 m of the Orakei core (Fig. ~~9~~11), supports this hypothesis, since we observe a dominance of finely- laminated sediment in much of the lower facies units 8-14, and much thicker laminations (unit 4) and fluvially in-washed sand (unit 3) in the upper part of the core. However, there is no significant link between lithology and sedimentation rate in other parts of the core as observed in the near constant sedimentation rate from the core base into the sandy facies unit 11 at ~65 m-ECD, and again in the alternating silts and sands of facies unit 9, and up to ~45 m-ECD in facies unit 8. All visible mass movement deposits have been removed from the sequence on the ECD used in this study; after removal of the sand bands (visible mass movement deposits), a constant sedimentation rate for the remaining matrix of laminated clay

and sand does not conflict with observed lithological changes. The slowest sedimentation rate of the entire sequence is observed in an interval of very fine laminations (facies unit 10; Fig. ~~9~~11), which is consistent with slow sedimentation in a quiet depositional environment dominated by in-lake production of biological particles and characterised by the absence of mass movement deposits indicative of instantaneous deposition.~~ Fine laminations generally indicate slower accumulation rates because only small amounts of sediment are slowly deposited at the lake bottom.~~ However, fine laminations observed below 70 m ECD in facies units 12 and 13 (Figs. 2, ~~9A~~11) also include multiple (mostly thin) mass movement deposits. Whilst these have been removed from the sequence, it is plausible that some thin mass movement deposits (< 1 mm thickness) could have been missed, thereby explaining the faster sedimentation rate compared to facies unit 10 (Fig. ~~9~~11).

The age model in the lower interval of the Orakei sediment sequence is additionally supported by the agreement within 2 σ between the tephra ages of Rotoehu (45,100 ± 3,300 (2 σ) yr BP; ~~(~~Danišík et al.~~,~~ (2012)) and "AVFaa" (119,200 ± 5,600 (2 σ) yr; ~~(~~Leonard et al.~~,~~ (2017)) and the solution obtained by the DTW alignment between the Orakei RPI and PISO (ca. 47,000 yr and ca. 124,500 yr, respectively; see Fig. 10) .

The laminated sediment interval above ~45 m ECD is characterised by a uniform acceleration in sedimentation consistent with the thicker laminations in this section of the core. Comparing sedimentation rate with the lithology is hampered by our poor understanding of the depositional mechanisms associated with facies units 5 to 7. A fast sedimentation rate is consistent with facies unit 6, a massive unit containing reworked basaltic tephra which may indicate near-instantaneous deposition and thicker laminations in facies unit 5. Generally, higher sedimentation rates agree well with thick laminations in facies unit 4, and fluvial sand bands in facies unit 3, as well as massive deposition in a shallow lake indicated by bioturbation in facies unit 2 (Fig. ~~9~~11). Very slow sedimentation inferred for facies unit 1 is reasonable considering that this is peat.

Overall, whilst limitations in any age-depth model are inevitable, we nevertheless find that the Orakei sedimentation rates agree reasonably well with the observed changes in sedimentary facies types and properties. Furthermore, our study improves substantially on the simple extrapolation age models previously employed in the AVF maar sequences, especially >40,000 years BP (e.g., Molloy et al., 2009).

6 Conclusions and outlook for chronology development of long sediment sequences

The importance of reliable chronologies for paleoenvironmental studies in lake sediment sequences cannot be overemphasized. For this reason, we developed a detailed chronology for the Orakei maar lake sediment sequence, the highest-resolution and most complete lake sediment record spanning the LGI from the terrestrial SW Pacific region. The chronology developed here significantly improves upon previous age models for AVF maar lakes, which until now have largely relied on sedimentation rate inter- and extrapolation, especially beyond the radiocarbon dating limit (e.g., Molloy et al., 2009; Hopkins et al., 2017). Our robust and high-resolution age model provides the essential chronological framework for event-based paleoenvironmental and -climatic reconstruction over the LGI without which such work would not be feasible.

Our study also highlighted difficulties involved in combining absolute ages with relative dating of RPI variability in Bayesian age-modelling. Estimating a realistic error for the tuning points so as to incorporate them into the Bayesian age-model is problematic, and potentially underestimates the 95% confidence range of the age model.

Several recommendations for future development of chronologies in comparable sediment sequences are proposed from this study:

(1) RPI variations are suitable for correlative dating with other records due to their independence from assumptions on climatic a-/synchroneity between regions, as long as independent age control is provided. In different depositional settings this may be successfully supplemented or replaced by Beryllium-10 variability, since both are indicators of magnetic field strength.

(2) We cannot over-emphasize the need for continuous and high-resolution sediment sequences for relative dating (tuning). Gaps in the proxy record complicate the alignment and increase age uncertainties. An improved uncertainty assessment of the DTW alignment and resulting tuning points is necessary.

(3) Sediment facies without datable, *in-situ* terrestrial macrofossils for radiocarbon dating are not well dated and suffer from the unknown estimation of the freshwater reservoir correction.

Despite the issues encountered with the development of the Orakei maar lake chronology, such an approach is necessary to enable robust records of past climate, especially at the event level, during the LGI that are well known from Northern Hemisphere equivalents such as Eifel maar lakes (Seelos et al., 2009). The ability to develop lake sedimentation chronologies independently of inferred links with climate events is of paramount importance for the reliable extraction of paleoclimate signals that can then be correlated with similar and well-dated time-series of climate change in both intra- and interhemispheric contexts. Only then can we produce the critical missing links between past climate drivers and subsequent events from the poles to the Equator from which to develop a robust understanding of the teleconnections and associated leads/lags within the Southern Hemisphere and global climate system.

The Orakei maar lake work is ongoing with further refinement of the Orakei chronology and paleoenvironmental and -climatic record expected and application of a similar approach to other select maar lake records from the AVF. It is anticipated that the Orakei maar chronology will form the master chronology against which those developed from the other AVF maar lakes will be compared. Such a comparison is particularly feasible given the widespread and excellent preservation of marker tephra layers in each maar lake sediment sequence that has already been used to develop the complete record of distal tephra to have reached the Auckland area, both from the TVZ and from the local AVF volcanic centre eruptions. The ability of the multi-method approach detailed here to produce robust ages for tephra and hence volcanic events beyond the limit of the radiocarbon method is of importance for reliable determination of past eruption frequencies and ~~associated~~ hazards associated with both the local AVF volcanic centres and those sourced from the TVZ. This is of particular relevance given the fact that Auckland City is built around 53 basaltic volcanoes, the last of which erupted only 504 ± 5 (2 σ)- cal yr BP (Needham et al., 2011).

Appendices

Appendix A: Tephra

~~**Re-calibrated radiocarbon ages for three tephra layers**~~

~~The ages for the Okareka, Maketu and Tahuna tephra layers were re-calculated using ^{14}C ages from (Molloy et al., 2009) as follows: the ages OZK291 and OZK293 (bulk sediment samples 10 mm above Maketu and Tahuna, respectively) were reservoir-corrected with the correction of 410 ± 120 years as both layers are located in facies unit 8 of the composite Orakei sediment sequence (section 4.2). The reservoir-corrected ages, as well as OZK292 and OZK294 (macrofossil charcoal samples 10 mm below Maketu and Tahuna, respectively), were calibrated with the SHCal13 calibration curve . The pairs from above and below the tephra (OZK291, OZK292 for Maketu; OZK293, OZK294 for Tahuna) were then combined in OxCal 4.3 (Bronk Ramsey, 2009) with the "C_combine" command to obtain a new age for the tephra layers.~~

~~Only ^{14}C ages from leaf fragments were accepted for the age determination of the Okareka tephra layer from the Molloy et al. (2009) ^{14}C dataset. The ^{14}C ages OZK262 and OZK263 were combined in OxCal 4.3 (Bronk Ramsey, 2009) with the "R_combine" command to obtain a combined conventional radiocarbon age for the Okareka tephra (used in section 3.2.1 for reservoir-correction determination), which was then calibrated with SHCal13 .~~

~~**ID of sample T66**~~

~~An unidentified basaltic tephra layers "T66" could not be matched stratigraphically or geochemically to any other Auckland Volcanic Field (AVF) tephra layer previously documented in Molloy et al. (2009) or Hopkins et al. (2015; 2017). Its occurrence between the layer AVF1 and the basal eruptive material sourced from the Orakei Volcanic Centre (Fig. A3) suggests that it is a new, previously undocumented tephra layer from a different AVF source. In order to test this hypothesis, electron microprobe analyses (EMPA) were conducted on sample T66 glass shards at Victoria University of Wellington following the method outlined in section 3.1. The results are presented in figures A3-A5. We confirmed that T66 is not a correlative to the Orakei Volcanic Centre and/or AVFa tephra layer (Fig. A3). Furthermore, glass shard geochemistry also obviates correlation to the AVF1 tephra layer (Fig. A4). We consider that T66 constitutes a basaltic tephra that has not so far been encountered in any AVF maar cores (Hopkins et al., 2015, 2017).~~

~~Based on the position of T66 between AVF1 (correlated to Domain/Grafton eruption) and AVFa (correlated to Orakei eruption; Hopkins et al. (2017)), several AVF volcanoes are potential sources for the T66 tephra (Hopkins et al., 2017; Leonard et al., 2017). Despite the difficulties in comparing whole rock and tephra material based on major element oxides, we compare data from sample T66 to the potential AVF source centres (Fig. A5): Grafton Park, Mt Albert, Mt Roskill, as well as the correlatives for AVF1 and AVFa, Domain and Orakei, respectively. Low FeO and SiO_2% in Mt Albert whole rock composition as well as in sample T66 suggests strongly that Mt Albert is the source of the T66 tephra layer (Fig. A5). The formative eruption of Mt Albert has been Ar-Ar dated to 119.2 ± 2.8 (1 sd) ka by (Leonard et al., 2017) which falls between the ages obtained for AVFa (126.15 ± 3.32 (2 sd), Hopkins et al., 2017) and AVF1 (106.17 ± 4.3 (2 sd) ka (Hopkins et al., 2017); 83.1 ka (Molloy et al., 2009)) giving further support for this identification. Hence, we conclude that sample T66 is sourced from Mt Albert with an eruptive age of 119. ± 2.8 ka. In order to maintain nomenclature consistency, we assign the name "AVFaa" to this tephra layer.~~

Appendix B: Luminescence dating

Methods

We undertook luminescence dating of polymineral fine-grained (4-11 µm) material from selected samples of the Orakei core, focusing on the feldspar signal. The fine-grained fraction was targeted in order to maximize the percentage component of non-volcanic, distally sourced dust, which is more likely to yield a reliable luminescence signal. Additionally, coarser grained (63-90 µm) aliquots of two selected samples (L15 and L20) were run.

The sediment cores were stored wrapped in light-proof plastic at 4˚C until opened and subsampled for luminescence dating under subdued orange light at the University of Auckland (New Zealand) taking care to only sample the innermost parts of the core for dating. Samples were taken to ensure maximal spread over the >45,000 years interval of the Orakei sequence following a preliminary age model by extrapolation of the sedimentation rate calculated between the two oldest identified and dated tephra layers (Tahuna and Rotoehu, see Table 2). Luminescence dating sample pre-treatment for polymineral fine grains (4-11 µm) was undertaken at the Max Planck Institute for Chemistry (Mainz, Germany) following published methods (Mauz and Lang, 2004), involving hydrochloric acid and hydrogen peroxide digestion, sieving and settling. Enough material remained after digestion, sieving and settling for production of 15 aliquots of the polymineral fine-grained component, except for sample L69 (A0119) which produced 10 aliquots. Each aliquot was pipetted onto 10 mm diameter stainless steel cups for equivalent dose (D_e) measurements. Additionally, K-feldspar was extracted from the coarser grained material (90-115 µm) if sample L20 (A0113) by density separation using lithium heterotungstate. Large aliquots (8 mm diameter) were prepared from this material for equivalent dose measurement.

Equivalent dose (De) was measured on the fine-grained samples using the post-infrared infrared (pIR-IRSL290) protocol, stimulated at 290°C to minimize the potential for feldspar signal fading (Buylaert et al., 2012; Thiel et al., 2011; Thiel et al., 2014), and based on equivocal results of the preheat plateau test which showed substantial inter-aliquot scatter irrespective of

measurement temperature (Figure 1). For the coarse-grained sample L20 (A0113), 12 aliquots were run using the pIR-IRSL290 protocol using an infrared (IR) preheat temperature of 50°c, and another 12 aliquots using the same protocol with an IR preheat temperature of 200°C, in order to compare luminescence characteristics in response to changing parameters. D_e measurements were undertaken using an automated Risø TL-DA-20 reader using infrared (IR) LEDs for illumination, with the resulting signal detected by an EMPI 9235QA photomultiplier tube with a D410 filter for feldspar (Bøtter-Jensen, 1997; Bøtter-Jensen et al., 1999). Irradiation was provided by a calibrated $^{90}Sr/^{90}Y$ beta source (Bøtter-Jensen et al., 2000). An internal alpha contribution of 0.12 was assumed for the samples, in order to account for the lower luminescence efficiency of alpha radiation relative to the beta and gamma components (Rees-Jones, 1995; Rees-Jones and Tite, 1997). The accepted aliquots of all samples yielded either normal distributions, which were typically very wide, or skewed distributions indicative of incomplete bleaching. In the first case, D_e values were calculated using the Central Age Model (CAM) (Galbraith et al., 1999); in the latter, D_e was calculated using the Minimum Age Model (MAM) (Olley et al., 2004) (Fig. B2). For the coarse-grained sample L20 (A0113), 2 out of 12 aliquots run with an IR50 preheat were not saturated with respect to dose, in comparison with 6 out of 12 aliquots from the IR200 preheat. Whilst this suggests better results using the higher preheat, the resulting equivalent doses were similar, as illustrated in the radial plot in Figure 3.

Samples for dose rate determination were digested with HNO_3 and HF at the Australian Nuclear Science and Technology Organisation (ANSTO, Sydney, Australia). U, Th concentrations were then obtained from these solutions on an Agilent 7700 inductively-coupled plasma mass spectrometer (ICP-MS) at the Mass Spectrometry Equipment Centre (University of Auckland, New Zealand). K concentrations were obtained from XRF measurements on fusion disks on a SPECTRO X-LAB 2000 polarizing energy dispersive X-ray fluorescence spectrometer at the University of Waikato (New Zealand). The measured activities of the radioactive elements K, Th, and U were converted to dose rates using published factors (Adamiec and Aitken, 1998; Guerin et al., 2011). Dose-rate attenuation was estimated using published values (Mejdahl, 1979) and the core sediment moisture content. Water content was estimated assuming saturation of the lacustrine sediments, taking into account water loss in the laboratory subsequent to core extraction (Lowick and Preusser, 2009). Substantial uncertainties in water content were included in order to mitigate potential inaccuracies in the dose rate calculations as a result of desiccation. Cosmic-ray dose rates were calculated based on sediment density estimates, altitude, latitude, longitude, and depth, following (Prescott and Hutton, 1994); these values were negligible (<0.01 Gy/ka) due to the depth within the lake sediments.

Results

Finer-grained samples

Results were obtained for the six samples measured in the series, and for the coarse-grained sample L20 (A0113). Samples L18, L20 and L29 (A0112-A0114 respectively) yielded insufficient natural signal for equivalent dose estimation (note that these are the youngest samples according to the depth, which explains why less charge has accumulated to date). The remarkably low sensitivity for feldspars may suggest a primary igneous origin. The remaining samples provided ages, although the luminescence characteristics were not optimal for age determination, as discussed below. Ages could only be calculated by relaxing the acceptance criteria for analysis; the results, however, broadly conform (within 2σ error) to the The polymineral fine-grained samples from the Orakei core do not exhibit optimal characteristics for the pIR-IRSL290 protocol. The samples are typically very dim, yielding generally low signal counts (Figure B4a) and low sensitivity. Late background subtraction was used to optimize the signal measured. The sensitivity to test dose over the regenerative cycles of the pIR-IRSL290 protocol typically decreased to 20-30% of the test dose sensitivity following the natural signal ~~measurement, and~~measurement and remained fairly constant over subsequent cycles (Figure B4b). Recuperation was very high, yielding values of up to 50%, and recycling ratios were variable but often exceeding 20% divergence from unity (Table B1). Dose-response curves could often, but not always, be fitted to an exponential or exponential-plus-linear function, and rarely passed through the origin due to the high degree of thermal transfer (Figure B4c). In order to obtain any results at all, aliquots were accepted if dose-response

curves could be reasonably fitted; threshold criteria for other quality control measurements such as recycling ratios, recuperation and sensitivity change were (by necessity) relaxed. expected ages based on the projected age model.

Additional quality control measurements were undertaken on sample L15 (A0111), which yielded the largest amount of dateable material and therefore the possibility to make extra aliquots for these tests. A dose recovery test on two aliquots of this sample provided a dose recovery ratio of 1.03 (Fig. B5), although it should be noted that thermal transfer remained high and the applied dose (c. 56 Gy) was substantially lower than the measured equivalent dose (c. 230 Gy) (the magnitude of applied dose can result in different dose recovery behaviours (Doerschner et al., 2016 and references therein)). There was no appreciable residual dose measured in sample L15 (A0111) (Fig. B5), therefore indicating that correction for inherited prior dose in the less easily bleached pIR signal is not necessary (Buylaert et al., 2012).

Residual dose tests were undertaken on samples L15. Residual dose in the order of 24 Gy was observed in one aliquot of sample L15 (A0111). Negligible residual signal, but also poor dose-response characteristics, were observed in the remaining two aliquots measured. Residual dose corrections of 24 Gy was made on the Orakei samples on the basis of the L15 aliquot, resulting in younger ages than first calculated. The residual-corrected age results are listed in italics in Table 4 of the main text.

Coarse-grain sample L20 (A0113)

The results for the comparative study of different IRSL preheat temperatures for the coarse-grained sample L20 (A0113) are summarized in Table B2.

By comparison with the fine-grained measurements, the coarse-grained sample exhibited better characteristics; namely, a brighter signal, overall better recycling and thermal transfer. However, sensitivity changes between regenerative doses remained substantial. While the equivalent doses were comparable between the aliquots measured with both preheats (Figure B3). Given the small number of aliquots accepted, we cannot confirm if this younger result is systematic or otherwise. Perhaps most critically, both sets of measurements yield ages that substantially overestimate the predicted age for this sample of c. 70 ka, and overestimate all ages calculated from fine grains. This result may suggest that the coarser grains were not completely bleached during transport, and therefore suggests two different sediment transport mechanisms for the fine and coarse grains. Ultimately, we cannot use the coarse-grained results for dating the Orakei core.

Appendix C: Paleomagnetism

Additional figures with paleomagnetic data.

Appendix D: Beryllium

10-Beryllium extraction from sediment samples at ANSTO:

All chemical reagents used are AR or Ultrapure grade.

1) Label and weigh empty and cleaned 50ml centrifuge tube (+lid)
2) Fill known weight (approx. 0.5g) dried, powdered and homogenized sediment into centrifuge tube and weigh
3) Slowly add 10ml 6M HCl to sediment (Adjust to 20ml 6M HCl for 1g samples).
4) Weigh together after reaction subsides.
5) Gently swirl and allow digesting for 2-3 hours.
6) Centrifuge at 3600rpm for 10 minutes and extract 2ml of supernatant into a labelled and rated 15 ml centrifuge tube and weigh.
7) Dilute sample in small centrifuge tube with MilliQ water to ca. 10 ml total volume and weigh accurately. This sample is sent for ICP-MS or ICP-AES for measurement of native ^{9}Be concentration.
8) Add 0.5 ml of Be carrier to remaining leachate in large centrifuge tube weighing carrier accurately
9) Swirl and let stand for ca. 2 hours
10) Centrifuge for 10 minutes at 3600 rpm and carefully pipette supernatant into new, labelled and cleaned 50 ml centrifuge tube.

11) Wash residue with 1 ml MilliQ water (2 ml for 1 g samples).
12) Centrifuge again and add supernatant to centrifuge tube from step 10. Repeat washing, centrifuging and pipetting.
13) Fill centrifuge tube with MilliQ water up to volume of 25 ml.

All further steps use the supernatant collected in the new centrifuge tube (see step 10). Sediment residue can be discarded after successful sample preparation.

The following preparation is identical to the steps used in the standard procedure for in situ samples (Child et al., 2000; White et al., 2019).

10-Beryllium extraction from sediment samples at Lund University/EAWAG method:

1) Add 9Be carrier to dried and homogenised sample in large beaker.
2) Add 1 ml 30% H2O2, 1 ml 37% HCl and 4 ml H2O
3) Mix and wait over night
4) Centrifuge and decant into beaker
5) Add 2 ml 37% HCl and 2 ml H2O to centrifuge tube, centrifuge and decant into same beaker. Discard precipitate
6) Add 1 ml 65% HNO3 and 1 ml 37% to beaker. Mix and wait until sample dissolved.
7) Transfer solution into small centrifuge tubes.
8) Add 2-4 ml 25% ammonia solution to reach hydroxide precipitation at pH 10. Mix and wait until precipitation.
9) Centrifuge and discard solution, keeping the precipitate. Wash sample and repeat.
10) Add 4 ml 40% NaOH (fresh!) to sample and wait >5h. Removal of Fe at pH 14.
11) Centrifuge and decant into small centrifuge tube discarding the precipitate.
12) Add 2-4 ml 37% HCl to solution to pH3. Wait 30 min at room temperature. Centrifuge and decant into small centrifuge tubes.
13) Add 2-4 ml 25% ammonia solution to precipitate 10Be at max pH 10. Wait 1-2 h, then centrifuge and wash sample twice.
14) Transfer precipitate to quartz crucible and dry.
15) Oxidize to BeO in muffle furnace (110°C, 600°C).
16) Press with Nb into AMS cathode.

Data availability

~~All datasets will be made available on Pangaea.de after publication. The doi will be provided as soon as it is available.~~The datasets are available on Pangaea.de under https://doi.org/10.1594/PANGAEA.920773 (Beryllium data), https://doi.org/10.1594/PANGAEA.921121 (Rhyolitic tephra), https://doi.org/10.1594/PANGAEA.921122 (Basaltic tephra), and https://doi.org/10.1594/PANGAEA.921134 (Paleomagnetic data). The resulting Orakei sediment sequence age-depth relationship with uncertainty is included as a supplementary material.

Author contributions

Leonie Peti: Formal Analysis, Funding acquisition (AINSE), Investigation, Visualization, Writing – original draft; **Kathryn Fitzsimmons:** Investigation, Supervision, Validation, Writing – review & editing; **Jenni Hopkins:** Investigation, Writing – review & editing; **Andreas Nilsson:** Methodology, Supervision, Writing – review & editing; **Toshiyuki Fujioka:** Supervision, Validation, Writing – review & editing; **David Fink:** Supervision, Writing – review & editing; **Charles Mifsud:** Methodology, Writing – review & editing; **Marcus Christl:** Investigation, Methodology, Writing – review & editing; **Raimund Muscheler:** Supervision, Validation, Writing – review & editing; **Paul Augustinus:** Conceptualization, Funding acquisition (Marsden), Supervision, Writing – review & editing

Competing interests

The authors declare no competing interests.

Acknowledgements and funding

LP thanks Hannah Marley for tephra, luminescence, radiocarbon and paleomagnetic sampling support, Phil Shane for discussing tephras and Craig Woodward for a discussion about age models.

The Orakei Basin drilling campaign in 2016 was co-funded by DEVORA (funded by the New Zealand Earthquake Commission and the Auckland Council and led by Jan Lindsay, University of Auckland, and Graham Leonard, GNS Science), and a grant from the Royal Society of New Zealand Marsden Fund (UOA1415 to Paul C. Augustinus). The paleomagnetic work at Lund University was funded by the same Marsden Fund UOA1415. We acknowledge the financial support for the Centre for Accelerator Science, at ANSTO, through the Australian National Collaborative Research Infrastructure Strategy (NCRIS). LP would like to thank AINSE Limited for providing financial assistance (Award – PGRA 12196) to enable work at the ANSTO Centre for Accelerator Science (radiocarbon dating and 10-Beryllium). This work was partially supported by the Swedish Research Council (grant DNR2013-8421 to RM).

We thank three anonymous reviewers, Quentin Simon for helpful reviews and Richard Staff for editorial handling and helpful comments which have all improved the quality of the age model and this manuscript.

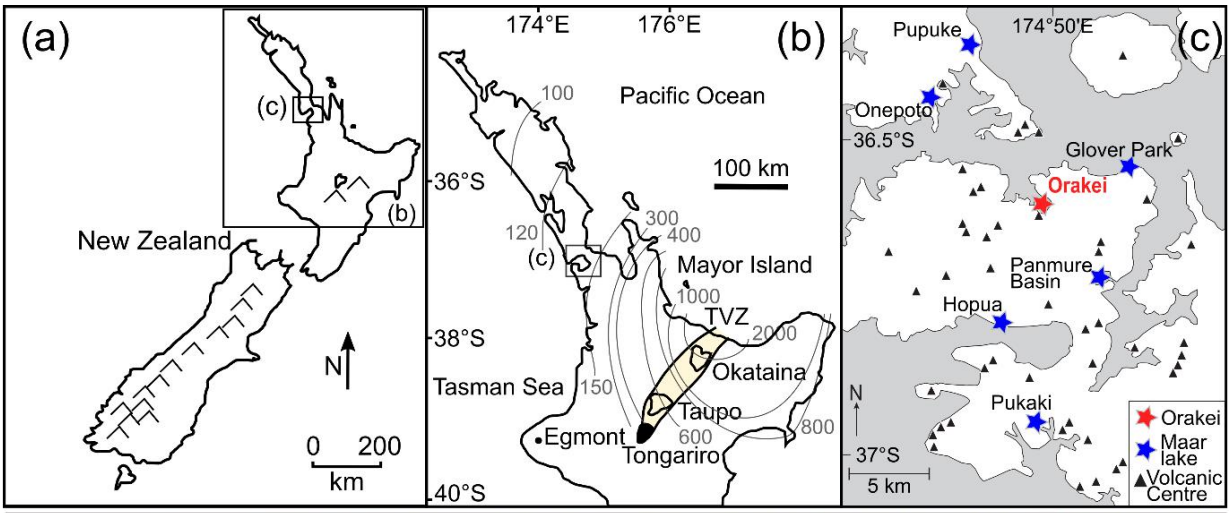

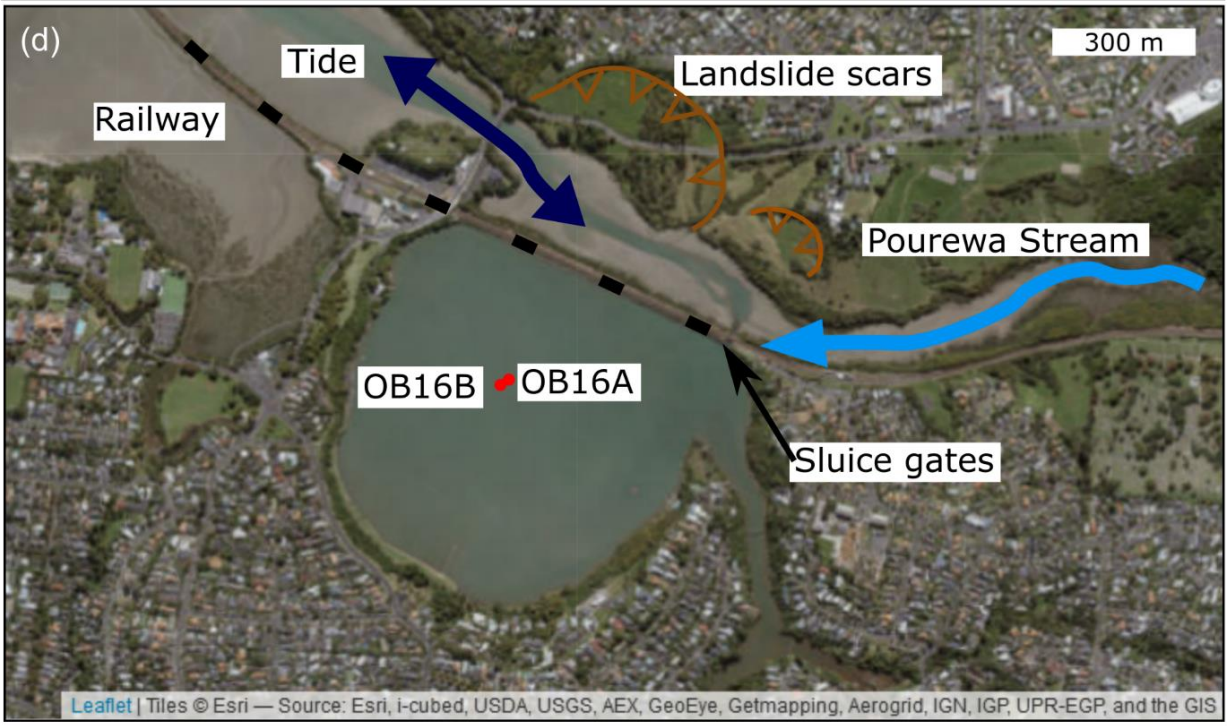

Figure 1: Map of the Orakei maar study area. (a) New Zealand with insets (b) and (c) marked. (b) New Zealand's North Island with Auckland (inset c) and the major volcanic source centres marked, the extent of the TVZ is shaded in yellow. Thin grey lines and numbers are isopachs (in mm) of the widespread Rotoehu tephra (modified from Lowe (2011)) highlighting the importance of the TVZ tephras as age markers in sediment records from New Zealand's North Island. (c) Auckland Volcanic Field showing the position of Orakei Basin. (d) Satellite image (ESRI world imagery) show the coring locations with red dots and other important features of the surroundings of the maar. Modified after Hopkins et al. (2017) and Peti and Augustinus (2019).

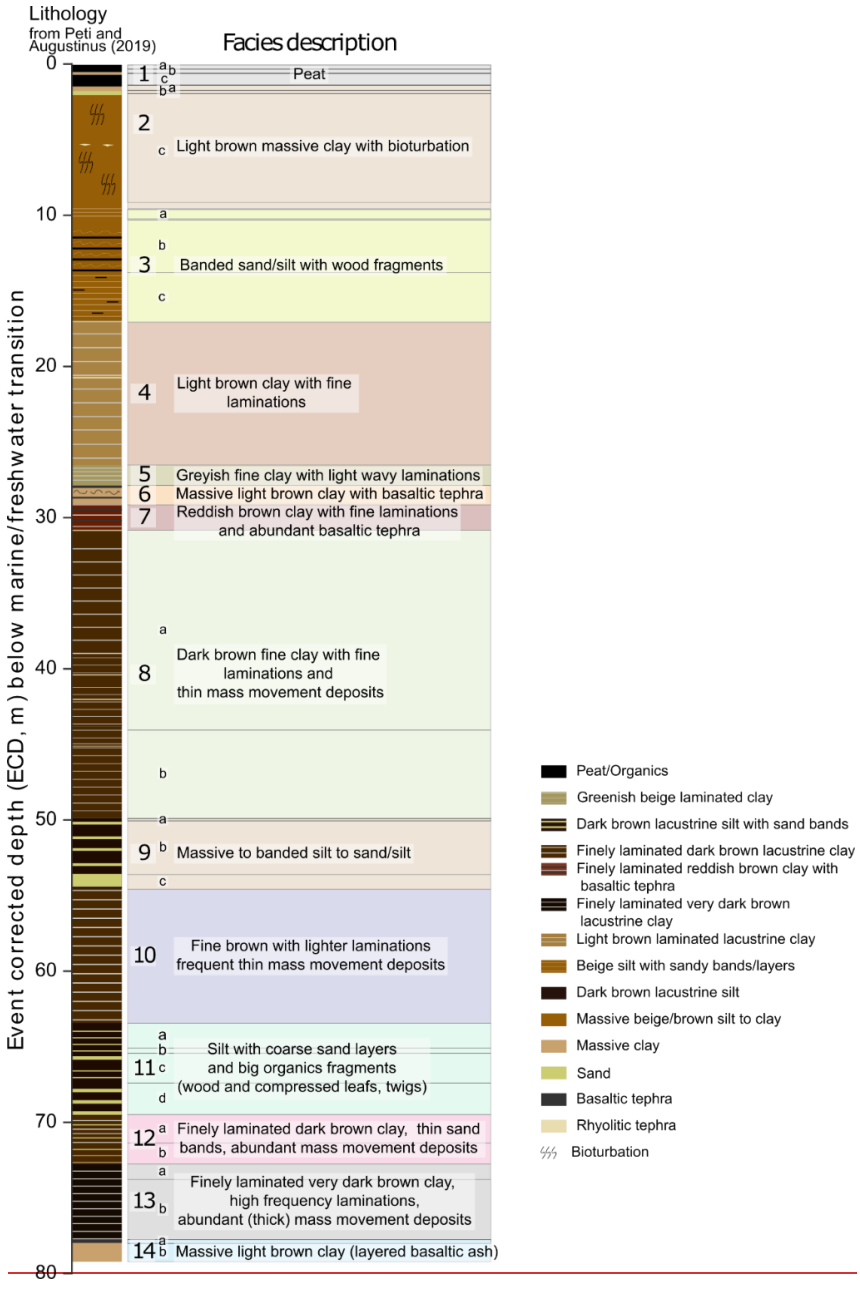
Lithology
from Peti and Augustinus (2019)
Facies description
Event corrected depth (ECD, m) below marine/freshwater transition
0
10
20
30
40
50
60
70
80
1 a b c b a Peat
2 c Light brown massive clay with bioturbation
a
3 b Banded sand/silt with wood fragments
c
4 Light brown clay with fine laminations
5 Greyish fine clay with light wavy laminations
6 Massive light brown clay with basaltic tephra
7 Reddish brown clay with fine laminations and abundant basaltic tephra
a
8 Dark brown fine clay with fine laminations and thin mass movement deposits
b
a
9 b Massive to banded silt to sand/silt
c
10 Fine brown with lighter laminations frequent thin mass movement deposits
a b
11 c Silt with coarse sand layers and big organics fragments (wood and compressed leafs, twigs)
d
12 a b Finely laminated dark brown clay, thin sand bands, abundant mass movement deposits
a
13 b Finely laminated very dark brown clay, high frequency laminations, abundant (thick) mass movement deposits
a b
14 Massive light brown clay (layered basaltic ash)
Peat/Organics
Greenish beige laminated clay
Dark brown lacustrine silt with sand bands
Finely laminated dark brown lacustrine clay
Finely laminated reddish brown clay with basaltic tephra
Finely laminated very dark brown lacustrine clay
Light brown laminated lacustrine clay
Beige silt with sandy bands/layers
Dark brown lacustrine silt
Massive beige/brown silt to clay
Massive clay
Sand
Basaltic tephra
Rhyolitic tephra
Bioturbation

1005

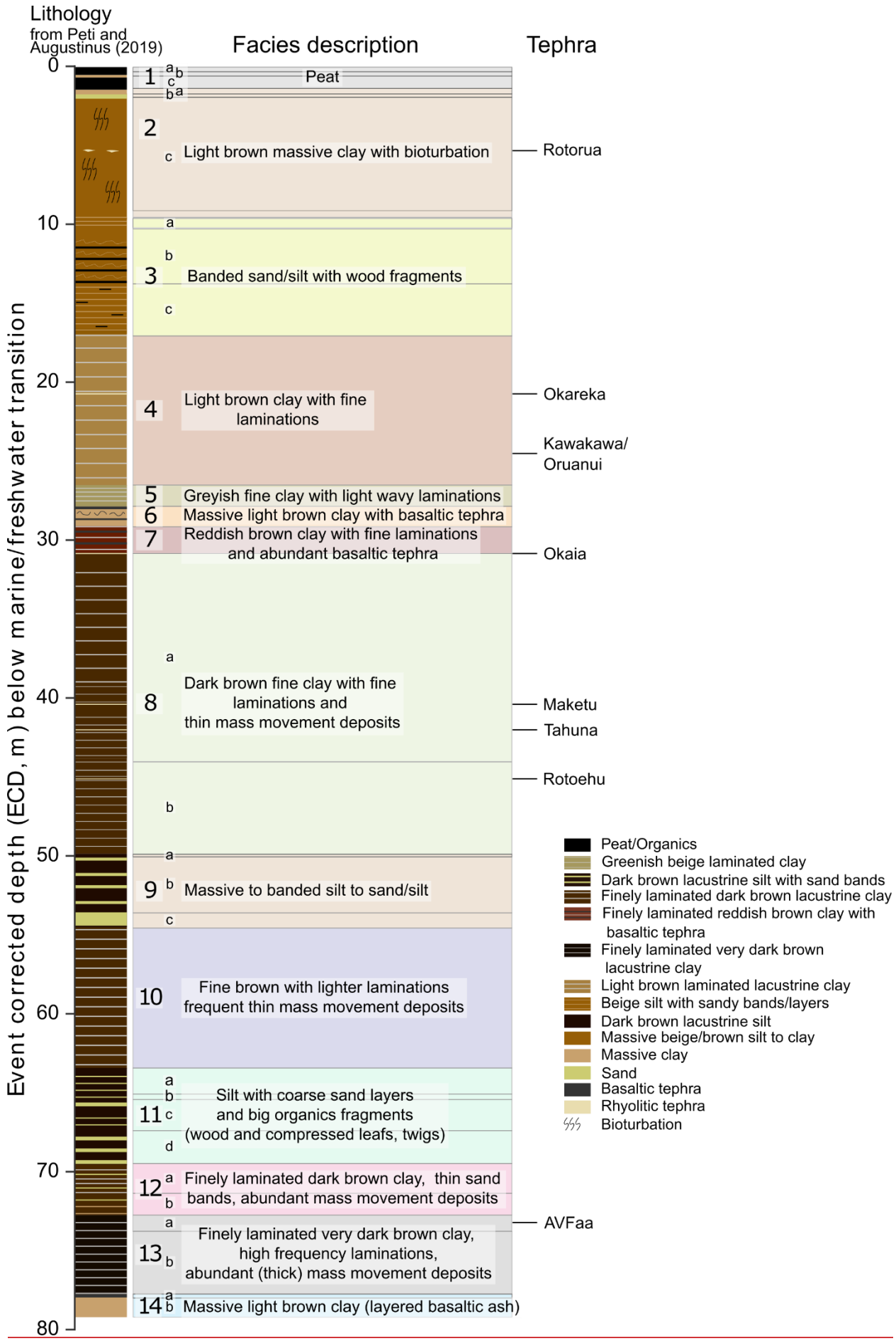

Figure 2: Simplified lithology and summarised facies unit description of the Orakei sediment sequence. After Peti and Augustinus (2019).

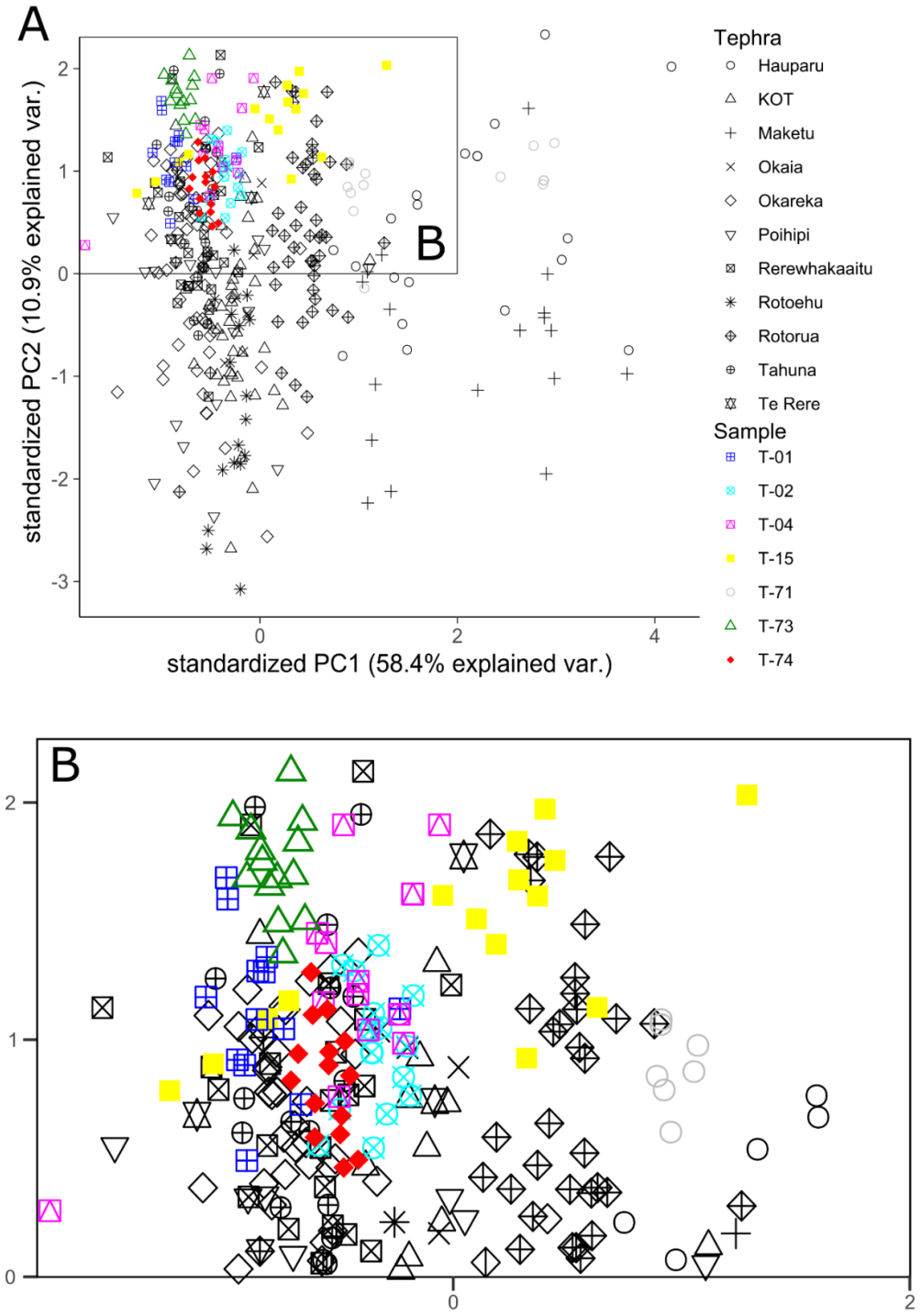

Figure 3: A: PCA individuals of reference tephra EMPA data (in black symbols from (Lowe et al., 2013; Molloy et al., 2009)) and Orakei samples (in coloured symbols). B: Enlarged inset from A. Symbols and references as in A.

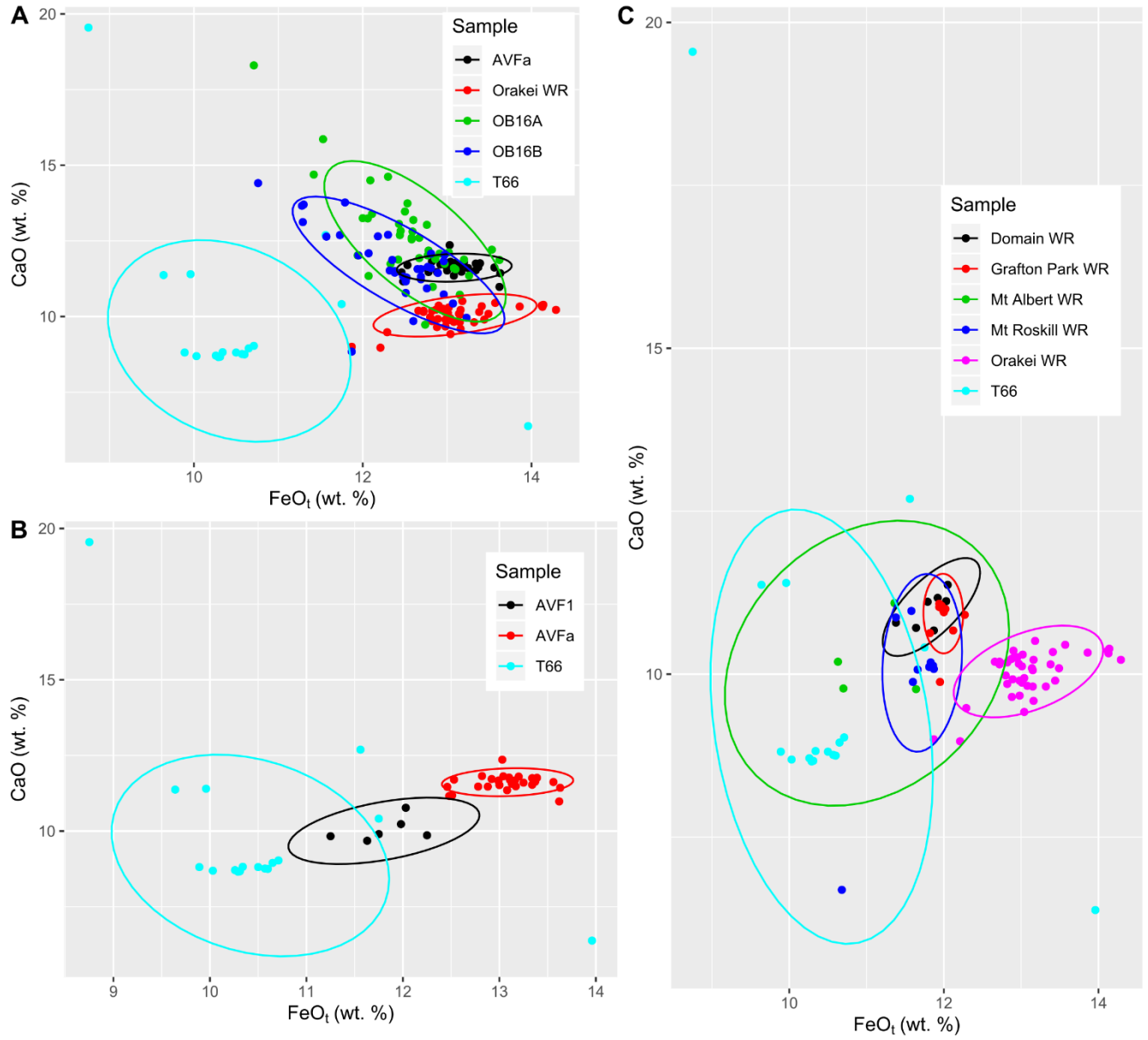

Figure 4: FeOt vs. CaO of sample T66 in comparison to tephra and whole-rock (WR) data from the Orakei eruption (A), in comparison with tephra data of the AVF1 and AVFa layers (B), and in comparison with WR data from potential AVF source centres for layer T66 (C) pointing to Mt Albert as the source for this tephra sample. Detailed figures with further major element oxides and extended explanations can be found in Figures A4 to A6.

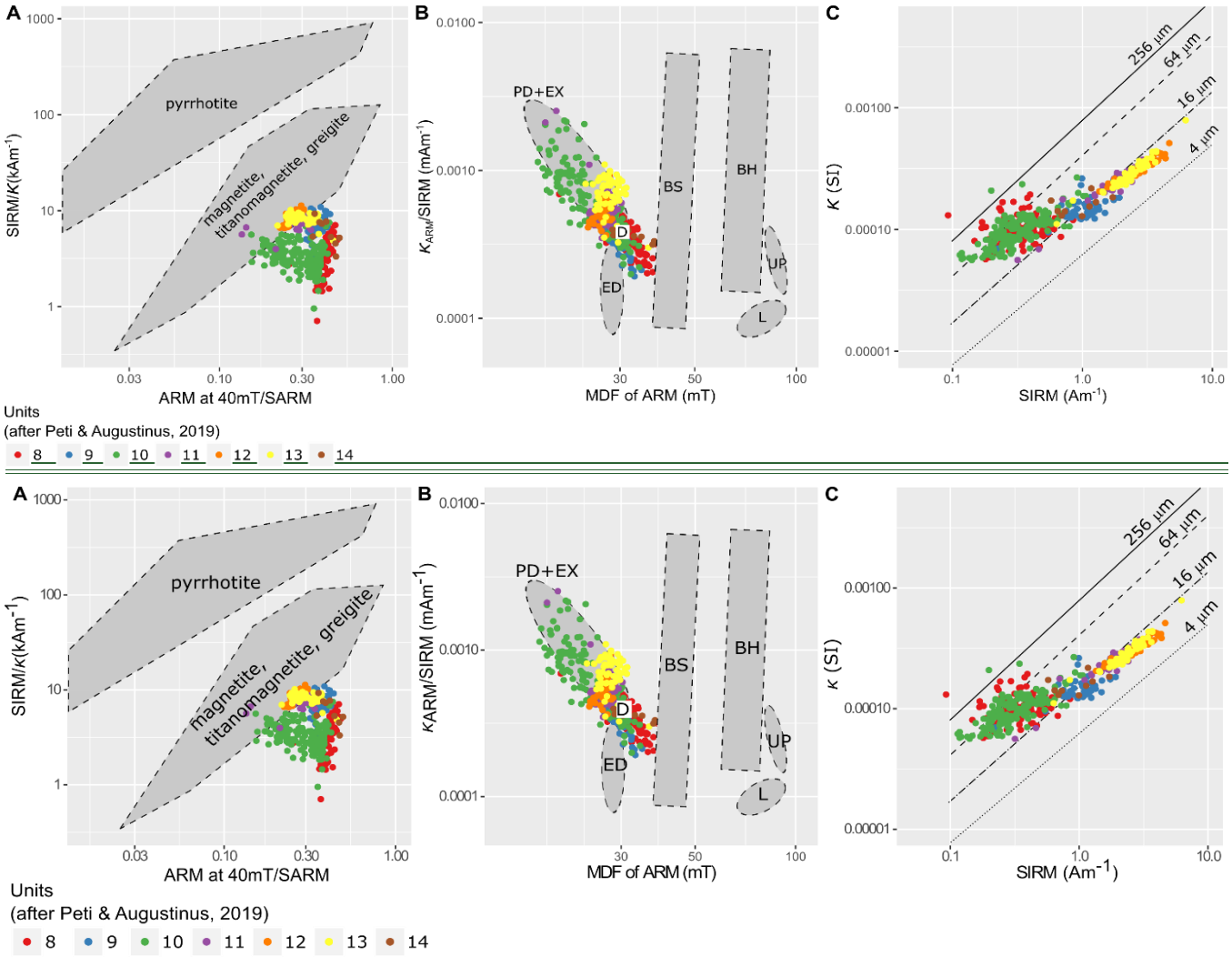

Figure ~~C~~5: Rockmagnetic characterisation of the Orakei sediment samples. (A) Qualitative identification of magnetic minerals following Peters and Thompson (1998). SARM: Saturated ARM at 0 mT. We note that the ARM at 40mT/SARM ratios are likely higher than the equivalent measurements of Peters and Thompson (1998) due to the lower maximum AF (80mT) used to induce the ARM. ~~The magnetic carrier in the Orakei sediment sequence is interpreted as dominantly magnetite/titanomagnetite.~~ (B) Magnetic components of Orakei samples in comparison to components defined by Egli (2004). MDF: Mean destructive field. κ_{ARM}: Susceptibility of ARM (SARM divided by applied bias field). BH: Biogenic hard, high-coercivity magnetosomes, BS: Biogenic soft, low-coercivity magnetosomes, D: detrital particles transported in water systems, ED: eolian dust/wind-blown particles, EX: ultrafine extracellular magnetite, L: maghemite component in loess, PD: pedogenic magnetite, UP: atmospheric particulate matter produced by urban pollution. ~~Orakei samples are classified as detrital and extracellular components.~~ (C) Estimated magnetic grain size indicator following Thompson and Oldfield (1986, p.31). SIRM: Saturated IRM at 0mT. ~~Most of the samples plot in the range of pseudo-single domain magnetite (0.1-20 µm). The increased scatter in the lower left half of the plot, suggesting increasing magnetic grain size, may partly reflect the importance of superparamagnetic (e.g. facies 10) and/or paramagnetic effects in samples with low magnetite concentration.~~

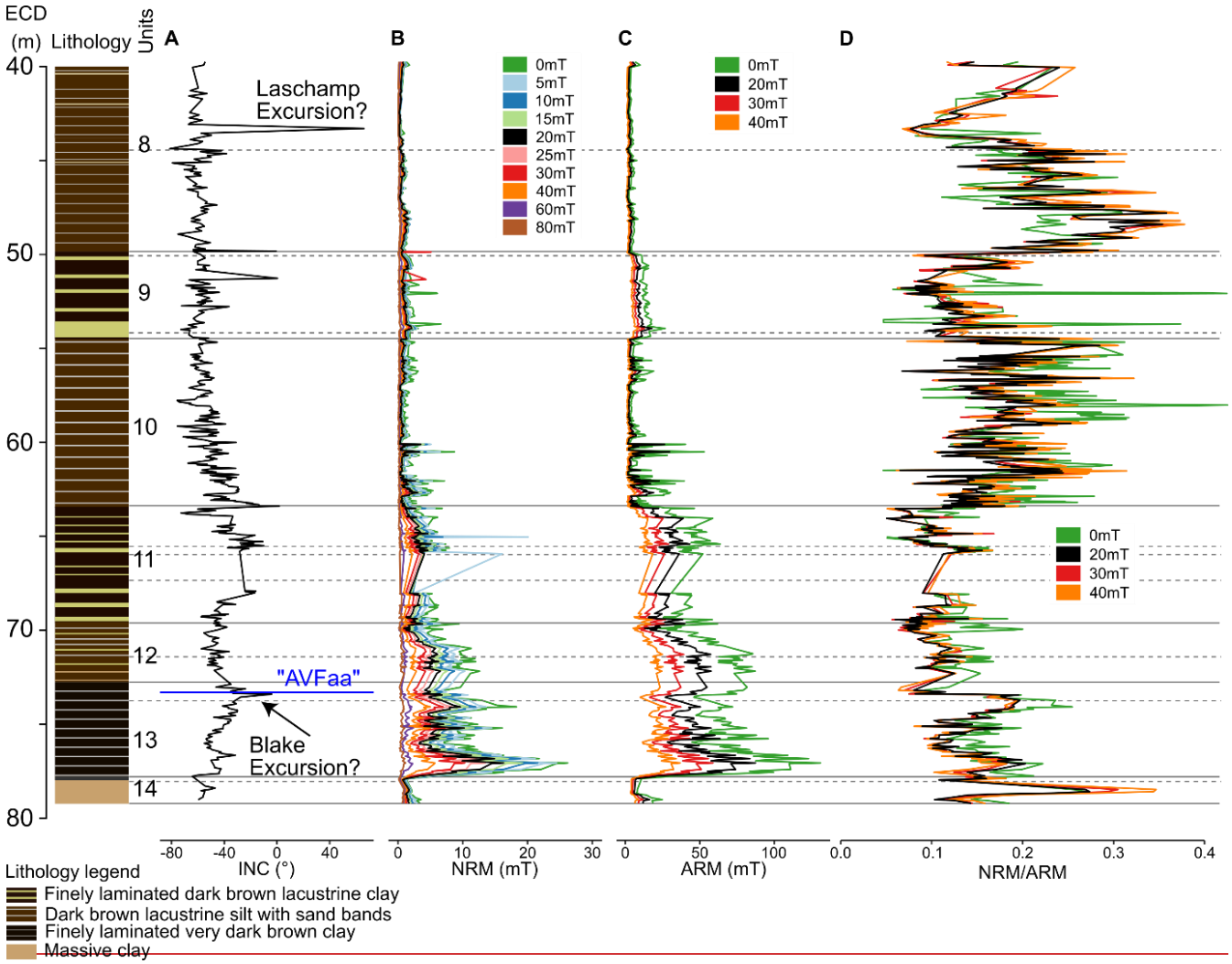
ECD
(m)
Lithology
Units
A
B
C
D
Laschamp
Excursion?
"AVFaa"
Blake
Excursion?
0mT
5mT
10mT
15mT
20mT
25mT
30mT
40mT
60mT
80mT
INC (°)
NRM (mT)
ARM (mT)
NRM/ARM
Lithology legend
Finely laminated dark brown lacustrine clay
Dark brown lacustrine silt with sand bands
Finely laminated very dark brown clay
Massive clay

1035

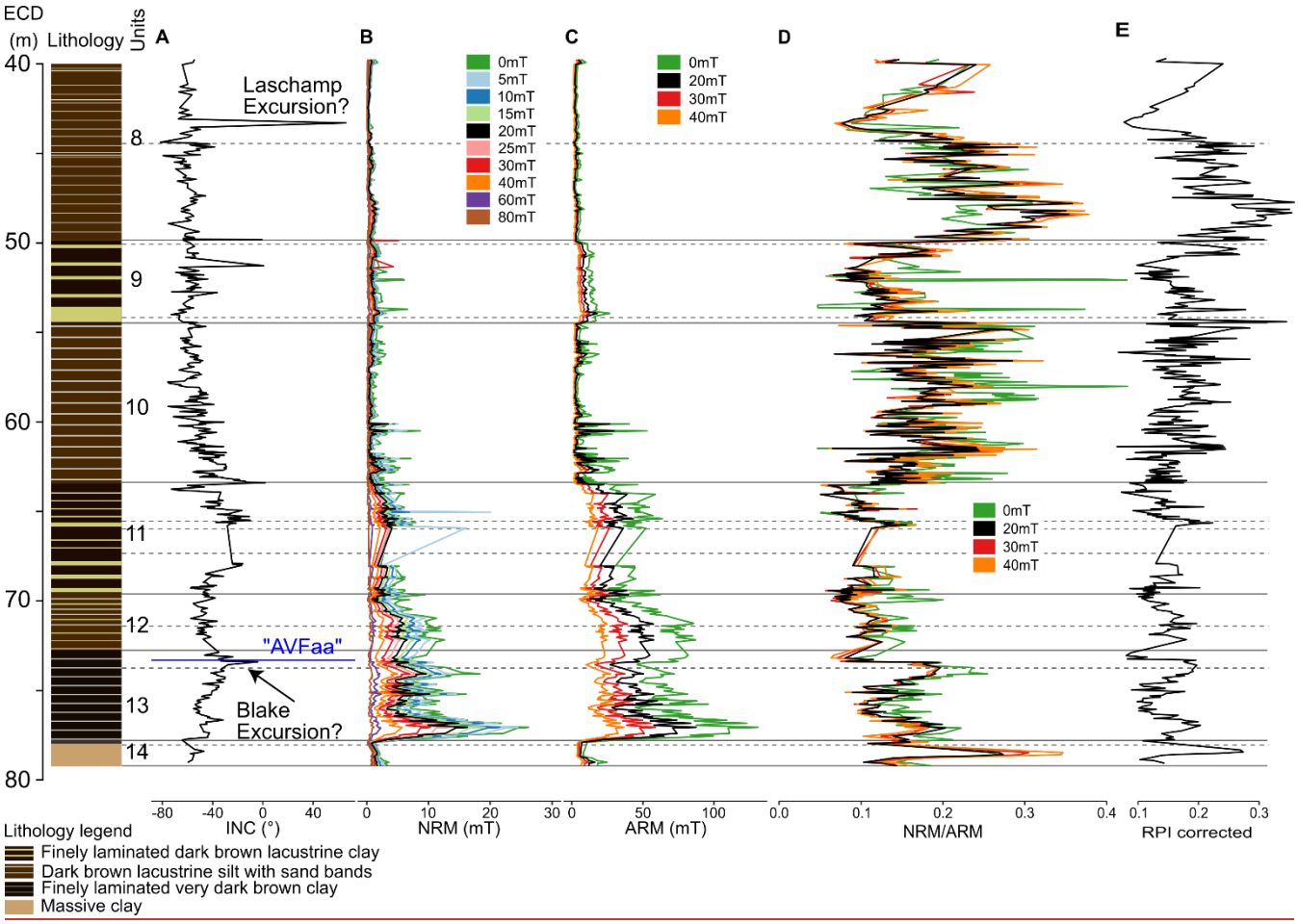

Figure 46: (A) Inclination, (B) NRM at different demagnetisation steps, (C) ARM at different demagnetisation steps, ~~and~~ (D) NRM/ARM at different demagnetisation steps, and (E) facies-corrected relative paleointensity (RPI) derived from NRM/ARM at 20mT of the Orakei sediment sequence. Horizontal gray lines mark facies unit boundaries (solid) and sub-unit boundaries (dashed) from Peti and Augustinus (2019).

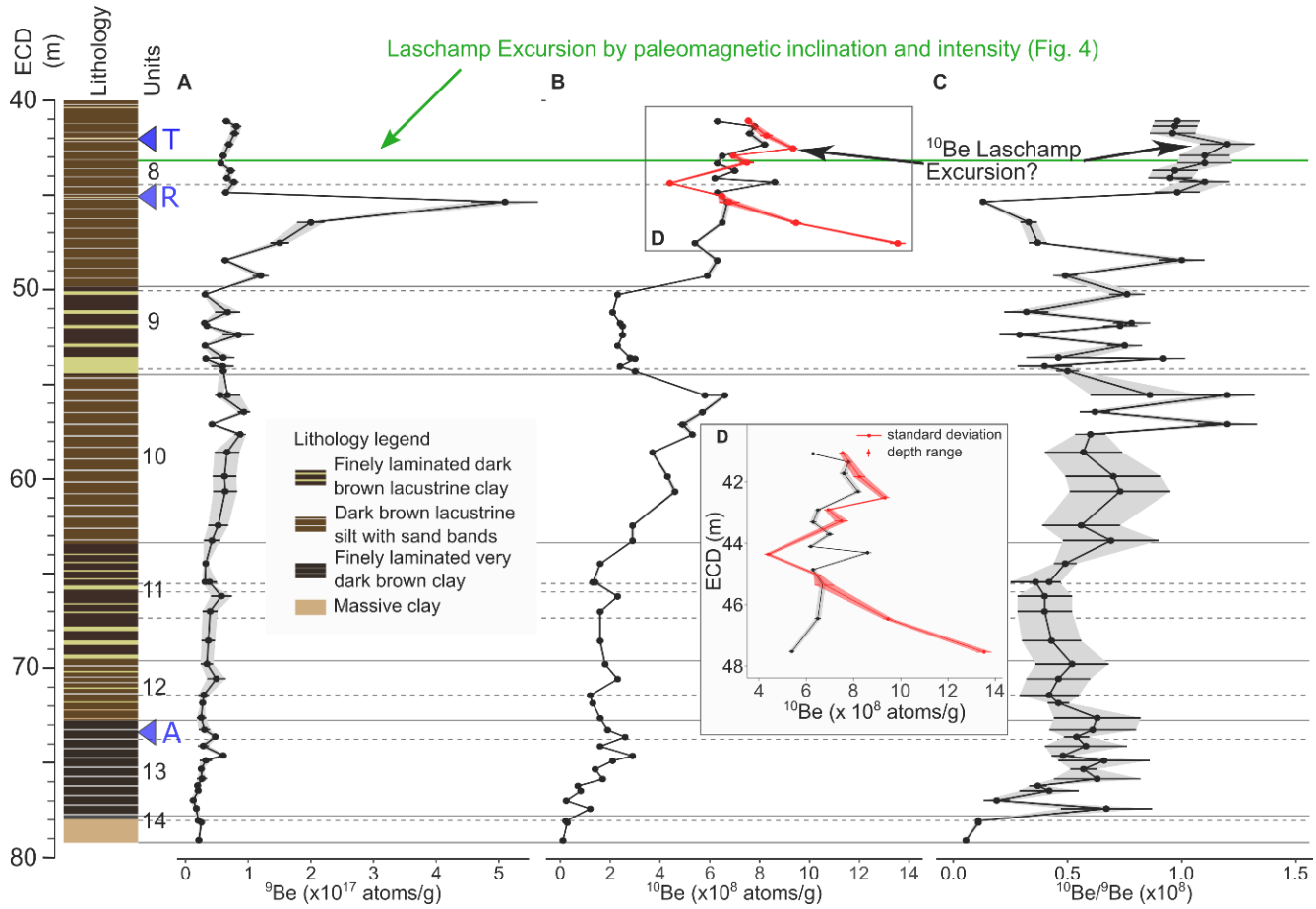

Figure ~~5~~7: Beryllium variation in the lower ~40 m of the Orakei sediment sequence alongside the simplified lithology and facies units boundaries (solid grey lines) and sub-unit boundaries (dashed grey lines) from Peti and Augustinus (2019). Green line marks the position of the Laschamp Excursion according to the paleomagnetic inclination and intensity (see Fig. 4 and section 4.4). Blue triangles mark positions of the tephra marker layers T: Tahuna (~~37~~38,~~485~~ 40 ± ~~932~~ 1,700 (2 σ) cal yr BP), R: Rotoehu (45,100 ± 3,300 (2 σ) yr BP), A: "AVFaa" from Mt. Albert (119,200 ± ~~25~~5,~~800~~ 600 (2 σ) yr). A: ^{9}Be concentration ± 1 standard error; B: ^{10}Be concentration ± 1 standard error from Lund (red) and ANSTO (black), enlarged interval in D; C: ^{10}Be/^{9}Be ratio ± 1 standard error. Grey/red shading to highlight the uncertainty interval. Where error bars are not visible, they are within the size of the datapoints.

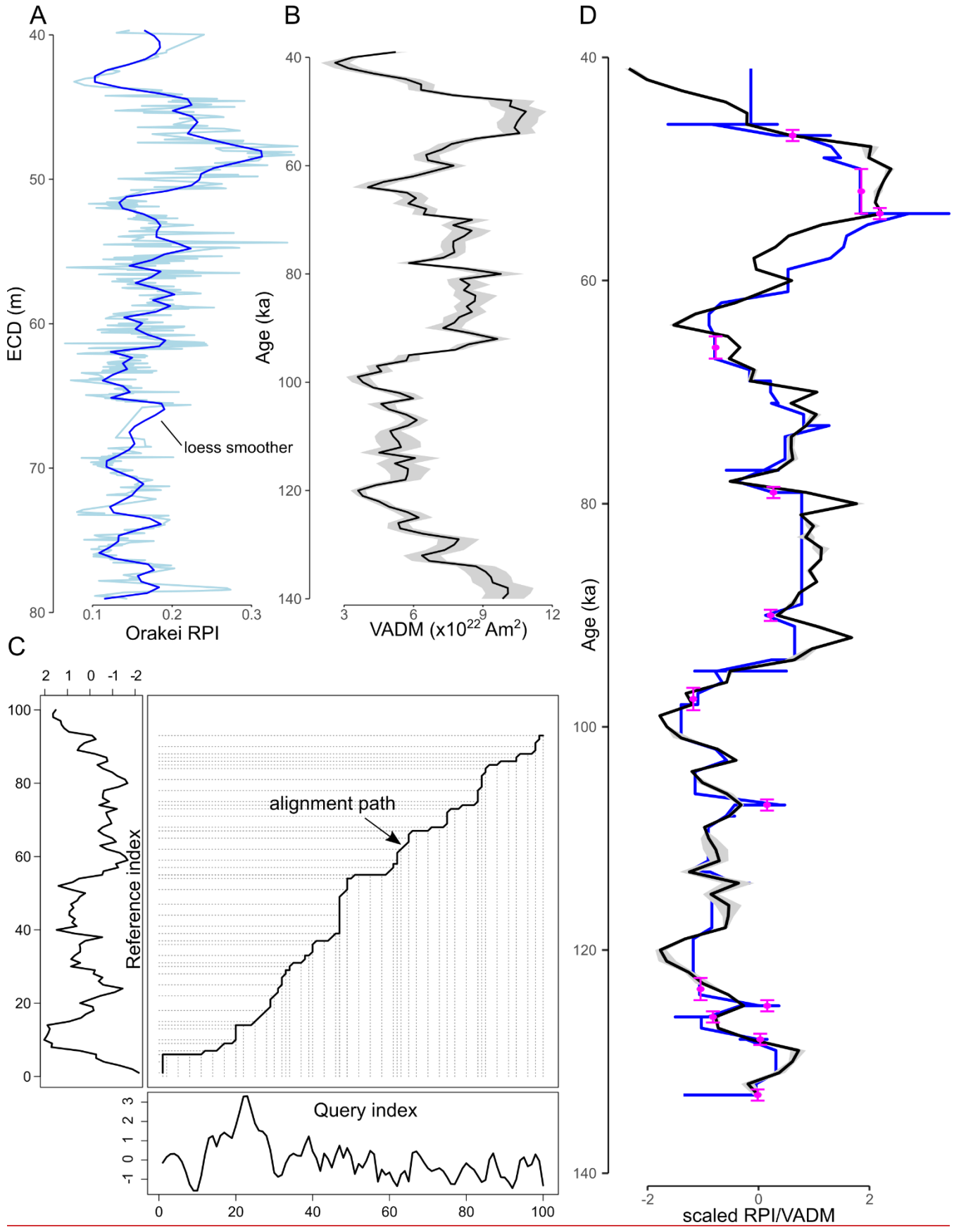
A
B
C
D
ECD (m)
Orakei RPI
loess smoother
Age (ka)
VADM (x10^22 Am^2)
Reference index
alignment path
Query index
Age (ka)
scaled RPI/VADM

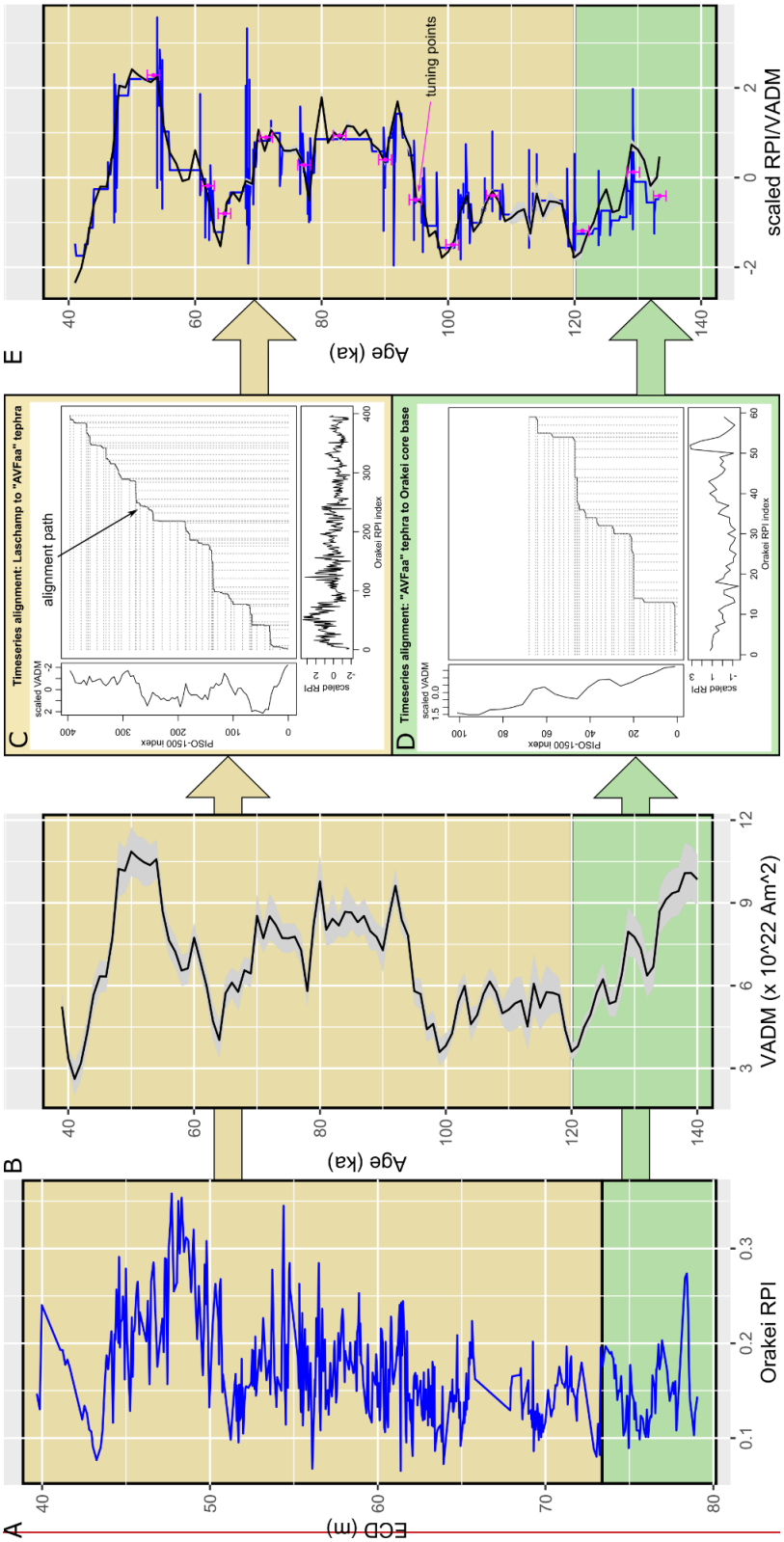

Figure ~~**6 [Landscape]**~~ **8: A: Orakei RPI (NRM/ARM at 20mT, ligthblue) with loess smoother (darkblue), B: PISO-1500 (Channell et al., 2009) ± standard error, C: DTW alignment path (solid black line)** ~~**for the upper core section (Laschamp Excursion to "AVFaa" tephra, orange background in A, B)**~~ **with scaled Orakei RPI as the query curve below and scaled PISO-1500 VADM as the reference curve to the left. Dotted grey lines highlight aligned points between both curves,** ~~**. D: Same as C for the lower core section ("AVFaa" tephra to the Orakei core base, green background in A, B). ED**~~**: Both curves scaled after DTW alignment on the same age scale with selected random tuning points ± age uncertainty of 2 σ.**

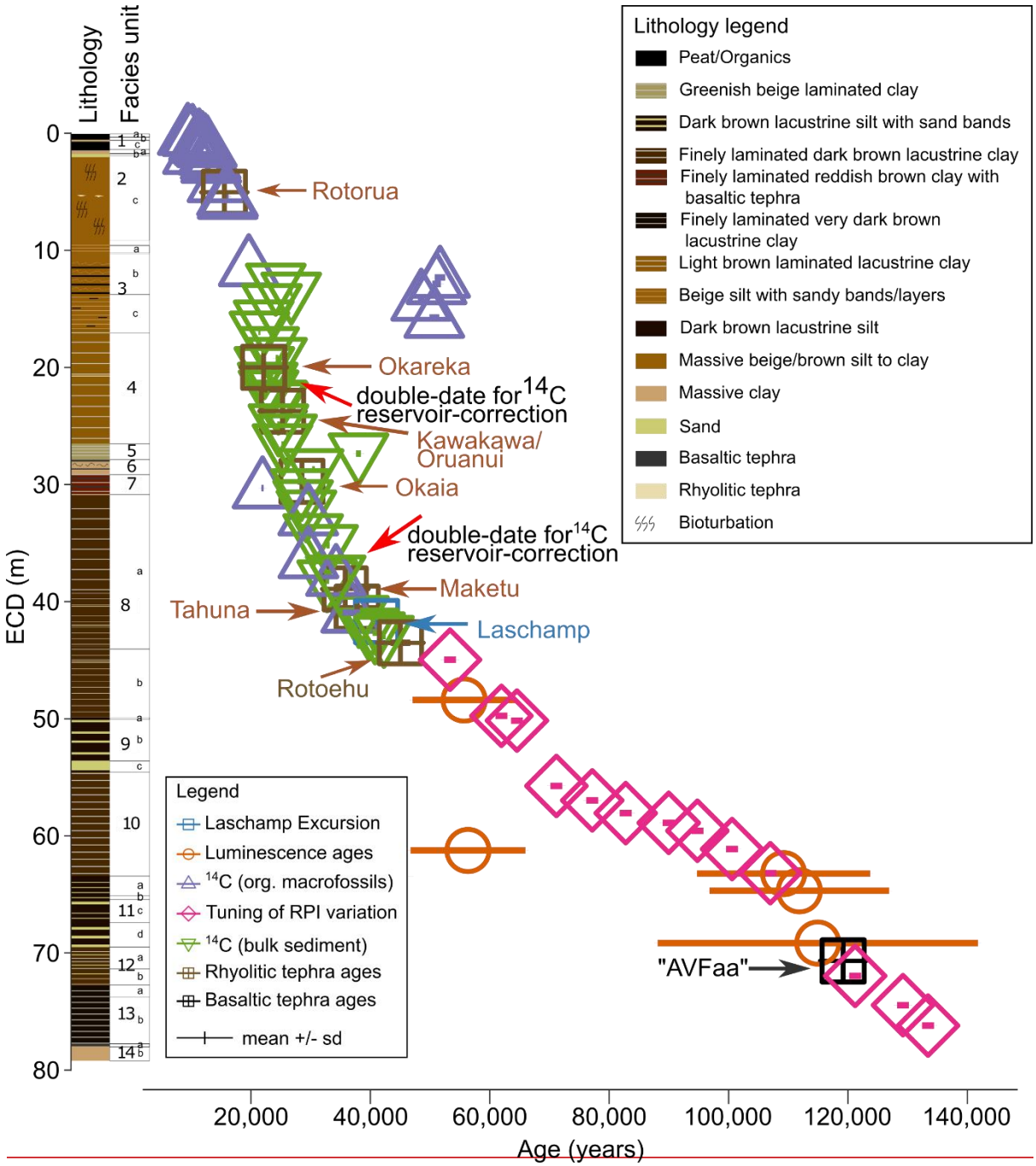
Lithology
Facies unit
ECD (m)
0
10
20
30
40
50
60
70
80
20,000
40,000
60,000
80,000
100,000
120,000
140,000
Age (years)
Lithology legend
Peat/Organics
Greenish beige laminated clay
Dark brown lacustrine silt with sand bands
Finely laminated dark brown lacustrine clay
Finely laminated reddish brown clay with basaltic tephra
Finely laminated very dark brown lacustrine clay
Light brown laminated lacustrine clay
Beige silt with sandy bands/layers
Dark brown lacustrine silt
Massive beige/brown silt to clay
Massive clay
Sand
Basaltic tephra
Rhyolitic tephra
Bioturbation
Legend
Laschamp Excursion
Luminescence ages
14C (org. macrofossils)
Tuning of RPI variation
14C (bulk sediment)
Rhyolitic tephra ages
Basaltic tephra ages
mean +/- sd
Rotorua
Okareka
double-date for 14C reservoir-correction
Kawakawa/ Oruanui
Okaia
double-date for 14C reservoir-correction
Maketu
Tahuna
Laschamp
Rotoehu
"AVFaa"

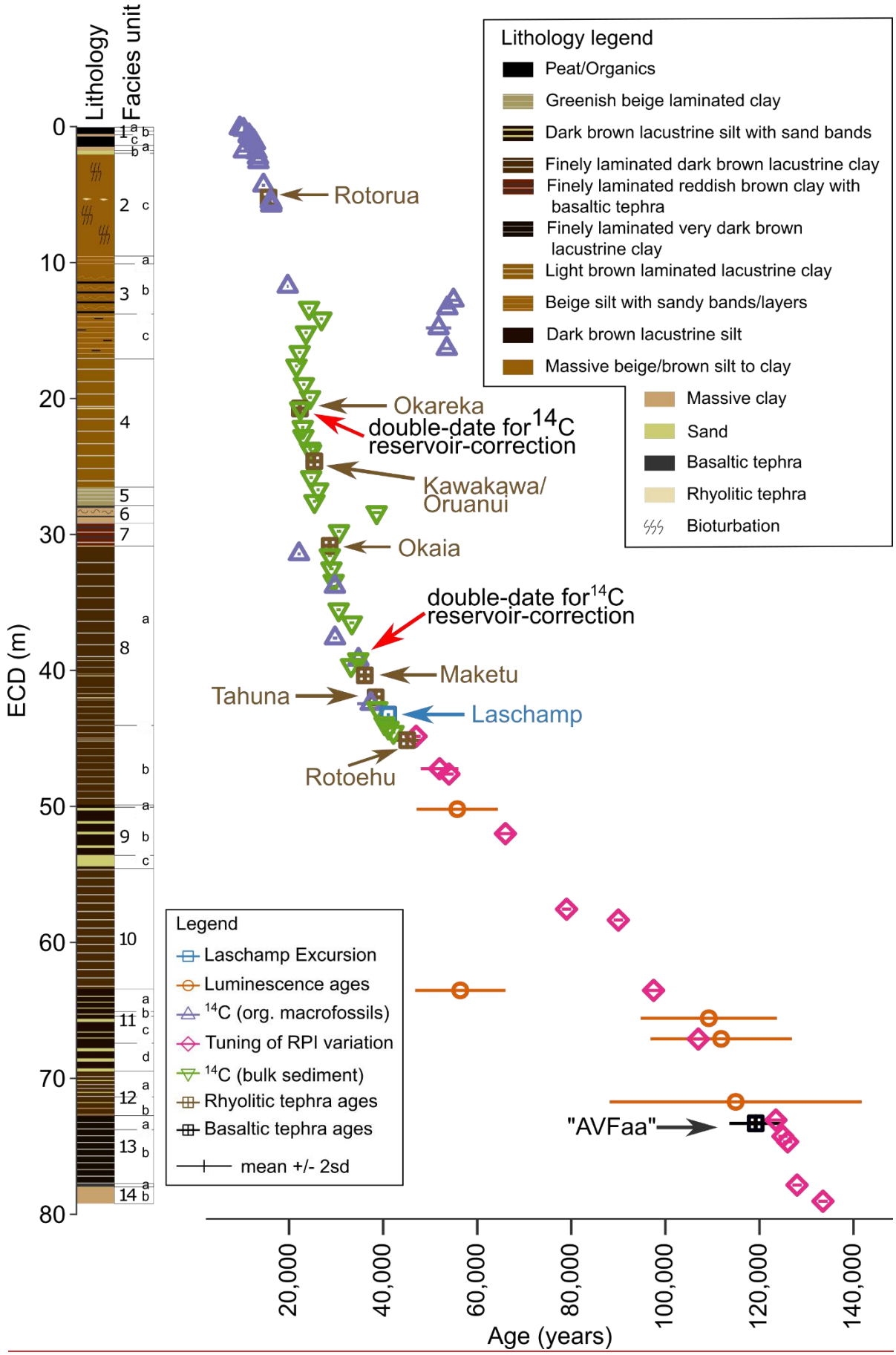

Figure ~~79~~: Simplified lithology and summarised facies units of the Orakei sediment sequence (from Peti and Augustinus (2019)) with ages (±2 σ) used in the current chronology study (identified tephras marked with names – for published and adjusted (this study) ages see Table 2). Red arrows mark double dates undertaken for ^{14}C reservoir-correction (see section 3.2). Note that radiocarbon dates have been calibrated and reservoir-corrected where applicable as noted in Table 1.

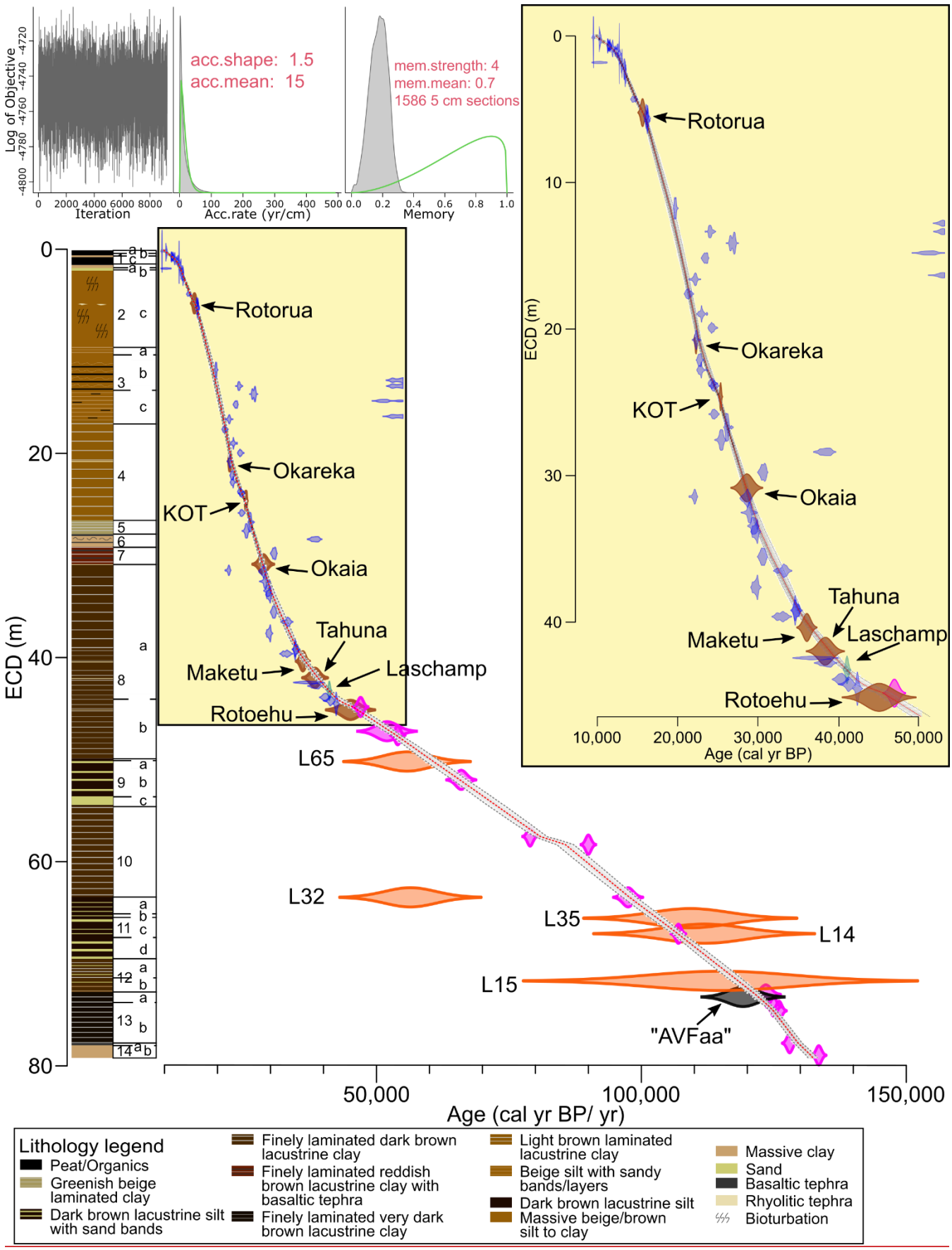
Log of Objective
-4720
-4740
-4760
-4780
-4800
0 2000 4000 6000 8000
Iteration
acc.shape: 1.5
acc.mean: 15
0 100 200 300 400 500
Acc.rate (yr/cm)
mem.strength: 4
mem.mean: 0.7
1586 5 cm sections
0.0 0.2 0.4 0.6 0.8 1.0
Memory
ECD (m)
0
20
40
60
80
Rotorua
Okareka
KOT
Okaia
Tahuna
Maketu
Laschamp
Rotoehu
L65
L32
L35
L14
L15
"AVFaa"
50,000
100,000
150,000
Age (cal yr BP/ yr)
10,000
20,000
30,000
40,000
50,000
Age (cal yr BP)
Lithology legend
Peat/Organics
Greenish beige laminated clay
Dark brown lacustrine silt with sand bands
Finely laminated dark brown lacustrine clay
Finely laminated reddish brown lacustrine clay with basaltic tephra
Finely laminated very dark brown lacustrine clay
Light brown laminated lacustrine clay
Beige silt with sandy bands/layers
Dark brown lacustrine silt
Massive beige/brown silt to clay
Massive clay
Sand
Basaltic tephra
Rhyolitic tephra
Bioturbation

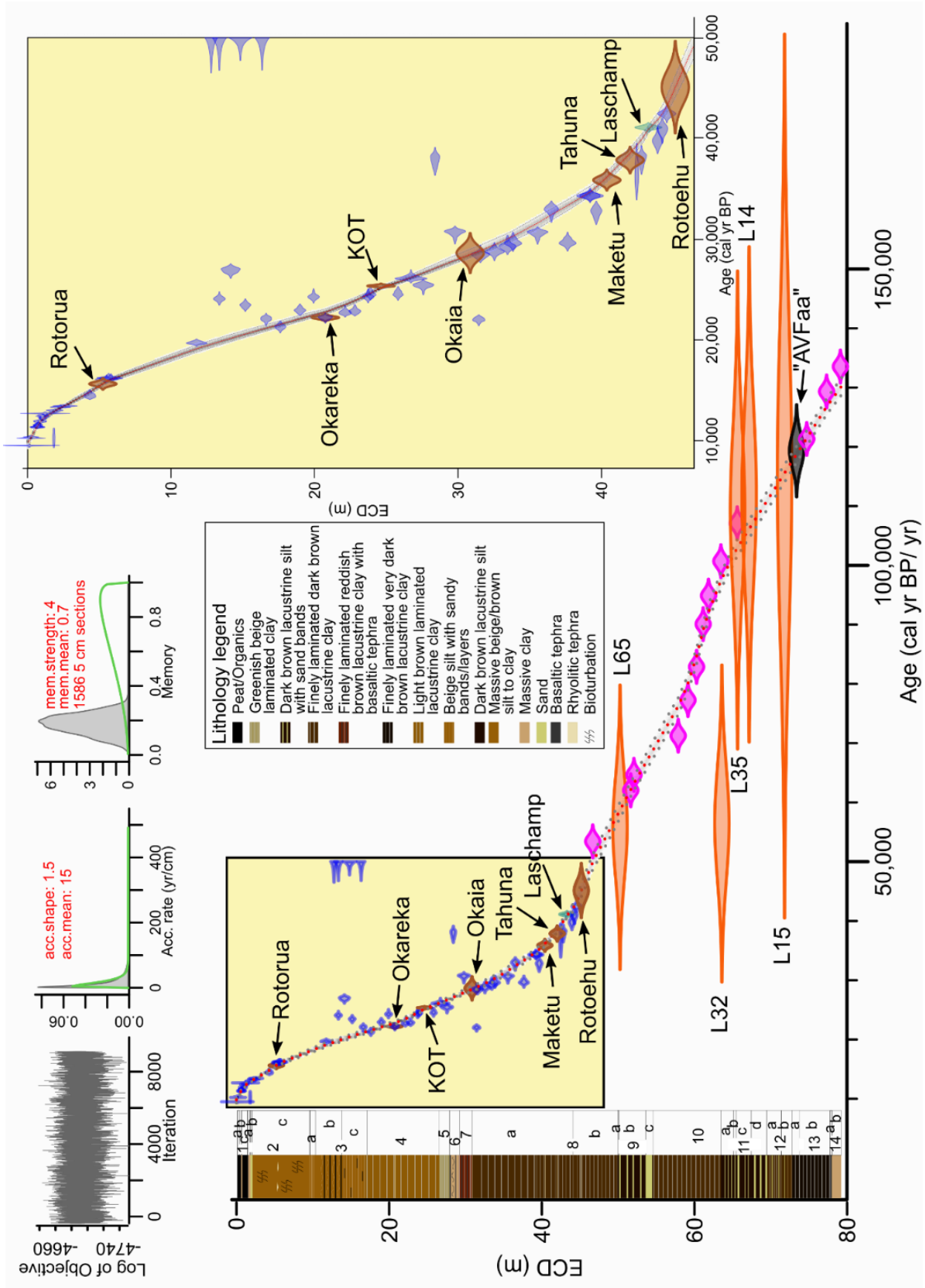

Figure ~~8~~ ~~10~~[~~Landscape~~]: Orakei age model spanning the entire sediment sequence using the event-corrected depth obtained by Bacon age modelling. Red dotted line marks the mean age model, grey dotted lines mark the 95% confidence limits. Inset enlarges the interval ca. 45,000 cal yr BP. Blue symbols mark calibrated radiocarbon ages, brown symbols mark rhyolitic tephra ages (marked by name), green symbol marks the age of the Laschamp Excursion, orange symbols mark luminescence ages (marked by sample codes), pink symbols mark tuning points from DTW alignment of Orakei RPI to PISO-1500 VADM, the black symbol marks the age of the basaltic "AVFaa" tephra identified as sourced from the Mt. Albert volcano. Lithology and facies units from Peti and Augustinus (2019).

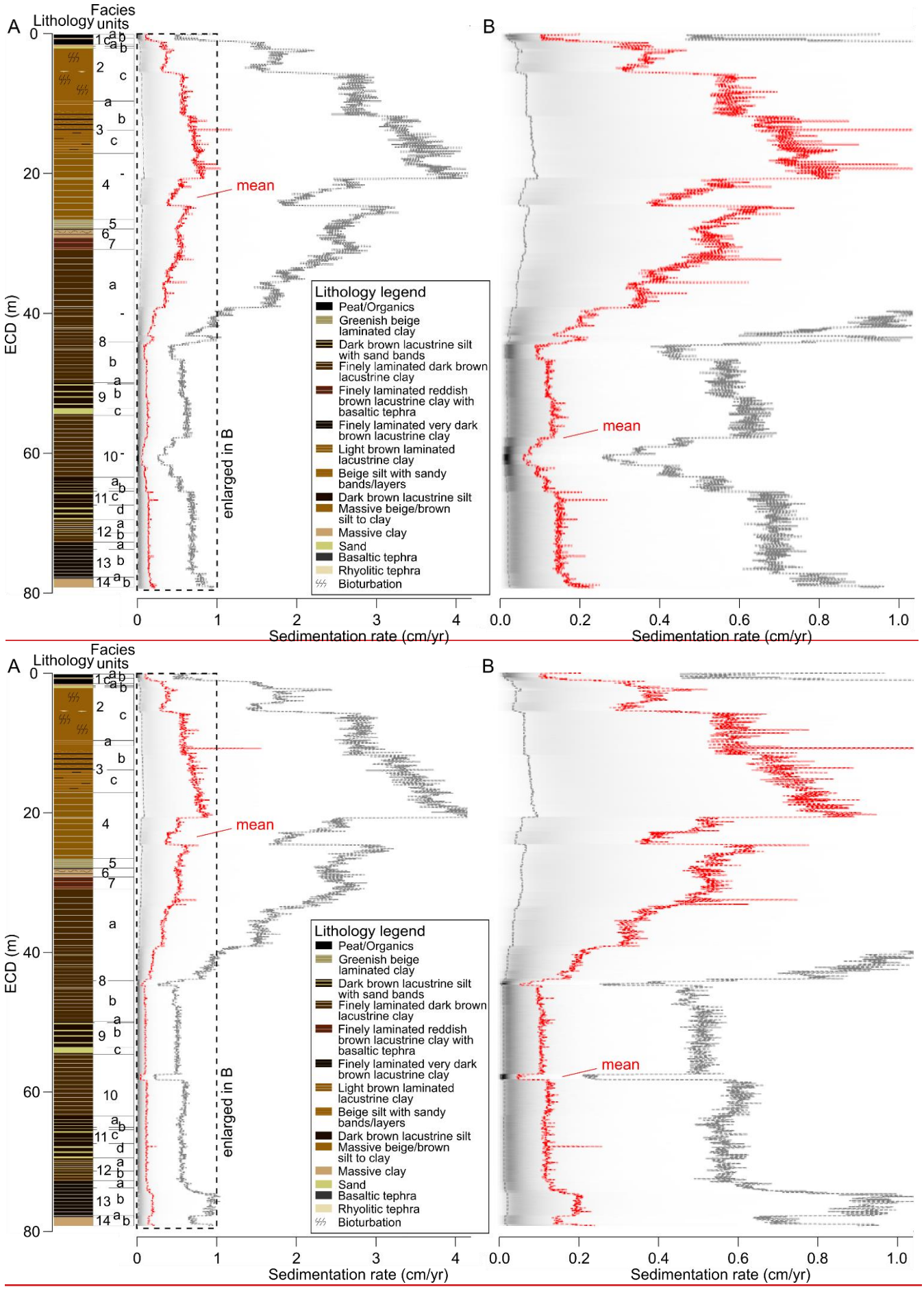

Figure ~~9~~11: A: Sedimentation rate variation of the Orakei sediment sequence in cm/yr from Bacon (Blaauw and Christen, 2020); B: Enlarged 0-1 cm/yr interval from A. Red dotted line marks the mean sedimentation rate, grey dotted lines mark the 95% confidence limits obtained by Bacon. Simplified lithology and facies units from Peti and Augustinus (2019).

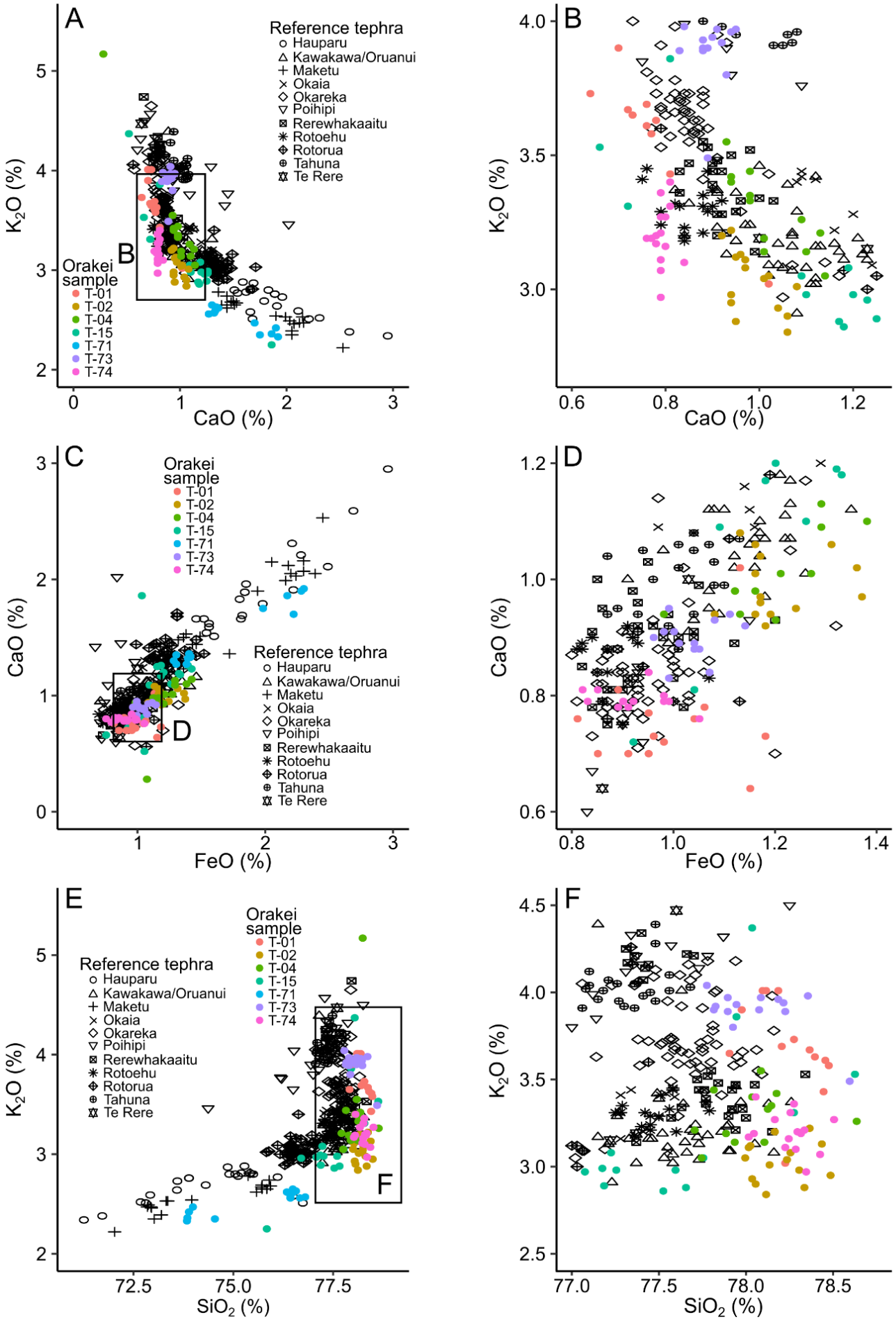
A
B
C
D
E
F
Reference tephra
Hauparu
Kawakawa/Oruanui
Maketu
Okaia
Okareka
Poihipi
Rerewhakaaitu
Rotoehu
Rotorua
Tahuna
Te Rere
Orakei sample
T-01
T-02
T-04
T-15
T-71
T-73
T-74
K2O (%)
CaO (%)
FeO (%)
SiO2 (%)

Figure A1: Major element oxide bivariate plots of reference tephra data (black) and Orakei samples (colourful points). Marked insets are enlarged on the ~~right hand~~right-hand side.

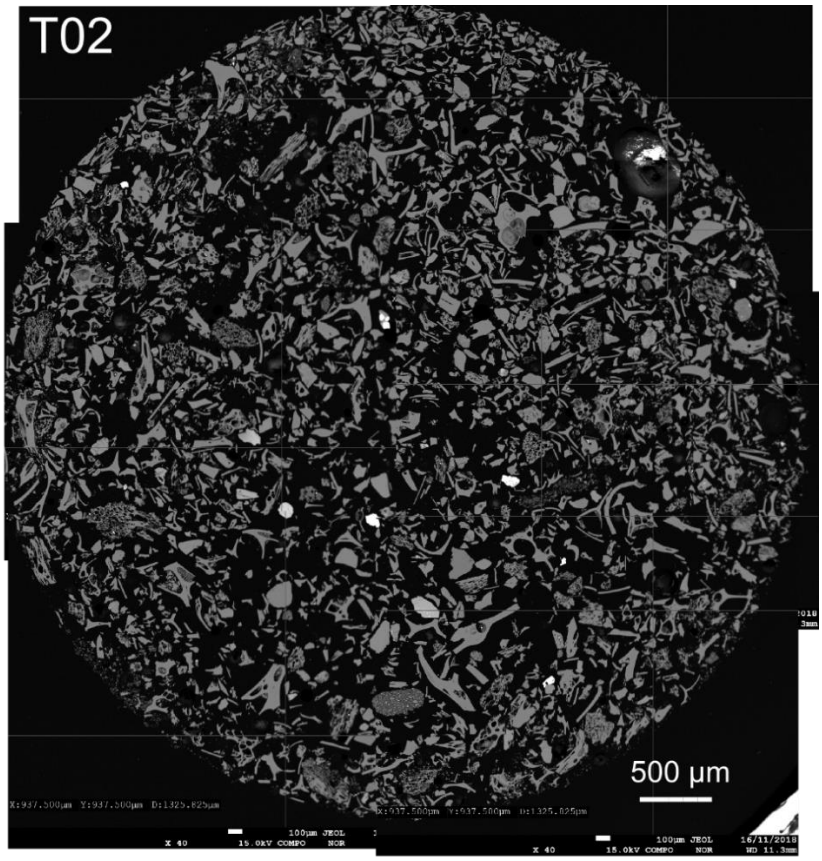

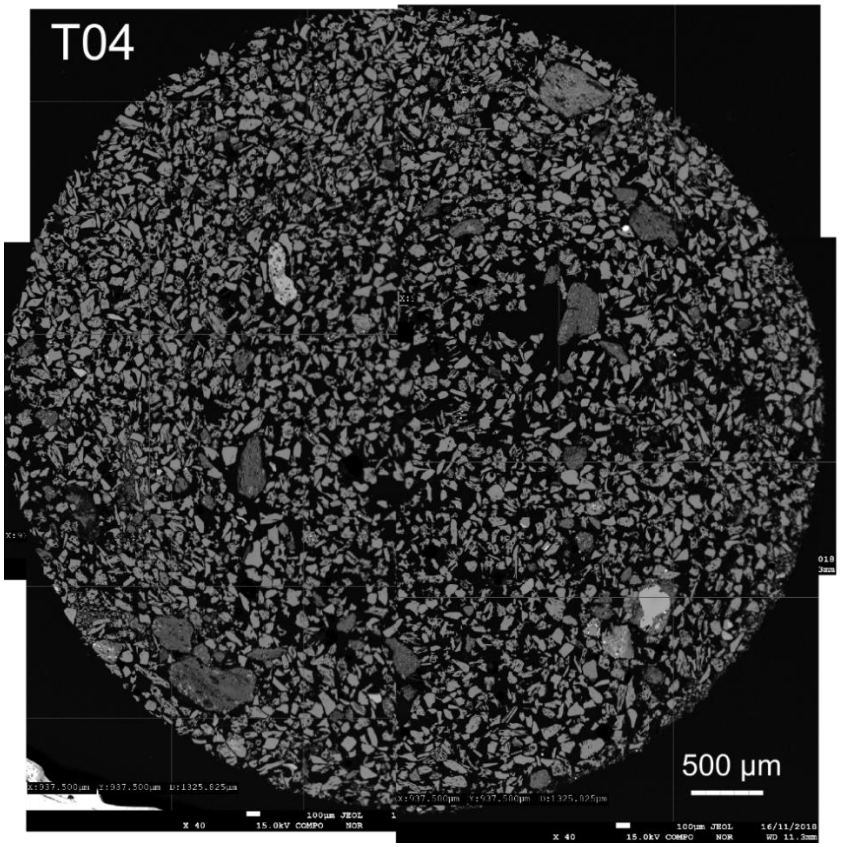

Figure A2: Backscatter images of samples T02 and T04. The large, cuspate shards with preserved thin bubble walls in T02 signify a very large, very explosive eruption, in comparison the small, blocky shards in T04, suggesting a smaller less explosive eruption.

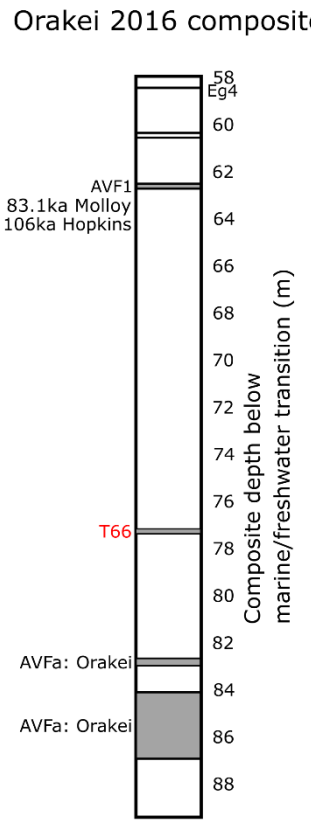

Figure A3: Lower section of the Orakei 2016 composite sequence highlighting the position of the T66 layers between the stratigraphically matched position of the AVF1 horizon and the primary eruptive material from the Orakei Volcanic Centre correlated to tephra layer AVFa by (Hopkins et al., 2017).

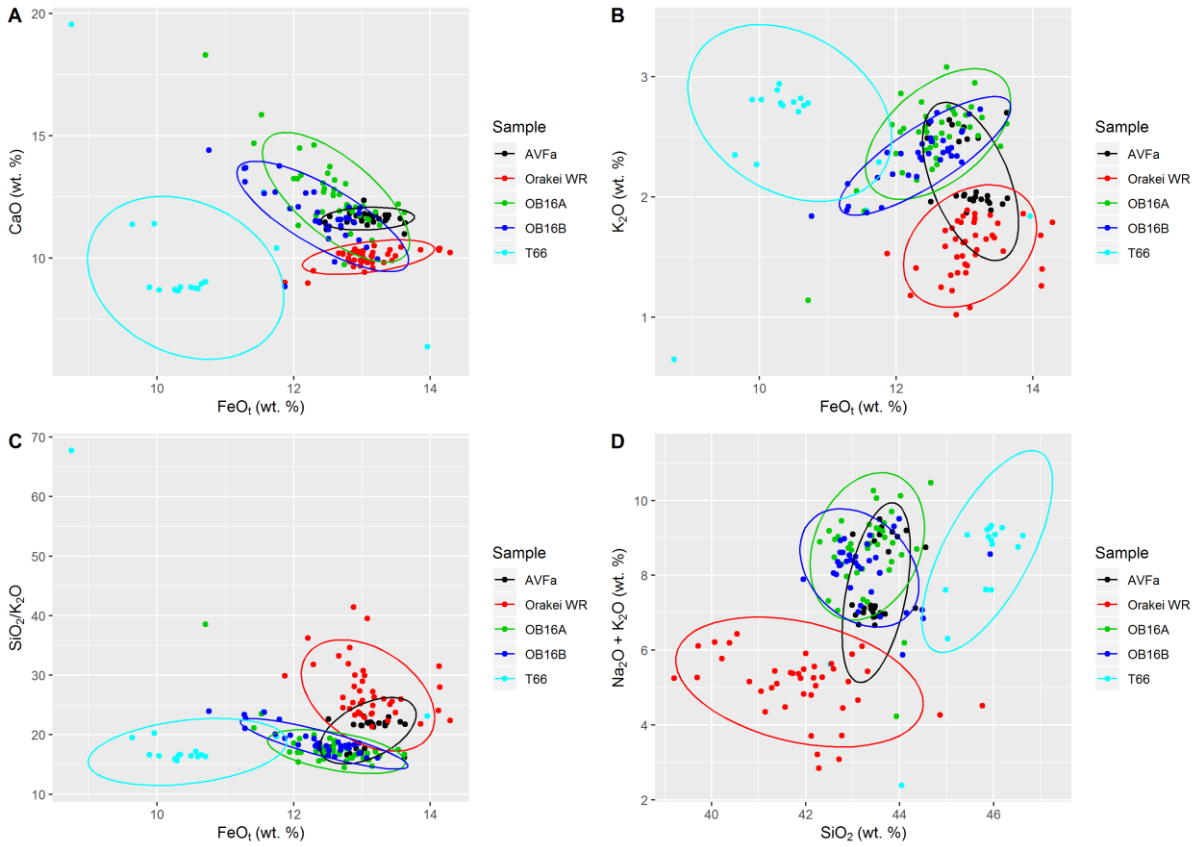

Figure A4: Comparison of sample T66 to AVFa (tephra layer from Glover Park core; correlated to the Orakei eruptive centre, (Hopkins et al., 2017)), Orakei whole rock (WR) data as well as eruptive material from Orakei in the A and B cores of this study (OB16A, OB16B). Note that T66 overlaps with neither of these samples suggesting that this is a tephra layer from a different eruption. Ellipses follow a multivariate t-distribution (Fox and Weisberg, 2011).

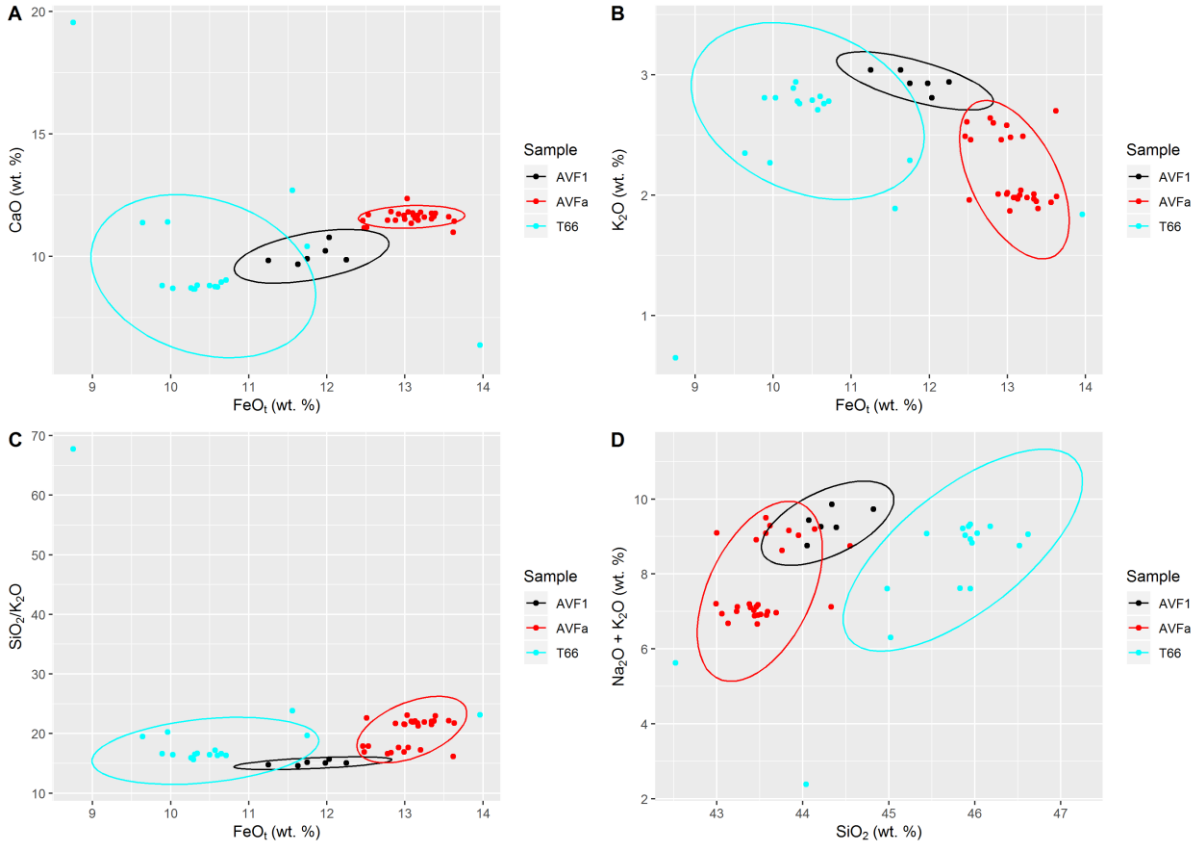

Figure A5: Comparison of sample T66 to AVF1 (tephra layer in Orakei 2007 core (Hopkins et al., 2015; Molloy et al., 2009) correlated to Domain: (Hopkins et al., 2017)) and AVFa (tephra layer from Glover Park core correlated to the Orakei Volcanic Centre (Hopkins et al., 2015, 2017)). Note that T66 overlaps with neither layer and thus is considered an eruption not previously found in the AVF maar cores. Ellipses follow a multivariate t-distribution (Fox and Weisberg, 2011).

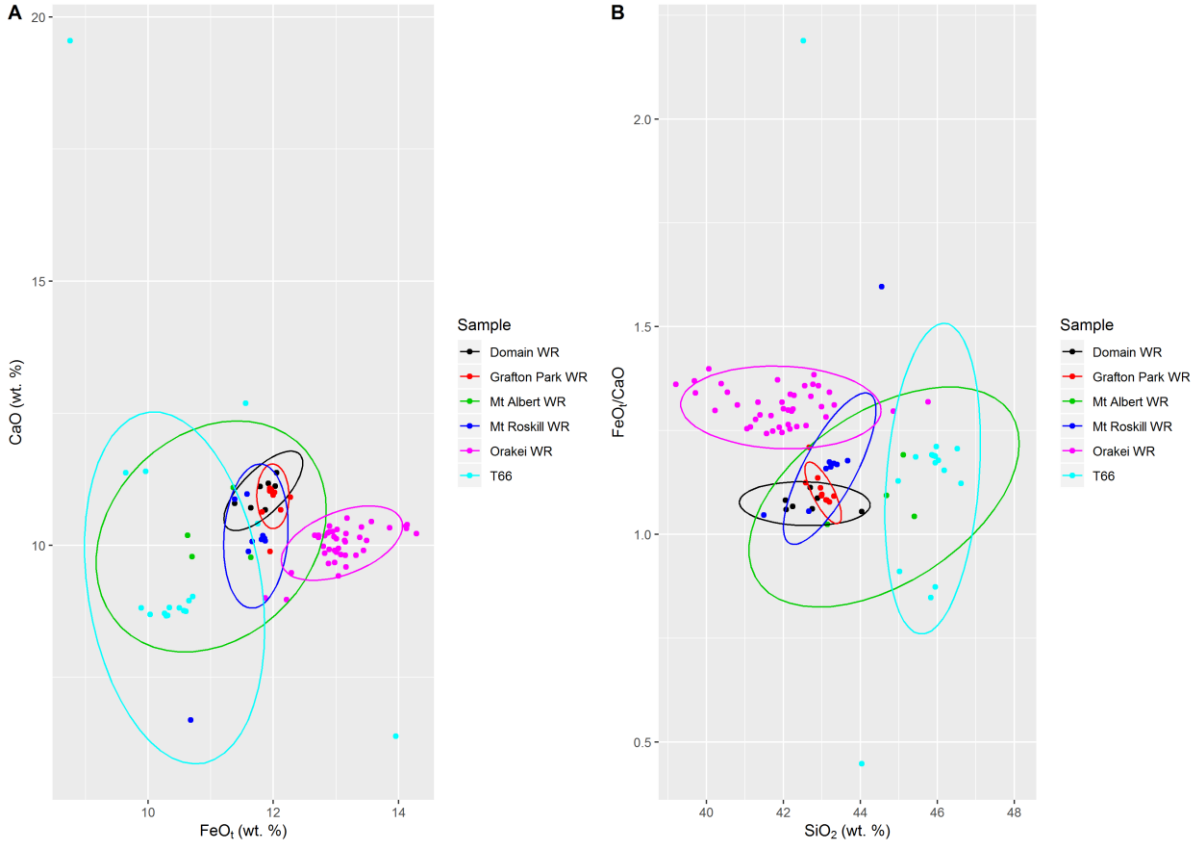

Figure A6: Matching of T66 to possible source volcanic centres (WR: whole rock data) for this tephra layers. Despite complications of correlating glass shard EMPA chemistry to whole rock geochemistry, the most likely source volcanic centre candidate for tephra

T66 is Mt. Albert as only the data and 95% confidence ellipse of Mt Albert WR data overlaps with the T66 tephra EMPA data. Ellipses follow a multivariate t-distribution (Fox and Weisberg, 2011).

1105

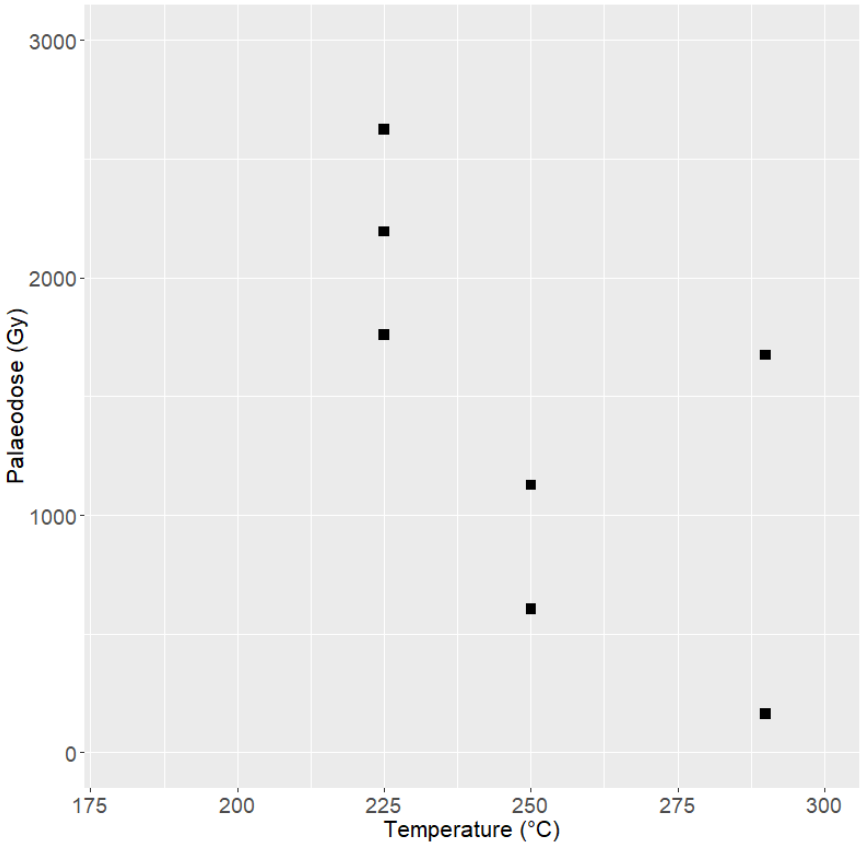

Figure B1: Preheat plateau for fine-grained sample L15 (A0111), showing substantial scatter between aliquots measured with the same preheat temperature, as well as between all aliquots.

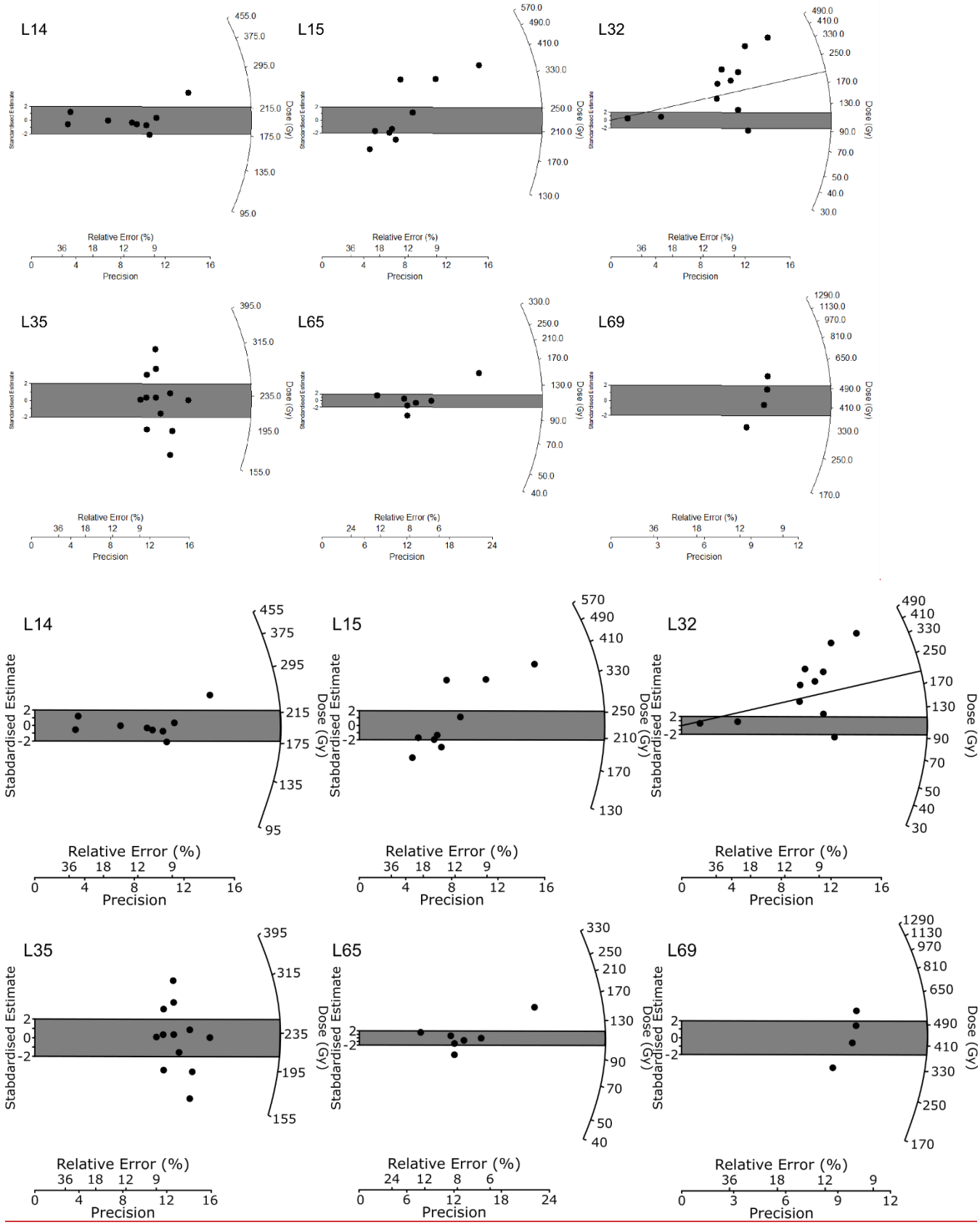

Figure B2: Radial plots showing the dose distributions of accepted aliquots for all fine-grained samples, as well as the calculated central age (shaded area). In the case of L32 (A0115), the shaded area corresponds to the minimum age calculated using the MAM, and the line corresponds to the equivalent dose which would yield the expected age according to a preliminary core age model.

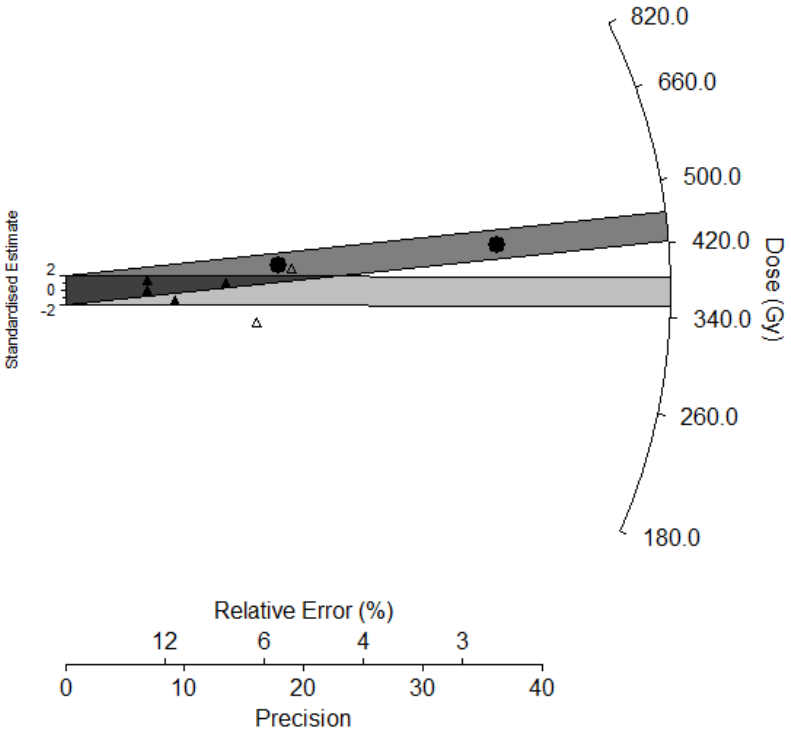

Figure B3: Radial plot showing the doses of accepted aliquots for the coarser-grained sample L20 (A0113). Aliquots run using the IR50 preheat are shown as black circles, with the darker grey shaded area; those run using the higher temperature preheat are shown as open triangles and the CAM age shaded in lighter grey.

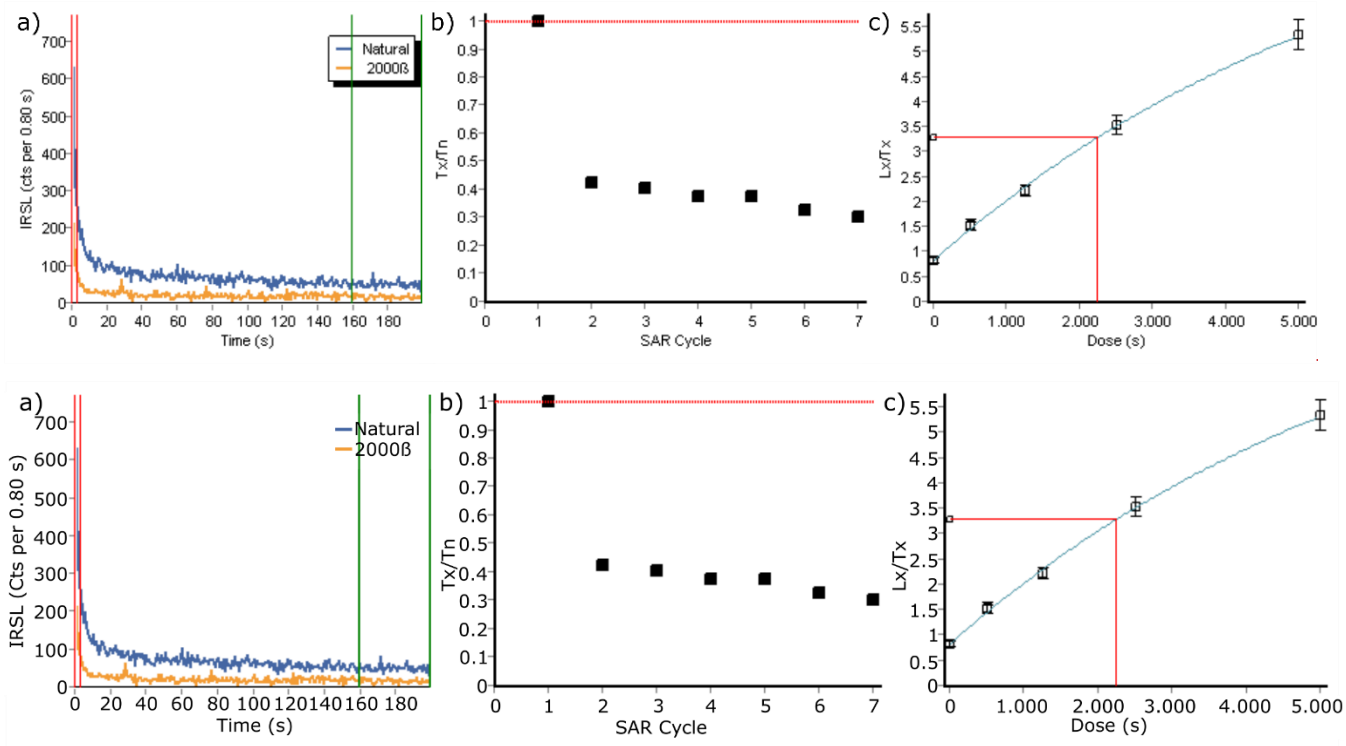

Figure B4: Illustration of luminescence characteristics of the Orakei core sediments using the post IR-IRSL$_{290}$ protocol: a) typical natural postIR-IRSL$_{290}$ signal decay for dateable sample L14 (A0110); b) change in sensitivity response to test dose over the regenerative dose cycles for sample L35 (A0116), showing reduction in effective charge transfer throughout the protocol in the typical sample; c) dose-response curve for representative aliquot of sample L35 (A0116), showing exponential fit but high Lx/Tx value for the zero dose step illustrating high degree of thermal transfer in the sediments.

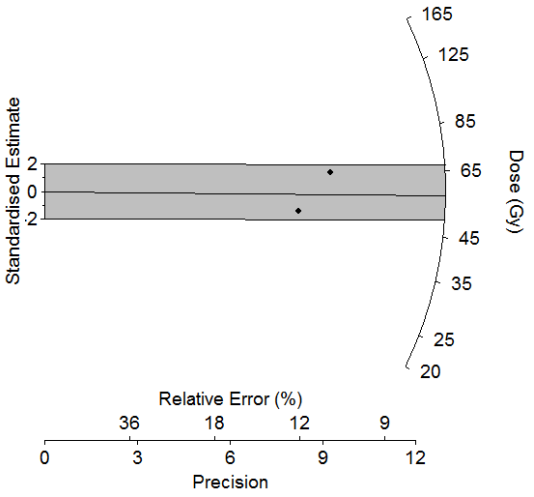

1125

Figure B5: Dose-recovery distribution from two aliquots of sample L15 (A0111). The shaded region corresponds to the standard deviation of the measured CAM dose; the line corresponds to the applied radiation dose.

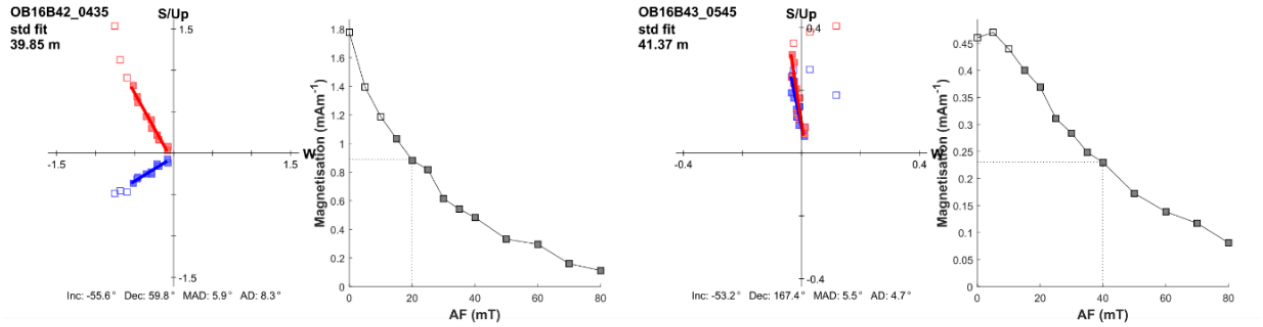
OB16B42_0435
std fit
39.85 m
S/Up
W
Inc: -55.6° Dec: 59.8° MAD: 5.9° AD: 8.3°
Magnetisation (mAm-1)
AF (mT)

OB16B43_0545
std fit
41.37 m
S/Up
W
Inc: -53.2° Dec: 167.4° MAD: 5.5° AD: 4.7°
Magnetisation (mAm-1)
AF (mT)

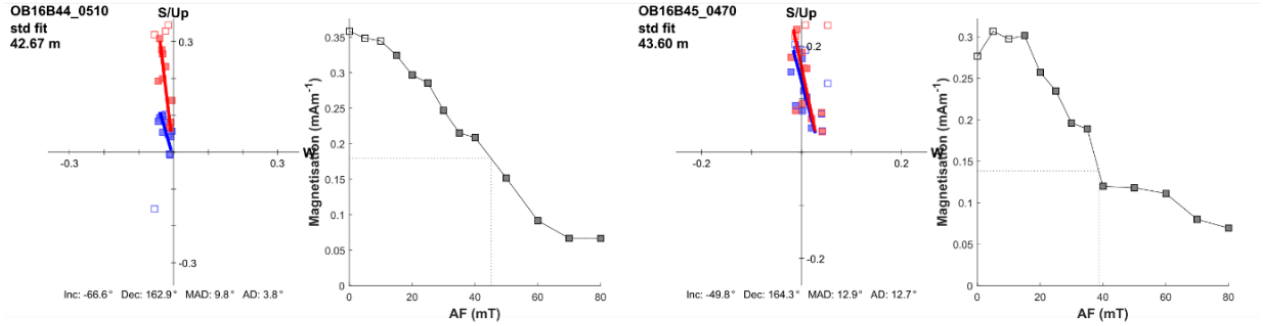
OB16B44_0510
std fit
42.67 m
S/Up
W
Inc: -66.6° Dec: 162.9° MAD: 9.8° AD: 3.8°
Magnetisation (mAm-1)
AF (mT)

OB16B45_0470
std fit
43.60 m
S/Up
W
Inc: -49.8° Dec: 164.3° MAD: 12.9° AD: 12.7°
Magnetisation (mAm-1)
AF (mT)

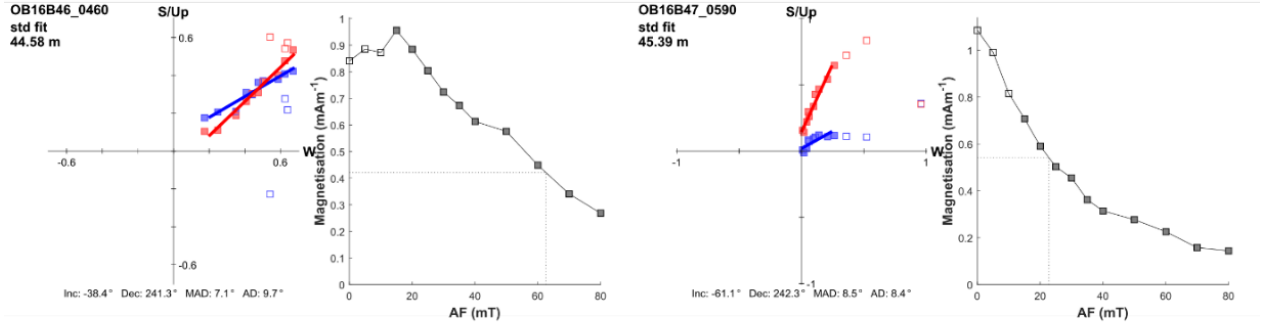
OB16B46_0460
std fit
44.58 m
S/Up
W
Inc: -38.4° Dec: 241.3° MAD: 7.1° AD: 9.7°
Magnetisation (mAm-1)
AF (mT)

OB16B47_0590
std fit
45.39 m
S/Up
W
Inc: -61.1° Dec: 242.3° MAD: 8.5° AD: 8.4°
Magnetisation (mAm-1)
AF (mT)

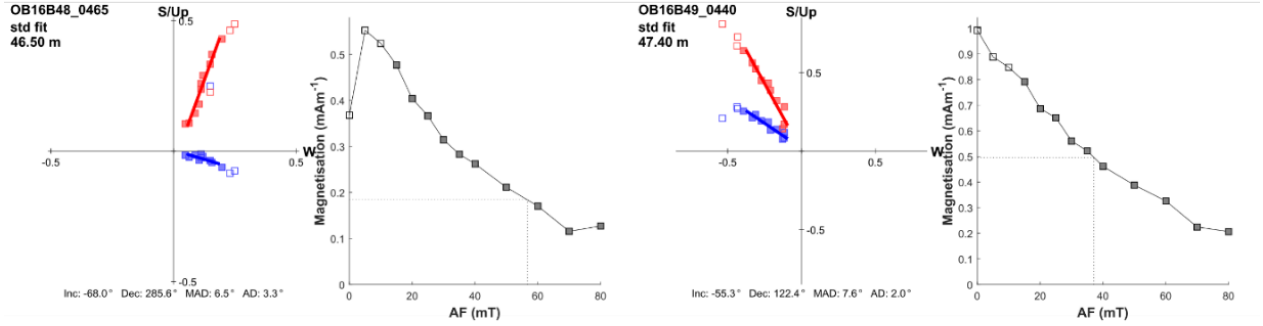
OB16B48_0465
std fit
46.50 m
S/Up
W
Inc: -68.0° Dec: 285.6° MAD: 6.5° AD: 3.3°
Magnetisation (mAm-1)
AF (mT)

OB16B49_0440
std fit
47.40 m
S/Up
W
Inc: -55.3° Dec: 122.4° MAD: 7.6° AD: 2.0°
Magnetisation (mAm-1)
AF (mT)

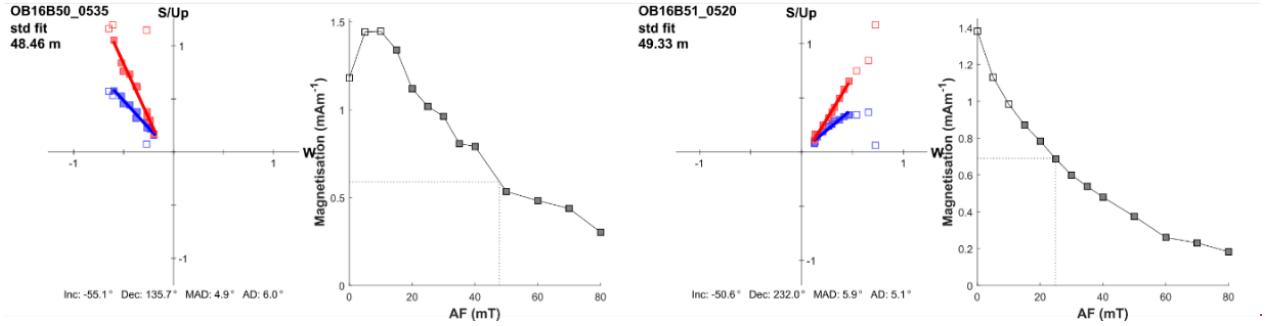
OB16B50_0535
std fit
48.46 m
S/Up
W
Inc: -55.1° Dec: 135.7° MAD: 4.9° AD: 6.0°
Magnetisation (mAm-1)
AF (mT)

OB16B51_0520
std fit
49.33 m
S/Up
W
Inc: -50.6° Dec: 232.0° MAD: 5.9° AD: 5.1°
Magnetisation (mAm-1)
AF (mT)

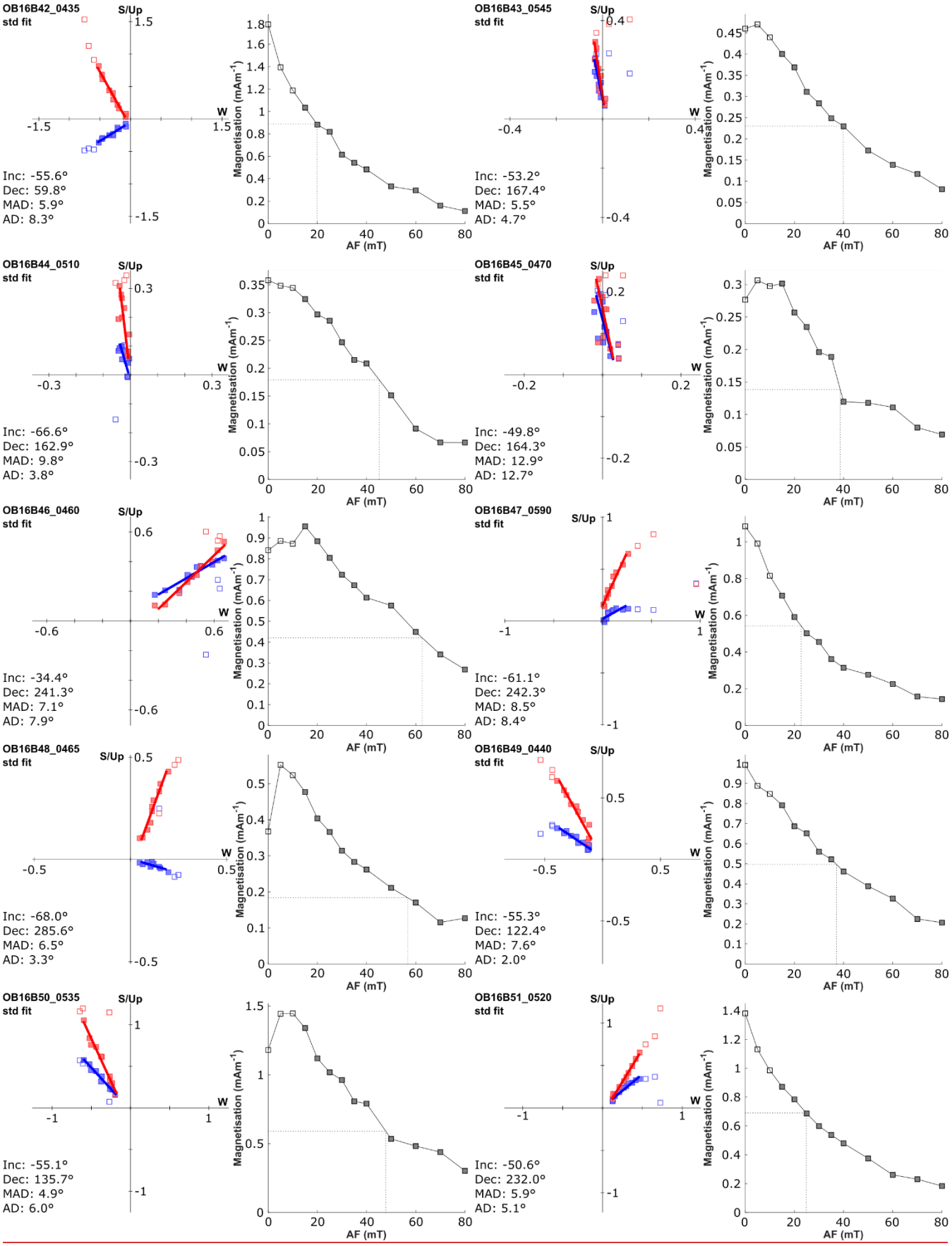

Figure C1: Orthogonal plots and intensity of magnetisation after step-wise demagnetisation of pilot samples OB16B42-51

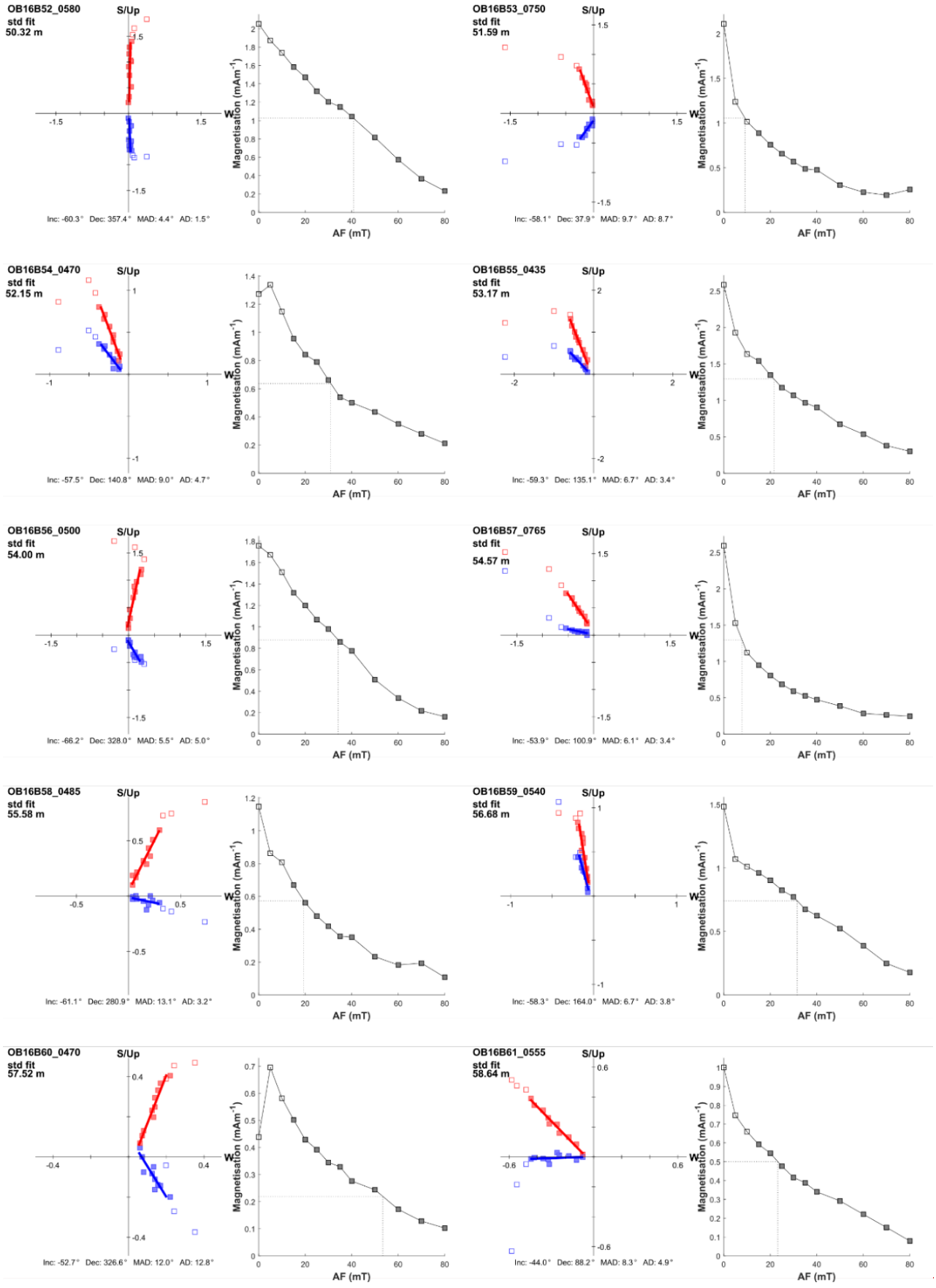
OB16B52_0580
std fit
50.32 m
S/Up
W
Inc: -60.3° Dec: 357.4° MAD: 4.4° AD: 1.5°
Magnetisation (mAm-1)
AF (mT)
OB16B53_0750
std fit
51.59 m
S/Up
W
Inc: -58.1° Dec: 37.9° MAD: 9.7° AD: 8.7°
Magnetisation (mAm-1)
AF (mT)
OB16B54_0470
std fit
52.15 m
S/Up
W
Inc: -57.5° Dec: 140.8° MAD: 9.0° AD: 4.7°
Magnetisation (mAm-1)
AF (mT)
OB16B55_0435
std fit
53.17 m
S/Up
W
Inc: -59.3° Dec: 135.1° MAD: 6.7° AD: 3.4°
Magnetisation (mAm-1)
AF (mT)
OB16B56_0500
std fit
54.00 m
S/Up
W
Inc: -66.2° Dec: 328.0° MAD: 5.5° AD: 5.0°
Magnetisation (mAm-1)
AF (mT)
OB16B57_0765
std fit
54.57 m
S/Up
W
Inc: -53.9° Dec: 100.9° MAD: 6.1° AD: 3.4°
Magnetisation (mAm-1)
AF (mT)
OB16B58_0485
std fit
55.58 m
S/Up
W
Inc: -61.1° Dec: 280.9° MAD: 13.1° AD: 3.2°
Magnetisation (mAm-1)
AF (mT)
OB16B59_0540
std fit
56.68 m
S/Up
W
Inc: -58.3° Dec: 164.0° MAD: 6.7° AD: 3.8°
Magnetisation (mAm-1)
AF (mT)
OB16B60_0470
std fit
57.52 m
S/Up
W
Inc: -52.7° Dec: 326.6° MAD: 12.0° AD: 12.8°
Magnetisation (mAm-1)
AF (mT)
OB16B61_0555
std fit
58.64 m
S/Up
W
Inc: -44.0° Dec: 88.2° MAD: 8.3° AD: 4.9°
Magnetisation (mAm-1)
AF (mT)

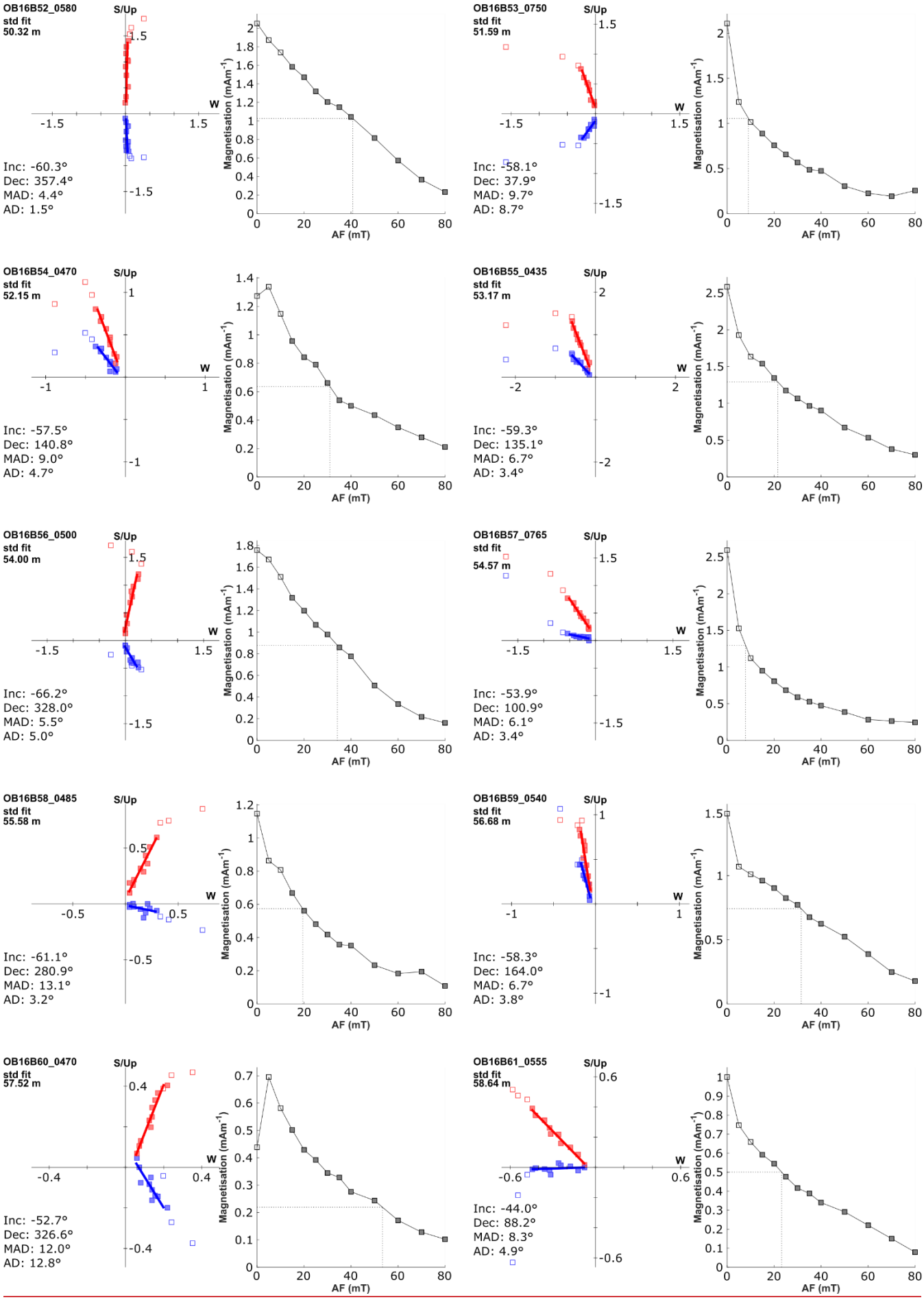

Figure C2: Orthogonal plots and intensity of magnetisation after step-wise demagnetisation of pilot samples OB16B52-61

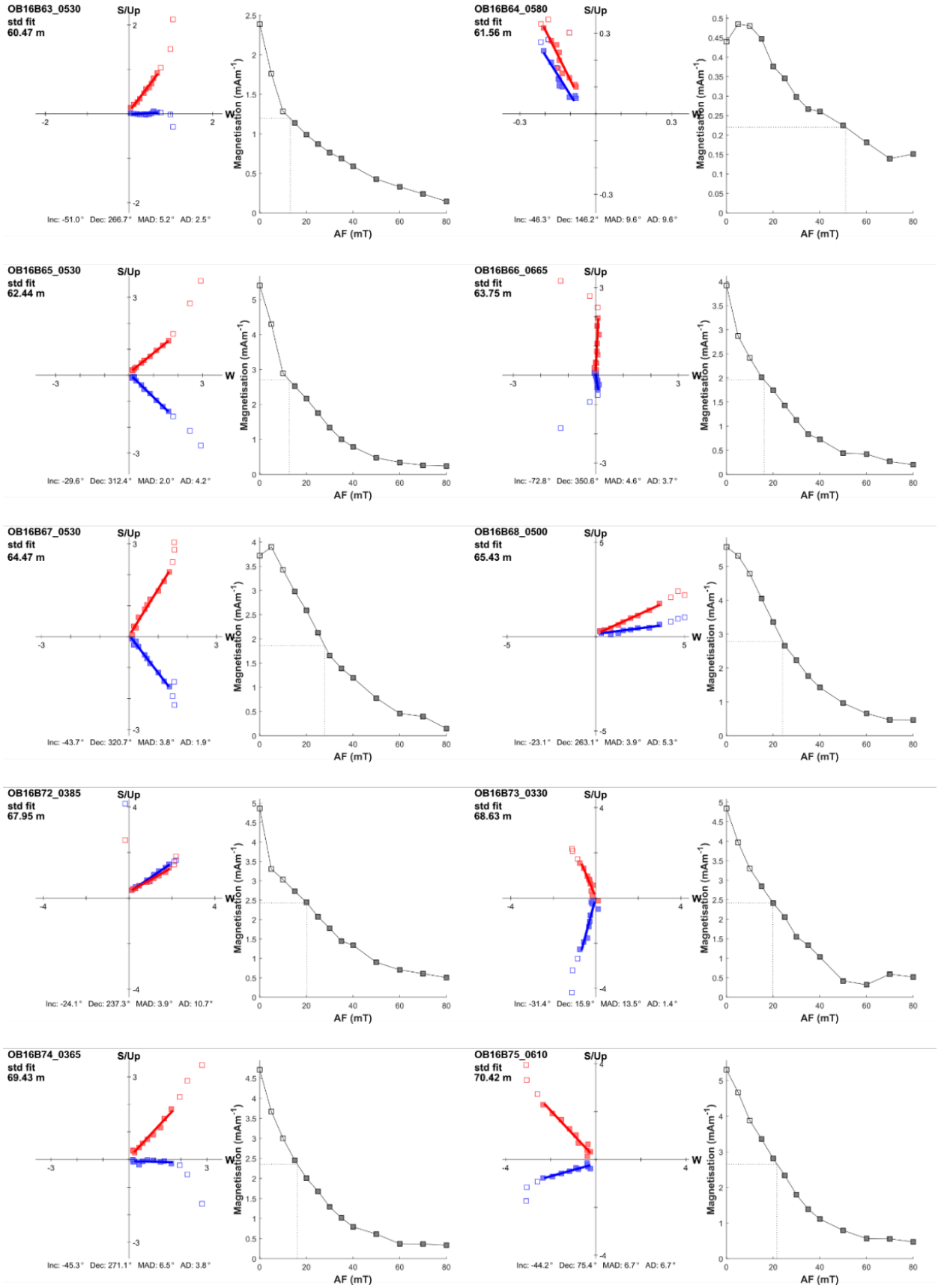
OB16B63_0530
std fit
60.47 m
S/Up
W
Inc: -51.0° Dec: 266.7° MAD: 5.2° AD: 2.5°
Magnetisation (mAm-1)
AF (mT)
OB16B64_0580
std fit
61.56 m
S/Up
W
Inc: -46.3° Dec: 146.2° MAD: 9.6° AD: 9.6°
Magnetisation (mAm-1)
AF (mT)
OB16B65_0530
std fit
62.44 m
S/Up
W
Inc: -29.6° Dec: 312.4° MAD: 2.0° AD: 4.2°
Magnetisation (mAm-1)
AF (mT)
OB16B66_0665
std fit
63.75 m
S/Up
W
Inc: -72.8° Dec: 350.6° MAD: 4.6° AD: 3.7°
Magnetisation (mAm-1)
AF (mT)
OB16B67_0530
std fit
64.47 m
S/Up
W
Inc: -43.7° Dec: 320.7° MAD: 3.8° AD: 1.9°
Magnetisation (mAm-1)
AF (mT)
OB16B68_0500
std fit
65.43 m
S/Up
W
Inc: -23.1° Dec: 263.1° MAD: 3.9° AD: 5.3°
Magnetisation (mAm-1)
AF (mT)
OB16B72_0385
std fit
67.95 m
S/Up
W
Inc: -24.1° Dec: 237.3° MAD: 3.9° AD: 10.7°
Magnetisation (mAm-1)
AF (mT)
OB16B73_0330
std fit
68.63 m
S/Up
W
Inc: -31.4° Dec: 15.9° MAD: 13.5° AD: 1.4°
Magnetisation (mAm-1)
AF (mT)
OB16B74_0365
std fit
69.43 m
S/Up
W
Inc: -45.3° Dec: 271.1° MAD: 6.5° AD: 3.8°
Magnetisation (mAm-1)
AF (mT)
OB16B75_0610
std fit
70.42 m
S/Up
W
Inc: -44.2° Dec: 75.4° MAD: 6.7° AD: 6.7°
Magnetisation (mAm-1)
AF (mT)

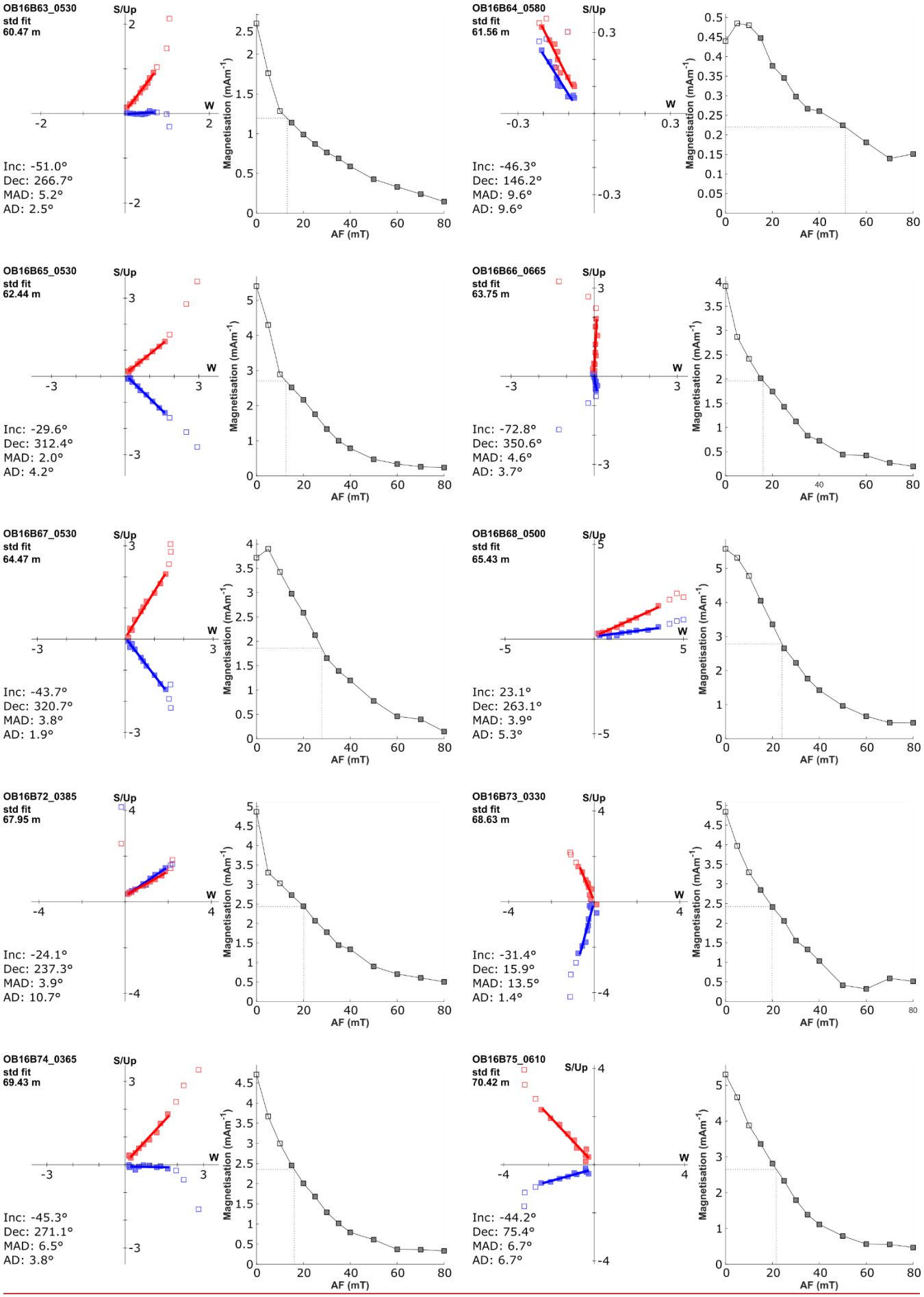

Figure C3: Orthogonal plots and intensity of magnetisation after step-wise demagnetisation of pilot samples OB16B63-75

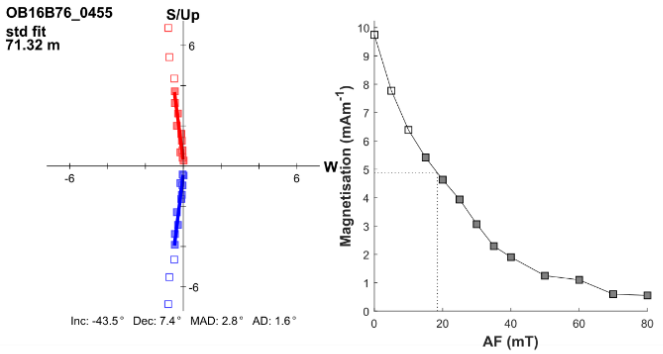
OB16B76_0455
std fit
71.32 m
S/Up
W
Inc: -43.5° Dec: 7.4° MAD: 2.8° AD: 1.6°
Magnetisation (mAm-1)
AF (mT)

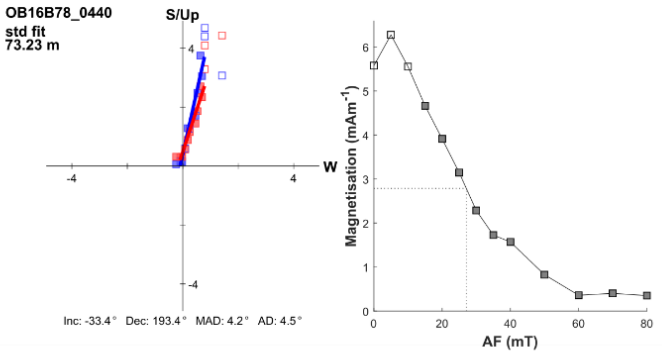
OB16B78_0440
std fit
73.23 m
S/Up
W
Inc: -33.4° Dec: 193.4° MAD: 4.2° AD: 4.5°
Magnetisation (mAm-1)
AF (mT)

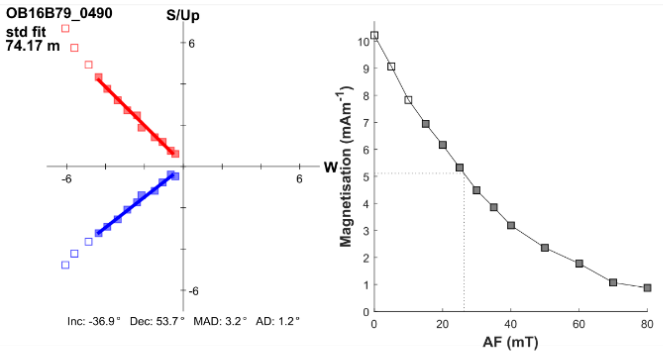
OB16B79_0490
std fit
74.17 m
S/Up
W
Inc: -36.9° Dec: 53.7° MAD: 3.2° AD: 1.2°
Magnetisation (mAm-1)
AF (mT)

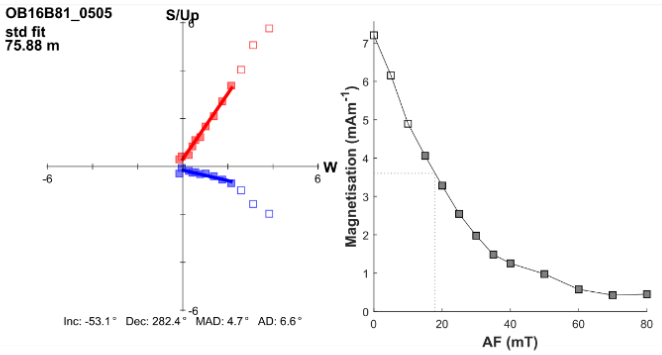
OB16B81_0505
std fit
75.88 m
S/Up
W
Inc: -53.1° Dec: 282.4° MAD: 4.7° AD: 6.6°
Magnetisation (mAm-1)
AF (mT)

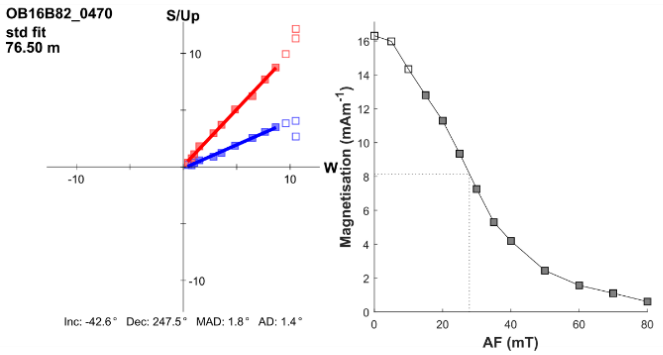
OB16B82_0470
std fit
76.50 m
S/Up
W
Inc: -42.6° Dec: 247.5° MAD: 1.8° AD: 1.4°
Magnetisation (mAm-1)
AF (mT)

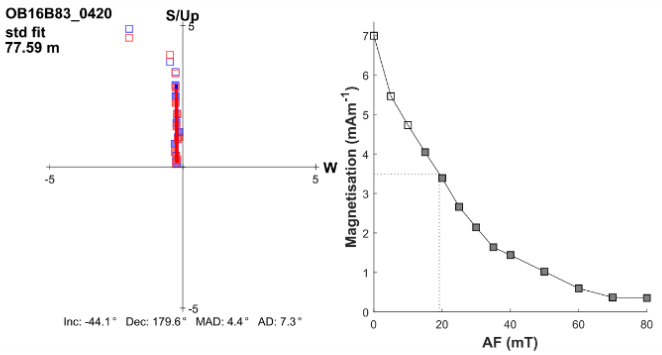
OB16B83_0420
std fit
77.59 m
S/Up
W
Inc: -44.1° Dec: 179.6° MAD: 4.4° AD: 7.3°
Magnetisation (mAm-1)
AF (mT)

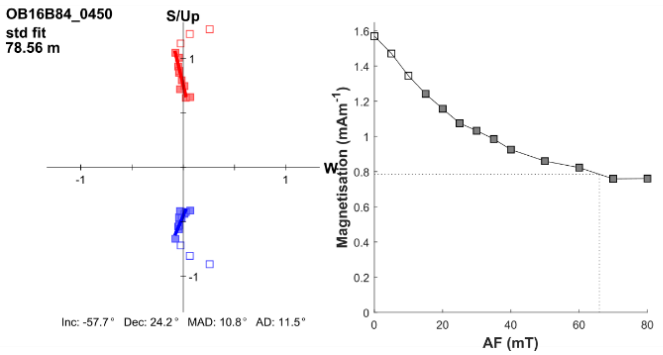
OB16B84_0450
std fit
78.56 m
S/Up
W
Inc: -57.7° Dec: 24.2° MAD: 10.8° AD: 11.5°
Magnetisation (mAm-1)
AF (mT)

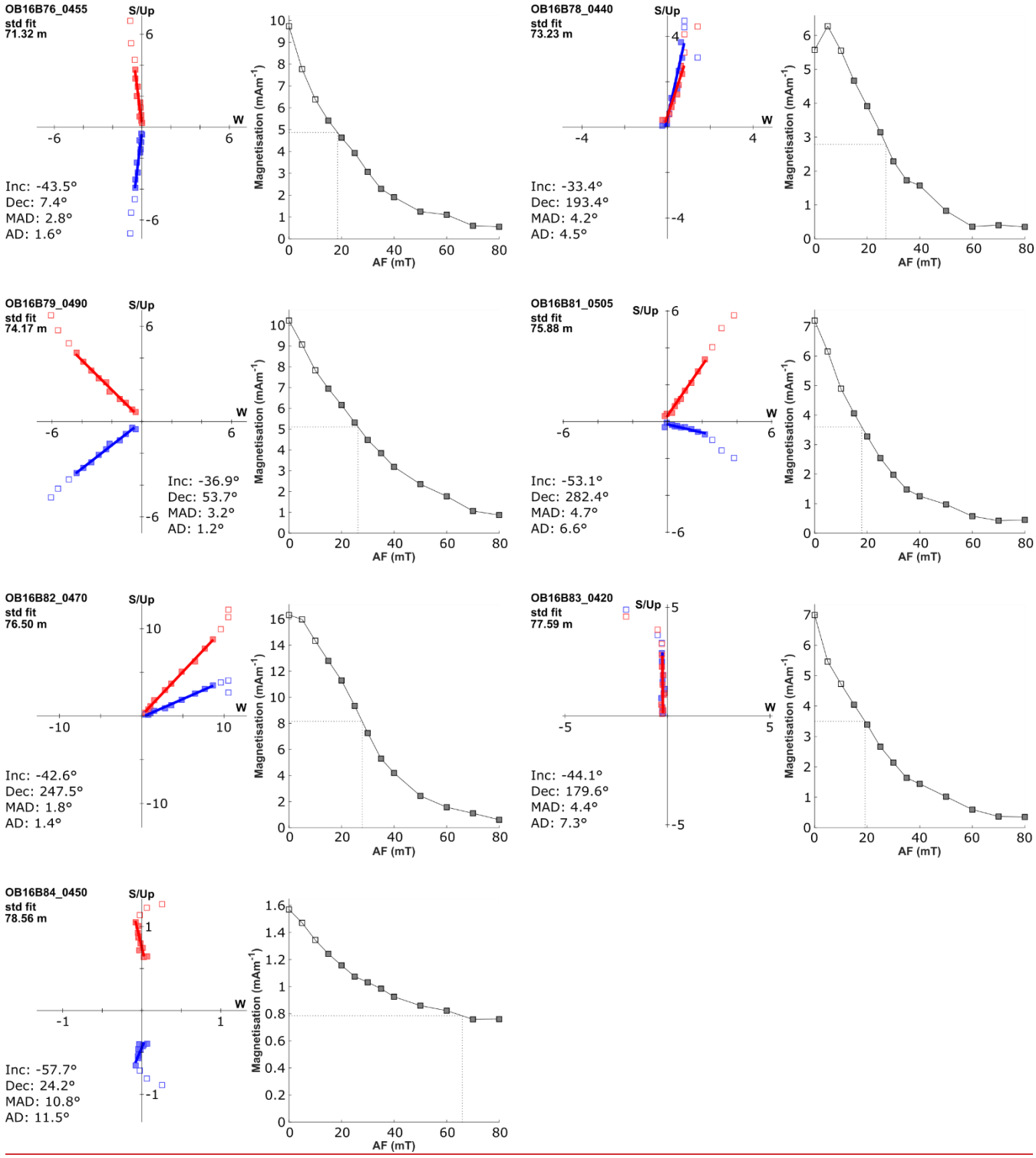

Figure C4: Orthogonal plots and intensity of magnetisation after step-wise demagnetisation of pilot samples OB16B76-84

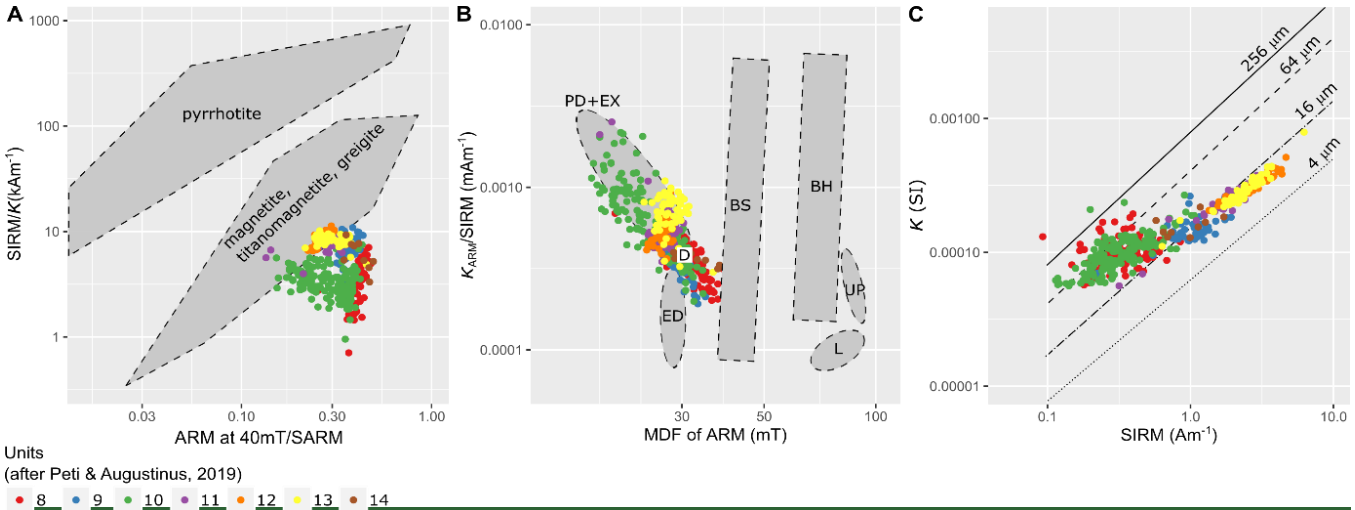

~~**Figure C5: Rockmagnetic characterisation of the Orakei sediment samples. (A) Qualitative identification of magnetic minerals following Peters and Thompson (1998). SARM: Saturated ARM at 0 mT. We note that the ARM at 40mT/SARM ratios are likely higher than the equivalent measurements of Peters and Thompson (1998) due to the lower maximum AF (80mT) used to induce the ARM. The magnetic carrier in the Orakei sediment sequence is interpreted as dominantly magnetite/titanomagnetite. (B) Magnetic components of Orakei samples in comparison to components defined by Egli (2004). MDF: Mean destructive field. κ_{ARM}: Susceptibility of ARM (SARM divided by applied bias field). BH: Biogenic hard, high-coercivity magnetosomes, BS: Biogenic soft, low-coercivity magnetosomes, D: detrital particles transported in water systems, ED: eolian dust/wind-blown particles, EX: ultrafine extracellular magnetite, L: maghemite component in loess, PD: pedogenic magnetite, UP: atmospheric particulate matter produced by urban pollution. Orakei samples are classified as detrital and extracellular components. (C) Estimated magnetic grain size indicator following Thompson and Oldfield (1986, p.31). SIRM: Saturated IRM at 0mT. Most of the samples plot in the range of pseudo-single domain magnetite (0.1-20 µm). The increased scatter in the lower left half of the plot, suggesting increasing magnetic grain size, may partly reflect the importance of superparamagnetic (e.g. facies 10) and/or paramagnetic effects in samples with low magnetite concentration.**~~

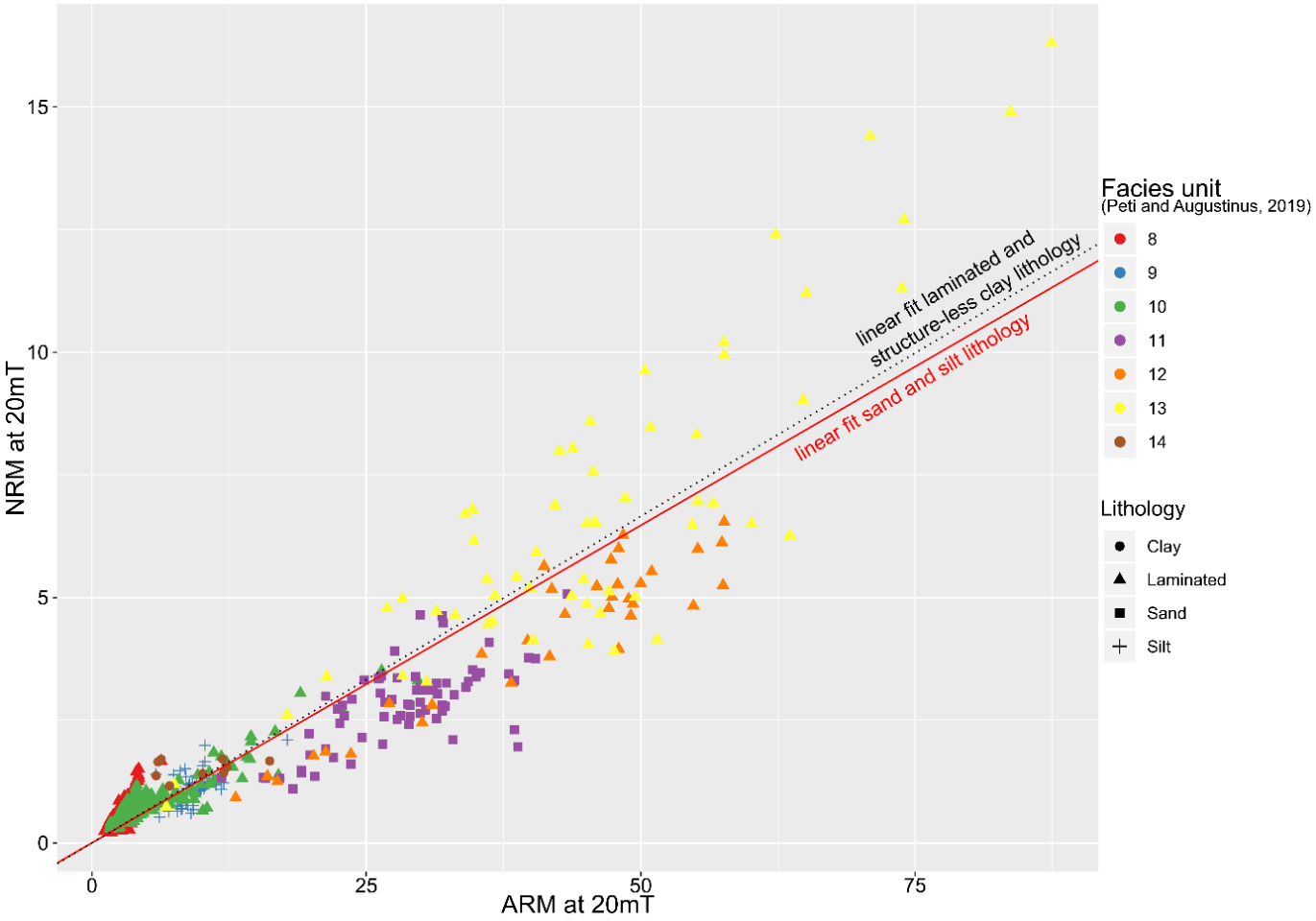

Figure ~~C6~~C5: Orakei ARM vs NRM at 20mT. Note how datapoints in coarser units with sandy and silty lithology follow a linear trend with a slightly shallower slope (red, solid) than clay-dominated lithologies (black dotted; laminated or structure-less).

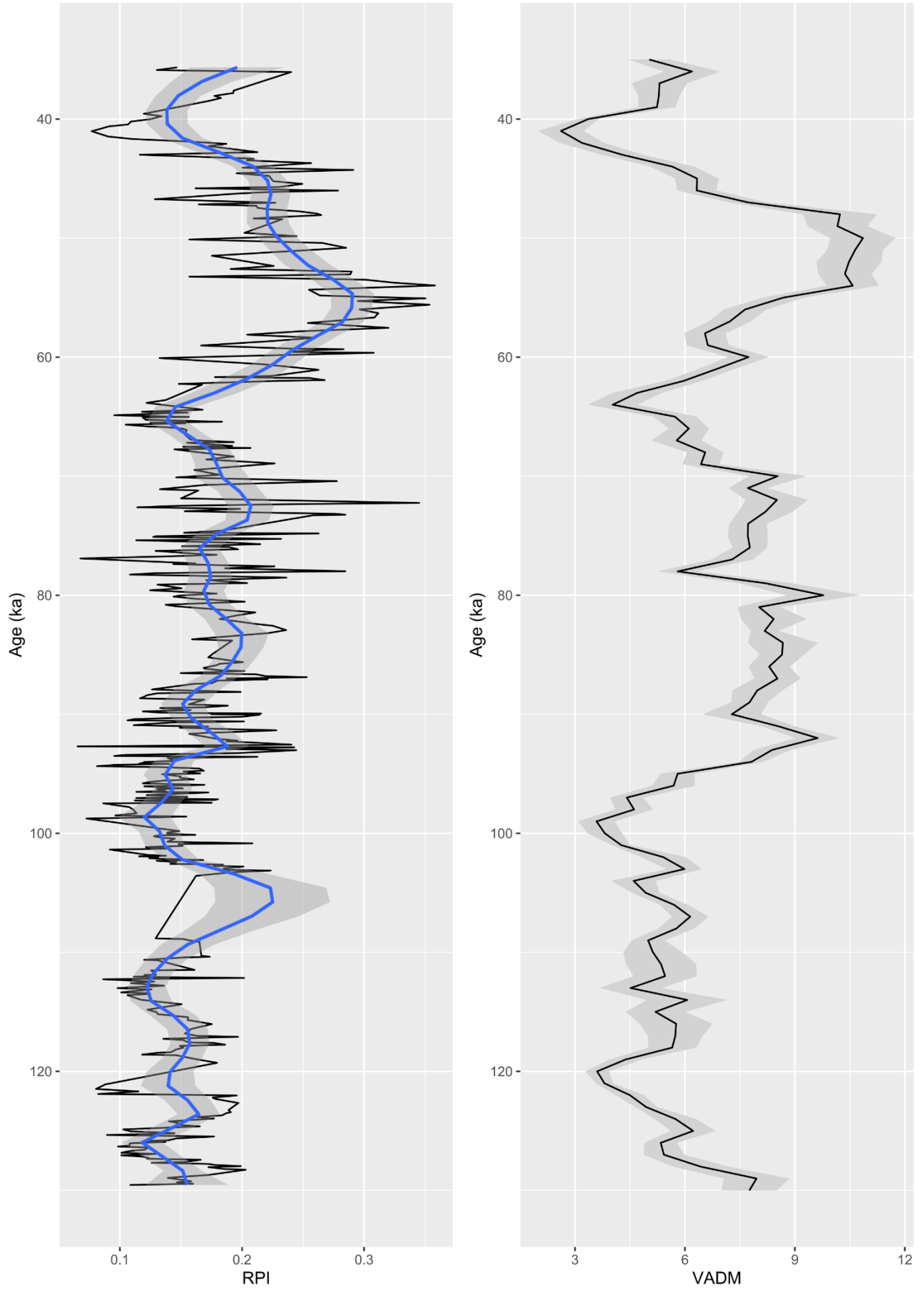
Age (ka)
40
60
80
100
120
0.1
0.2
0.3
RPI
Age (ka)
40
60
80
100
120
3
6
9
12
VADM

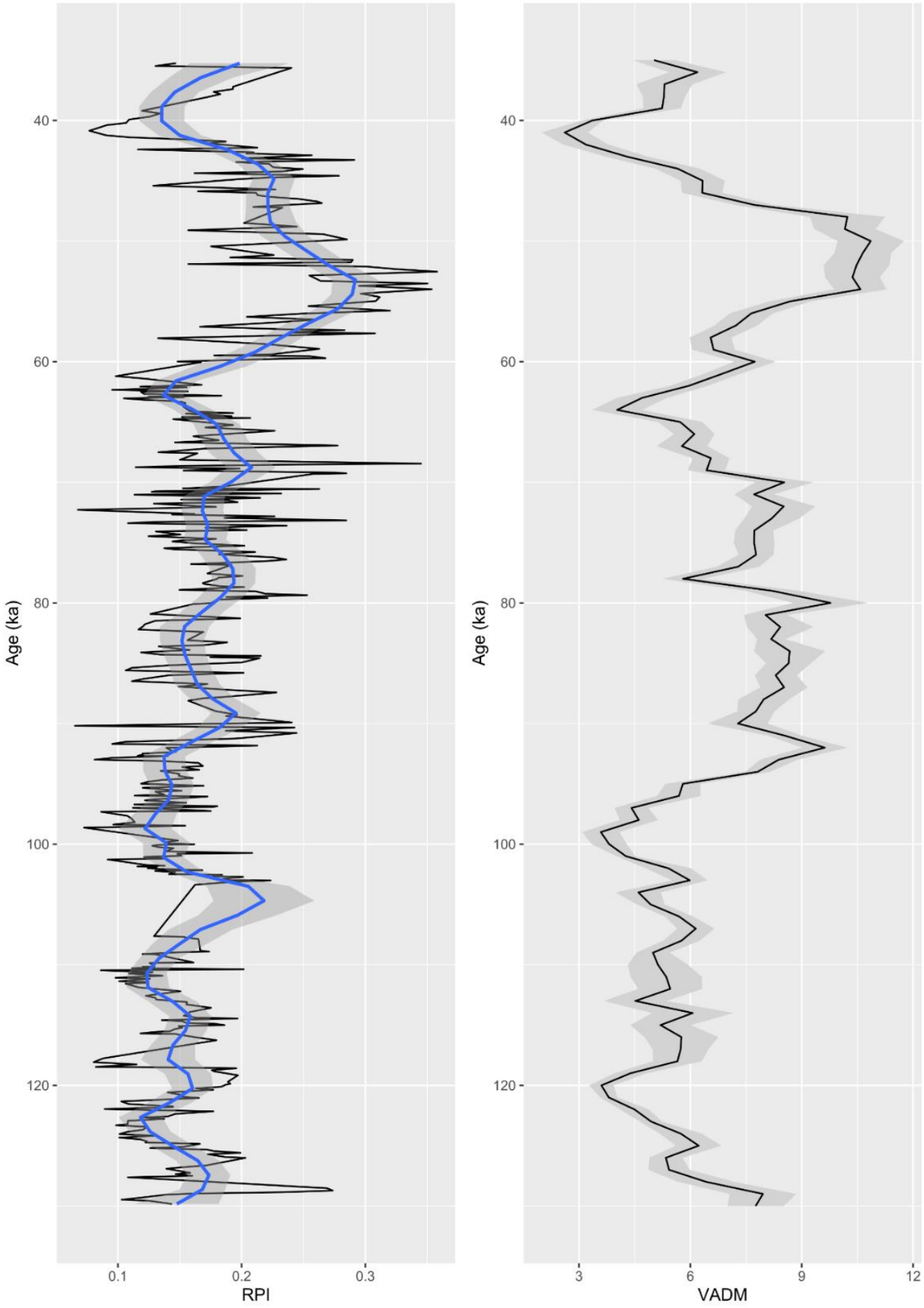

Figure C67: Comparison of Orakei RPI (left) and PISO VADM (right) after the age modelling process in Bacon. Note the very good alignment between the smoothed RPI curved and the PISO stack.~~but small offsets are caused by the consideration of absolute ages for the "AVFaa" tephra and luminescence ages as well as the smoothness of the age model introduced by Bacon, which does not always follow the palaeomagnetic tuning points as established by dynamic time warping.~~

Table 1: Bacon prior parameters

Accumulation mean (acc.mean) (cm/year)	Accumulation shape (acc.shape)	Memory strength (mem.strength)	Memory mean (mem.mean)	thick (cm)
15	1.5	4	0.7	5

Table 2: Identified rhyolitic tephra layers in the Orakei sediment sequence. For source locations see figure 1.

Orakei sample code	Tephra name	ECD (m)	Thickness (mm)	Age (cal yr BP) ± 2 σ	Source volcanic centre	Original dating method	Reference
T-15	Rotorua	5.23	20	15,635 ± 412	Okataina	combined ^{14}C ages above, below and within the tephra layer	(Lowe et al., 2013)
T-01	Okareka	20.74	1	22,~~213~~2295 ± 192~~278~~	Okataina	^{14}C of leaf fragments 10 mm above and below tephra	Original age from Molloy et al. (2009) calibrated with SHCal20 (Hogg et al., 2020)~~13 (Hogg et al., 2013)~~. ~~See Appendix A.~~
T-02	Kawakawa/ Oruanui	24.62	25	25,360 ± 160	Taupo	22 macrofossil ^{14}C ages from four sites incorporated in Bayesian model	(Vandergoes et al., 2013) supported by an ice core age (Dunbar et al., 2017)
T-04	Okaia	30.84	5	28,621 ± 1,428	Taupo	^{14}C ages	(Lowe et al., 2013)
T-71	Maketu	40.37	18	~~35~~36,~~866~~100 ± ~~738~~900#	Okataina	Integrated Bayesian modelling of zircon double dating and ^{14}C dating~~14C of bulk sediment and macrofossil charcoal~~	(Danišík et al., 2020)~~Original age from freshwater reservoir effect corrected (for bulk sediment age, see section 3.2, 4.2), and calibrated with SHCal13 (Hogg et al., 2013). See Appendix A.~~
T-73	Tahuna^	41.99	2	~~37~~38,~~854~~40 ± ~~940~~1700# ^	Taupo	Integrated Bayesian modelling of zircon double dating and ^{14}C dating ~~^{14}C of bulk sediment and macrofossil charcoal~~	(Danišík et al., 2020)~~Original age from freshwater reservoir effect corrected (for bulk sediment age, see section 3.2, 4.2), and calibrated with SHCal13 . See Appendix A.~~

T-74	Rotoehu	45.14	>300 (partially reworked)	45,100 ± 3,300 47,400 ± 3,000		Okataina	$^{238}U/^{230}Th$ disequilibrium and (U-Th)/He zircon $^{40}Ar/^{39}Ar$	(Danišík et al., 2012)* (Flude and Storey, 2016)

Note that (Danišík et al., 2020) calculated non-symmetrical errors of + 900 – 800 cal yr BP (Maketu) and +1700 -1400 cal yr BP (Tahuna) but Bacon does not accommodate non-symmetrical errors by default so that we use the larger term of each error respectively in the positive and negative directions.

^ We note that Loame et al. (2019) dated the Tahuna layer to 38,870 ± 1,106 (2 σ) cal yr BP. However, we prefer ~~an~~ the more recent age constrained by several samples ~~above and below the tephra layer (Molloy et al., 2009) but highlight the agreement between both ages~~and two techniques (Danišík et al., 2020) but note their strong agreement.~~.~~

* Many ages for the Rotoehu tephra (Rotoiti eruption) have been proposed based on a variety of direct and indirect dating methods spanning approximately the age range 40 – 60 ka. The combined $^{238}U/^{230}Th$ disequilibrium and (U-Th)/He zircon age of 45,100 ± 3,300 (2 σ) years, concordant with radiocarbon ages (Danišík et al., 2012) is in better agreement with the radiocarbon ages of this study (see Table 3) and thus used in the presented chronology.

Table 3: Overview of radiocarbon samples and ages. Reservoir-corrected ages in italics. Outliers in grey. All are calibrated by ~~SHCal13~~ SHCal20 (Hogg et al., 2020)~~.~~

Lab Code	Material	ECD (m)	Facies unit (from Peti and Augustinus (2019))	^{14}C age (years BP ± 1~~2~~σ)	Reservoir correction (years ± 2σ)	Calibrated mean ± 2~~1~~σ age (cal. yr BP) (reservoir ~~corrected where~~ corrected where
NZA28865* ^	Wood	0.12	1a (Peat)	8,565 ± ~~30~~60		9,512 ± 40~~19~~
OZW872	Wood	0.22	1a (Peat)	9,175 ± 8~~4~~0		10,~~303~~ 314 ± ~~61~~132
OZW871	Wood	0.62	1c (Peat)	10,000 ± 8~~4~~0		11,4~~05~~33 ± ~~109~~236
OZW870	Wood	0.70	1c (Peat)	9,995 ± ~~48~~0		11,~~396~~ 426 ± ~~107~~238
OZW869	Wood	0.71	1c (Peat)	10,065 ± 90~~45~~		11,~~519~~ 509 ± ~~122~~252
OZW868	Wood	0.85	1c (Peat)	10,265 ± 90~~45~~		11,~~908~~ 915 ± 188~~94~~
OZW876	Wood	1.04	1c (Peat)	10,505 ± 90~~45~~		12,~~351~~ 420 ± ~~142~~296
OZW875	Wood	1.20	1c (Peat)	10,815 ± 10~~5~~0		12,~~700~~ 739 ± ~~2~~756
OZW874	Wood	1.81	2b (Sand)	9,130 ± 102~~51~~0		10,~~380~~ 389 ± ~~71~~41440

OZW873	Wood	1.87	2b (Sand)	11,150 ± 9045		1213,965–040 ± 73114
OZW878	Wood	2.27	2c (Clay)	11,535 ± 9045		13,342–380 ± 55102
OZW877	Wood	2.60	2c (Clay)	11,645 ± 9045		13,430–472 ± 58122
OZW879	Wood	4.32	2c (Clay)	12,445 ± 1050		14,488–552 ± 183382
OZW882	Wood	5.49	2c (Clay)	13,405 ± 1050		16,074–089 ± 100192
OZW881	Wood	5.63	2c (Clay)	13,530 ± 1050		16,237–266 ± 105190
OZW880	Wood	5.79	2c (Clay)	13,495 ± 1050		16,187–212 ± 101186
OZW883	Wood	11.76	3b (Sand)	16,370 ± 1260		19,718–716 ± 1101900
OZW885	Wood	12.78	3b (Sand)	51,590 ± 172860		51,733 ± 889out of range
OZW884	Wood	13.35	3b (Sand)	51,050 ± 711420		5153,147–648 ± 7261548
OZX869	Bulk sed.	13.35	3b (Sand)	21,090 ± 22110	1026 ± 117?	*24,235–244 ± 208398*
OZX889	Bulk sed.	14.14	3c (Sand/Silt)	23,690 ± 26130	1026 ± 117?	*26,822–877 ± 190354*
OZW886	Wood	14.81	3c (Sand/Silt)	48,520 ± 108540		4851,575–788 ± 5472688
OZX888	Bulk sed.	15.16	3c (Sand/Silt)	20,540 ± 2100	1026 ± 117?	*23,604–607 ± 194362*
OZW887	Wood	16.33	3c (Sand/Silt)	50,640 ± 168120		5053,767–525 ± 8341660
OZX870	Bulk sed.	16.61	3c (Sand/Silt)	19,320 ± 26130	1026 ± 117?	*22,209–250 ± 206378*
OZX349	Bulk sed.	17.60	4 (Clay)	18,690 ± 1260	1026 ± 117	*21,502–565 ± 164312*
OZX871	Bulk sed.	18.97	4 (Clay)	20,120 ± 1890	1026 ± 117	*23,120–134 ± 190352*
OZX887	Bulk sed.	19.92	4 (Clay)	21,270 ± 22110	1026 ± 117	*24,441–452 ± 209394*
OZX348	Bulk sed.	20.74	4 (Clay)	19,430 ± 1260	1026 ± 117	*22,329–362 ± 161292*
OZX872	Bulk sed.	22.12	4 (Clay)	19,920 ± 2100	1026 ± 117	*22,889–904 ± 198360*

OZX886	Bulk sed.	22.80	4 (Clay)	20,040 ± 1890	1026 ± 117	23,029–043 ± 191348
OZX885	Bulk sed.	23.72	4 (Clay)	21,280 ± 2100	1026 ± 117	24,452–464 ± 202380
OZX350	Bulk sed.	23.88	4 (Clay)	21,480 ± 1470	1026 ± 117	24,674–691 ± 181330
OZX884	Bulk sed.	25.81	4 (Clay)	21,490 ± 2100	1026 ± 117	24,683–700 ± 196366
OZX351	Bulk sed.	26.71	5 (Clay)	22,980 ± 1470	1026 ± 117	26,140–175 ± 174328
OZX883	Bulk sed.	27.57	5 (Clay)	22,170 ± 26130	1026 ± 117?	25,368–392 ± 187362
OZX882	Bulk sed.	28.39	6 (Clay)	34,650 ± 34580	1026 ± 117?	38,079–615 ± 421836
OZX873	Bulk sed.	29.78	7 (Clay)	26,920 ± 38190	410 ± 170?	30,567611 ± 231478
OZX340	Wood	31.44	8a (Clay)	18,210 ± 28140		22,027–107 ± 184340
OZX874	Bulk sed.	31.55	8a (Clay)	24,870 ± 30150	410 ± 170	28,467–666 ± 253484
OZX875	Bulk sed.	32.53	8a (Clay)	25,180 ± 28140	410 ± 170	2829,804–003 ± 510255
OZX876	Bulk sed.	33.44	8a (Clay)	25,670 ± 28140	410 ± 170	29,375–481 ± 303476
OZX342	Wood	33.83	8a (Clay)	25,560 ± 19380		29,676–741 ± 293478
OZX877	Bulk sed.	35.54	8a (Clay)	26,820 ± 32160	410 ± 170	30,499–538 ± 228464
OZX344	Bulk sed.	36.50	8a (Clay)	29,260 ± 24120	410 ± 170	3233,990–343 ± 261540
OZX343	Wood	37.63	8a (Clay)	25,580 ± 38190		29,704–762 ± 294480
OZX341	Wood	39.20	8a (Clay)	30,360 ± 28140		34,324–738 ± 164392
OZX347	Bulk sed.	39.20	8a (Clay)	30,770 ± 32160	410 ± 170	34,261–710 ± 237502
OZX878	Bulk sed.	39.63	8a (Clay)	29,140 ± 4200	410 ± 170	3233,843–180 ± 330712
LuS9636*	Wood	42.45	8a (Clay)	32,400 ± 12400		3637,859–368 ± 14202886
OZX879	Bulk sed.	42.79	8a (Clay)	34,140 ± 6300	410 ± 170	38,155–746 ± 421926

OZX880	Bulk sed.	43.91	8a (Clay)	35,650 ± 6633~~0~~	±	410 ± 170	~~39,808~~40,297 ± ~~434~~746
OZX881	Bulk sed.	44.24	8a (Clay)	36,740 ± 7437~~0~~	±	410 ± 170	~~4041~~,~~848~~ 151 ± ~~397~~656
OZX346	Bulk sed.	44.55	8b (Clay)	38,830 ± 6633~~0~~	±	410 ± 170	42,~~339~~ 192 ± ~~294~~426

* From correlated Orakei 2007 core

^ From ~~(~~Hayward et al.~~,~~ (2008)

? Reservoir effect assumed from stratigraphically closest facies unit with calculated reservoir effect (see section 4.2).

Table 4. Equivalent dose (D_e), total dose rate data and pIR-IRSL$_{290}$ age estimates for the Orakei 4-11 µm polymineral fine-grained samples.

Sample code *Lab code*	ECD (m)	D_e (Gy)	K (%)	Th (ppm)	U (ppm)	Total dose rate (Gy/ka)	Age (years) ± 2σ *
L65 *A0118*	50.21	111 ± 10[a]	0.81 ± 0.04	4.27 ± 0.21	0.86 ± 0.04	1.56 ± 0.16	71,200 ± 9,800 *55,760 ± 8,630*
L32 *A0115*	63.54	105 ± 11[b]	0.77 ± 0.04	3.75 ± 0.19	0.79 ± 0.04	1.44 ± 0.15	73,100 ± 10,800 *56,400 ± 9,620*
L35 *A0116*	65.59	230 ± 17[a]	0.96 ± 0.05	5.21 ± 0.26	1.08 ± 0.05	1.89 ± 0.20	122,000 ± 16,000 *109,230 ± 14,500*
L14 *A0110*	67.11	198 ± 12[a]	0.90 ± 0.09	3.92 ± 0.30	0.81 ± 0.30	1.57 ± 0.18	126,000 ± 17,000 *111,860 ± 15,030*
L15 *A0111*	71.74	230 ± 41[a]	0.87 ± 0.10	5.07 ± 0.30	1.08 ± 0.40	1.79 ± 0.22	128,000 ± 28,000 *114,950 ± 26,810*
L69[c] *A0119*	74.41	440 ± 59[a]	0.83 ± 0.04	4.93 ± 0.25	1.24 ± 0.06	1.81 ± 0.19	243,000 ± 41,000

[a] Calculated using the CAM.

[b] Calculated using the MAM.

[c] Only 4 aliquots of sample L69 were acceptable but scattered. Hence, we decided against residual dose correction and reject sample L69 as an outlier given insufficient D_e data.

* Ages corrected for residual dose (24 Gy) based on tests on sample L15 are provided in italics. Water contents of 20±10% were used for all samples.

Table 5. Tuning points obtained by dynamic time warping alignment of the Orakei RPI data to the PISO-1500 VADM (Channell et al., 2009). ~~A standard deviation of ±1000 years is assumed for all points which equals the temporal resolution of the PISO-1500 stack.~~

Tuning point	ECD (m)	Age (years)	Age uncertainty (2σ)
~~TuP93~~TuP14	~~46~~44.85~~.64~~	~~53~~47,~~400~~000	1,000
TuP20~~175~~	~~51~~47.24~~.61~~	~~62~~52,000	4,000
~~TuP193~~TuP21	~~52~~47.63~~.03~~	~~64~~54,~~600~~000	1,000
TuP~~297~~32	~~57~~52.01~~.82~~	~~71~~66,~~200~~000	2,000

TuP46343	5957.57.10	7779,200000	1,000
TuP48384	6058.37.23	8290,800000	1,000
TuP61434	6163.54.09	9097,0500	2,000
TuP70464	6167.12.79	94107,0,80000	1,000
TuP85529	6373.08.41	100123,600500	2,000
TuP88589	65.5574.28	107125,000	1,000
TuPex18TuP89	74.6568	121126,200000	1,000
TuPex82TuP97	7777.86.24	129128,200000	1,000
TuPex115100	79.05	133133,400500	1,000

Table B1. Summary of luminescence characteristics arising from postIR-IRSL$_{290}$ protocol measurements.

Sample	Number of aliquots accepted	Recycling ratio	Overdispersion (%)
L14 *A0110*	9/15	1.35 ± 0.35	12.4
L15 *A0111*	9/15	1.38 ± 0.69	52
L32 *A0115*	11/15	1.04 ± 0.09	67
L35 *A0116*	12/15	1.10 ± 0.08	24.3
L65 *A0118*	7/15	1.10 ± 0.10	22.7
L69 *A0119*	4/10	1.00 ± 0.10	24.7

Table B2: Results for the coarse-grained sample L20 (A0113) of different IRSL preheat temperatures.

IRSL preheat (°C)	No. aliquots accepted	Recycling ratio	Recuperation (%)	D_e (Gy)	Total dose rate (Gy/ka)	Age (ka) ± 2 σ
50	2/12	1.03 ± 0.04	0.5 ± 0.1	439 ± 11	2.19 ± 0.27	200 ± 25
200	6/12	0.95 ± 0.18	1.9 ± 1.3	368 ± 28		168 ± 24

References

Adamiec, G. and Aitken, M.: Dose-rate conversion factors: update, Anc. TL, 16(2), 37–50, 1998.

Aitchison, J.: The statistical analysis of compositional data, Chapman and Hall, London; New York., 1986.

Allen, J.: Holocene coastal lowlands in NW Europe : autoeompaction and the uncertain ground, in Coastal and Estuarine Enviromnents: sedimentology, geomorphology and geoarchaeolog, edited by K. Pye and J. Allen, pp. 239–252, The Geological Society of London, London., 2000.

Alley, R. B., Marotzke, J., Nordhaus, W. D., Overpeck, J. T., Peteet, D. M., Pielke Jr, R. A., Pierrehumbert, R. T., Rhines, P. B., Stocker, T. F., Talley, L. D. and Wallace, J. M.: Abrupt Climate Change, Science (80-.)., 299(5615), 2005–2010, 2003.

Alloway, B. V, Lowe, D. J., Barrell, D. J. A., Newnham, R. M., Almond, P. C., Augustinus, P. C., Bertler, N. A. N., Carter, L., Litchfield, N. J., McGlone, M. S., Shulmeister, J., Vandergoes, M. J., Williams, P. W. and NZ-INTIMATE members: Towards a Climate Event Stratigraphy for New Zealand over the past 30000 years (NZ-INTIMATE project), J. Quat. Sci., 22(1), 9–35, doi:Doi 10.1002/Jqs.1079, 2007.

Augustinus, P., Cochran, U., Kattel, G., D'Costa, D. and Shane, P.: Late Quaternary paleolimnology of Onepoto maar, Auckland, New Zealand: Implications for the drivers of regional paleoclimate, Quat. Int., 253, 18–31, doi:10.1016/j.quaint.2011.02.028, 2012.

Augustinus, P. C.: NZ-Maars: Extracting High Resolution Paleoclimate Records from Maar Crater Lakes, Auckland, New Zealand, Past Clim. Dyn. A South. Perspect., 15(2), 18–20, 2007.

Augustinus, P. C.: Probing the history of New Zealand's Orakei maar, Eos, Trans. Am. Geophys. Union, 97(September), 1–7, doi:10.1029/2016EO059227, 2016.

Barrell, D. J. A., Almond, P. C., Vandergoes, M. J., Lowe, D. J. and Newnham, R. M.: A composite pollen-based stratotype for inter-regional evaluation of climatic events in New Zealand over the past 30,000 years (NZ-INTIMATE project), Quat. Sci. Rev., 74, 4–20, doi:10.1016/j.quascirev.2013.04.002, 2013.

Bird, M. I., Fifield, L. K., Chua, S. and Goh, B.: CALCULATING SEDIMENT COMPACTION FOR RADIOCARBON DATING OF INTERTIDAL SEDIMENTS, Radiocarbon, 46(1), 421–435, 2004.

Blaauw, M.: Methods and code for "classical" age-modelling of radiocarbon sequences, Quat. Geochronol., 5(5), 512–518, doi:10.1016/j.quageo.2010.01.002, 2010.

Blaauw, M.: Out of tune: The dangers of aligning proxy archives, Quat. Sci. Rev., 36, 38–49, doi:10.1016/j.quascirev.2010.11.012, 2012.

Blaauw, M. and Christen, J. A.: Flexible paleoclimate age-depth models using an autoregressive gamma process, Bayesian Anal., 6(3), 457–474, doi:10.1214/11-BA618, 2011.

Blaauw, M. and Christen, J. A.: rbacon: Age-Depth Modelling using Bayesian Statistics. R package version 2.4.2., 2020.

Bleil, U. and Gard, G.: Chronology and correlation of Quaternary magnetostratigraphy and nanno- fossil biostratigraphy in Norwegian-Greenland Sea sediments, Geol. Rundschau, 78(3), 1173–1187, 1989.

van den Boogaart, K. G., Tolosana-Delgado, R. and Bren, M.: compositions: Compositional Data Analysis R package version 1.40-2., [online] Available from: https://cran.r-project.org/package=compositions, 2018.

Bøtter-Jensen, L.: Luminescence techniques: Instrumentation and methods, Radiat. Meas., 27(5–6), 749–768, doi:10.1016/S1350-4487(97)00206-0, 1997.

Bøtter-Jensen, L., Mejdahl, V. and Murray, A. S.: New light on OSL, Quat. Sci. Rev., 18(2), 303–309, doi:10.1016/S0277-3791(98)00063-8, 1999.

Bøtter-Jensen, L., Bulur, E., Duller, G. A. T. and Murray, A. S.: Advances in luminescence measurement systems, Radiat. Meas., 32, 523–528 [online] Available from: https://ac.els-cdn.com/S1350448700000391/1-s2.0-S1350448700000391-main.pdf?_tid=59d7ff0e-0665-4ed0-ad3a-18d268a28765&acdnat=1522418437_118cb0422d9cedbfc9e26c4244650ea9,

2000.

Bourlès, D., Raisbeck, G. M. and Yiou, F.: 10Be and 9Be in marine sediments and their potential for dating, Geochim. Cosmochim. Acta, 53, 443–452, 1989.

Broecker, W. S.: Does the Trigger for Abrupt Climate Change Reside in the Ocean or in the Atmosphere?, Science (80-.)., 300(5625), 1519–1522, 2003.

Bronk Ramsey, C.: Bayesian Analysis of Radiocarbon Dates, Radiocarbon, 51(01), 337–360, doi:10.1017/S0033822200033865, 2009.

Buylaert, J. P., Jain, M., Murray, A. S., Thomsen, K. J., Thiel, C. and Sohbati, R.: A robust feldspar luminescence dating method for Middle and Late Pleistocene sediments, Boreas, 41(3), 435–451, doi:10.1111/j.1502-3885.2012.00248.x, 2012.

Carolin, S. A., Cobb, K. M., Adkins, J. F., Clark, B., Conroy, J. L., Lejau, S., Malang, J. and Tuen, A. A.: Varied Response of Western Pacific Hydrology to Climate Forcings over the Last Glacial Period, Science (80-.)., 340, 1564–1567, 2013.

Cassata, W. S., Singer, B. S. and Cassidy, J.: Laschamp and Mono Lake geomagnetic excursions recorded in New Zealand, Earth Planet. Sci. Lett., 268(1–2), 76–88, doi:10.1016/j.epsl.2008.01.009, 2008.

Channell, J. E. T., Hodell, D. A. and Lehman, B.: Relative geomagnetic paleointensity and δ18O at ODP Site 983 (Gardar Drift, North Atlantic) since 350 ka, Earth Planet. Sci. Lett., 153, 103–118, 1997.

Channell, J. E. T., Stoner, J. S., Hodell, D. A. and Charles, C. D.: Geomagnetic paleointensity for the last 100 kyr from the sub-antarctic South Atlantic: a tool for inter-hemispheric correlation, Earth Planet. Sci. Lett., 175, 145–160, 2000.

Channell, J. E. T., Xuan, C. and Hodell, D. A.: Stacking paleointensity and oxygen isotope data for the last 1.5 Myr (PISO-1500), Earth Planet. Sci. Lett., 283(1–4), 14–23, doi:10.1016/j.epsl.2009.03.012, 2009.

Child, D., Elliott, G., Mifsud, C., Smith, A. M. and Fink, D.: Sample processing for earth science studies at ANTARES, Nucl. Instruments Methods Phys. Res. B, 172, 856–860, 2000.

Christen, J. A. and Pérez E, S.: A New Robust Statistical Model for Radiocarbon Data, Radiocarbon, 51(03), 1047–1059, doi:10.1017/s003382220003410x, 2009.

Christl, M., Vockenhuber, C., Kubik, P. W., Wacker, L., Lachner, J., Alfimov, V., Synal, H.-A. and Synal, H.: The ETH Zurich AMS facilities: Performance parameters and reference materials, Nucl. Inst. Methods Phys. Res. B, 294, 29–38, doi:10.1016/j.nimb.2012.03.004, 2013.

Czymzik, M., Muscheler, R., Brauer, A., Adolphi, F., Ott, F., Kienel, U., Dräger, N., Słowiński, M., Aldahan, A. and Possnert, G.: Solar cycles and depositional processes in annual 10Be from two varved lake sediment records, Earth Planet. Sci. Lett., 428, 44–51, doi:10.1016/j.epsl.2015.07.037, 2015.

Danišík, M., Shane, P., Schmitt, A. K., Hogg, A., Santos, G. M., Storm, S., Evans, N. J., Keith Fifield, L. and Lindsay, J. M.: Re-anchoring the late Pleistocene tephrochronology of New Zealand based on concordant radiocarbon ages and combined238U/230Th disequilibrium and (U-Th)/He zircon ages, Earth Planet. Sci. Lett., 349–350, 240–250, doi:10.1016/j.epsl.2012.06.041, 2012.

Danišík, M., Lowe, D. J., Schmitt, A. K., Friedrichs, B., Hogg, A. G. and Evans, N. J.: Sub-millennial eruptive recurrence in the silicic Mangaone Subgroup tephra sequence , New Zealand , from Bayesian modelling of zircon double-dating and radiocarbon ages, Quat. Sci. Rev., 246, 106517, doi:10.1016/j.quascirev.2020.106517, 2020.

Doerschner, N., Hernandez, M. and Fitzsimmons, K. E.: Sources of variability in single grain dose recovery experiments: Insights from Moroccan and Australian samples, Anc. TL, 34(1), 2016.

Dunbar, N. W., Iverson, N. A., Van Eaton, A. R., Sigl, M., Alloway, B. V., Kurbatov, A. V., Mastin, L. G., McConnell, J. R. and Wilson, C. J. N.: New Zealand supereruption provides time marker for the Last Glacial Maximum in Antarctica, Sci. Rep., 7(1), 3–10, doi:10.1038/s41598-017-11758-0, 2017.

Egli, R.: Characterization of individual rock magnetic components by analysis of remanence curves, 1. Unmixing natural sediments, Stud. Geophys. Geod., 48(2), 391–446, 2004.

Elsasser, W., Ney, E. P. and Winckler, J. R.: Cosmic-Ray intensity and geomagnetism, Nature, 178, 1226–1227, 1956.

EPICA Community Members: One-to-one coupling of glacial climate variability in Greenland and Antarctica, Nature, 444(7116), 195–198, doi:10.1038/nature05301, 2006.

Fink, D., Hotchkis, M., Hua, Q., Jacobsen, G., Smith, A. M., Zoppi, U., Child, D., Mifsud, C., Gaast, H. Van Der, Williams, A. and Williams, M.: The ANTARES AMS facility at ANSTO, Nucl. Instruments Methods Phys. Res. B, 223–224, 109–115, doi:10.1016/j.nimb.2004.04.025, 2004.

Flude, S. and Storey, M.: 40Ar/39Ar age of the Rotoiti Breccia and Rotoehu Ash, Okataina Volcanic Complex, New Zealand, and identification of heterogeneously distributed excess40Ar in supercooled crystals, Quat. Geochronol., 33, 13–23, doi:10.1016/j.quageo.2016.01.002, 2016.

Fox, J. and Weisberg, S.: An R Companion to Applied Regression, 2nd ed., SAGE Publications, Thousand Oaks, Calif., 2011.

Frank, M., Schwarz, B., Baumann, S., Kubik, P. W., Suter, M. and Mangini, A.: A 200 kyr record of cosmogenic radionuclide production rate and geomagnetic field intensity from 10Be in globally stacked deep-sea sediments, Earth Planet. Sci. Lett., 149(1), 121–129, doi:10.1016/S0012-821X(97)00070-8, 1997.

Frank, M., Backman, J., Jakobsson, M., Moran, K., Regan, M. O., King, J., Haley, B. A., Kubik, P. W. and Garbe-Schönberg, D.: Beryllium isotopes in central Arctic Ocean sediments over the past 12.3 million years: Stratigraphic and paleoclimatic implications, Paleoceanography, 23, 1–12, doi:10.1029/2007PA001478, 2008.

Froggatt, P. C. and Lowe, D. J.: A review of late quaternary silicic and some other tephra formations from New Zealand: Their stratigraphy, nomenclature, distribution, volume, and age, New Zeal. J. Geol. Geophys., 33(1), 89–109, doi:10.1080/00288306.1990.10427576, 1990.

Galbraith, R. F., Roberts, R. G., Laslett, G. M., Yoshida, H. and Olley, J. M.: Optical Dating of Single and Multiple Grains of Quartz From Jinmium Rock Shelter, Northern Australia: Part I, Experimental Design and Statistical Models, Archaeometry, 41(2), 339–364, 1999.

Giorgino, T.: Computing and Visualizing Dynamic Time Warping Alignments in R : The dtw Package, J. Stat. Softw., 31(7), 2009.

Guerin, G., Mercier, N. and Adamiec, G.: Dose-rate conversion factors: update, Anc. TL, 29(1), 5–8, 2011.

Hagen, C. J., Reilly, B. T., Stoner, J. S. and Creveling, J. R.: Dynamic Time Warping of Paleomagnetic Secular Variation Data, Geophys. J. Int., 1–45, 2020.

Hatfield, R. G., Stoner, J. S., Solada, K. E., Morey, A. E., Woods, A., Chen, C. Y., McGee, D., Abbott, M. B. and Rodbell, D. T.: Paleomagnetic Constraint of the Brunhes Age Sedimentary Record From Lake Junín, Peru, Front. Earth Sci., 8, 1–18, doi:10.3389/feart.2020.00147, 2020.

Hay, C. C., Creveling, J. R., Hagen, C. J., Maloof, A. C. and Huybers, P.: A library of early Cambrian chemostratigraphic correlations from a reproducible algorithm, , 47(5), 457–460, 2019.

Hayward, B. W., Morley, M. S., Sabaa, A. T., Grenfell, H. R., Daymond-King, R., Molloy, C., Shane, P. A. and Augustinus, P. A.: FOSSIL RECORD OF THE POST-GLACIAL MARINE BREACHING OF AUCKLAND ' S VOLCANIC MAAR CRATERS, Rec. Auckl. Museum, 45, 79–99, 2008.

Hayward, C. M. and Hayward, B. W.: HUMAN IMPACT ON ORAKEI BASIN, AUCKLAND, Tane, 37, 137–152, 1999.

Heiken, G.: Morphology and Petrography of Volcanic Ashes, Geol. Soc. Am. Bull., 83, 1961–1988, 1972.

Hessell, J. W. D.: The climate and weather of the Auckland region, , (20), 1988.

Hogg, A. G., Heaton, T. J., Hua, Q., Palmer, J. G., Turney, C. S. M., Southon, J., Bayliss, A., Blackwell, P. G., Boswijk, G., Bronk Ramsey, C., Pearson, C., Petchey, F., Reimer, P., Reimer, R. and Wacker, L.: SHCal20 SOUTHERN HEMISPHERE CALIBRATION, 0–55,000 YEARS CAL BP, Radiocarbon, 62(4), 759–778, doi:10.1017/RDC.2020.59, 2020.

Hopkins, J. L., Millet, M. A., Timm, C., Wilson, C. J. N., Leonard, G. S., Palin, J. M. and Neil, H.: Tools and techniques for developing tephra stratigraphies in lake cores: A case study from the basaltic Auckland Volcanic Field, New Zealand, Quat.

Sci. Rev., 123, 58–75, doi:10.1016/j.quascirev.2015.06.014, 2015.

Hopkins, J. L., Wilson, C. J. N., Millet, M. A., Leonard, G. S., Timm, C., McGee, L. E., Smith, I. E. M. and Smith, E. G. C.: Multi-criteria correlation of tephra deposits to source centres applied in the Auckland Volcanic Field, New Zealand, Bull. Volcanol., 79(7), doi:10.1007/s00445-017-1131-y, 2017.

Hurnard, S. M.: Auckland's climate, in Natural History of Auckland: an Introduction, edited by P. J. Brook, pp. 31–34, Auckland Institute and Museum, Auckland., 1979.

Ingham, E., Turner, G. M., Conway, C. E., Heslop, D., Roberts, A. P., Leonard, G., Townsend, D. and Calvert, A.: Volcanic records of the Laschamp geomagnetic excursion from Mt Ruapehu, New Zealand, Earth Planet. Sci. Lett., 472, 131–141, doi:10.1016/j.epsl.2017.05.023, 2017.

Kemp, C. W., Tibby, J., Arnold, L. J., Barr, C., Gadd, P. S., Marshall, J. C., Mcgregor, G. B. and Jacobsen, G. E.: Climates of the last three interglacials in subtropical eastern Australia inferred from wetland sediment geochemistry, Palaeogeogr. Palaeoclimatol. Palaeoecol., 538(November 2019), 109463, doi:10.1016/j.palaeo.2019.109463, 2020.

Kidson, J. W.: An Analysis of New Zealand Synoptic Types and Their Use in Defining Weather Regimes, Int. J. Climatol., 20, 299–316, 2000.

King, R. F.: THE REMANENT MAGNETISM OF ARTIFICIALLY DEPOSITED SEDIMENTS, Geophys. Suppl. to Mon. Not. R. Astron. Soc., 7(3), 115–134, doi:doi.org/10.1111/j.1365-246X.1955.tb06558.x, 1955.

Kirschvink, J. L.: The least-squares line and plane and the analysis of palaeomagnetic data, Geophys. J. Int., 62(3), 699–718, 1980.

Laj, C. and Channell, J. E. T.: Geomagnetic Excursions, in Treatise on Geophysics, pp. 343–383, Elsevier B.V., 2015.

Laj, C., Kissel, C. and Beer, J.: High Resolution Global Paleointensity Stack Since 75 kyr (GLOPIS-75) Calibrated to Absolute Values, in Timescales of the paleomagnetic field, vol. 145, edited by J. E. T. Channell, D. V Kent, W. Lowrie, and J. G. Meert, pp. 255–265, American Geophysical Union, Washington, DC., 2004.

Laj, C., Guillou, H. and Kissel, C.: Dynamics of the earth magnetic field in the 10–75 kyr period comprising the Laschamp and Mono Lake excursions: New results from the French Chaîne des Puys in a global perspective, Earth Planet. Sci. Lett., 387, 184–197, doi:10.1016/j.epsl.2013.11.031, 2014.

Lascu, I., Feinberg, J. M., Dorale, J. A., Cheng, H. and Edwards, R. L.: Age of the Laschamp excursion determined by U-Th dating of a speleothem geomagnetic record from North America, Geology, 44(2), 139–142, doi:10.1130/G37490.1, 2016.

Leonard, G. S., Calvert, A. T., Hopkins, J. L., Wilson, C. J. N., Smid, E. R., Lindsay, J. M. and Champion, D. E.: High-precision 40Ar/39Ar dating of Quaternary basalts from Auckland Volcanic Field, New Zealand, with implications for eruption rates and paleomagnetic correlations, J. Volcanol. Geotherm. Res., 343, 60–74, doi:10.1016/j.jvolgeores.2017.05.033, 2017.

Lézine, A., Grafenstein, U. Von, Andersen, N., Belmecheri, S., Bordon, A., Caron, B. and Cazet, J.: Lake Ohrid, Albania, provides an exceptional multi-proxy record of environmental changes during the last glacial – interglacial cycle, Palaeogeogr. Palaeoclimatol. Palaeoecol., 287, 116–127, doi:10.1016/j.palaeo.2010.01.016, 2010.

Lindsay, J., Leonard, G., Smid, E. and Hayward, B.: Age of the Auckland Volcanic Field: a review of existing data, New Zeal. J. Geol. Geophys., 54(4), 379–401, doi:10.1080/00288306.2011.595805, 2011.

Liu, E. J., Cashman, K. V and Rust, A. C.: Optimising shape analysis to quantify volcanic ash morphology, GeoResJ, 8, 14–30, doi:10.1016/j.grj.2015.09.001, 2015.

Liu, J., Nowaczyk, N. R., Panovska, S., Korte, M. and Arz, H. W.: The Norwegian-Greenland Sea, the Laschamps, and the Mono Lake Excursions Recorded in a Black Sea Sedimentary Sequence, J. Geophys. Res. Solid Earth, 125, 1–22, doi:10.1029/2019JB019225, 2020.

Loame, R. C., Villamor, P., Lowe, D. J., Milicich, S. D., Pittari, A., Barker, S. L. L., Rae, A., Gomez-vasconcelos, M. G., Martinez-, M. and Ries, W. F.: Using paleoseismology and tephrochronology to reconstruct fault rupturing and hydrothermal activity since c. 40 ka in Taupo Rift, New Zealand, Quat. Int., 500, doi:10.1016/j.quaint.2019.02.031, 2019.

Løvlie, R.: Palaeomagnetic excursions during the last interglacial/glacial cycle: A synthesis, Quat. Int., 3/4, 5–11, 1989.

Lowe, D. J.: Tephrochronology and its application: A review, Quat. Geochronol., 6(2), 107–153, doi:10.1016/j.quageo.2010.08.003, 2011.

Lowe, D. J., Blaauw, M., Hogg, A. G. and Newnham, R. M.: Ages of 24 widespread tephras erupted since 30,000 years ago in New Zealand, with re-evaluation of the timing and palaeoclimatic implications of the Lateglacial cool episode recorded at Kaipo bog, Quat. Sci. Rev., 74, 170–194, doi:10.1016/j.quascirev.2012.11.022, 2013.

Lowick, S. E. and Preusser, F.: A method for retrospectively calculating the water content for silt-dominated desiccated core samples, Anc. TL, 27(1), 9–14, 2009.

Lund, S., Schwartz, M. and Stott, L.: Long-term palaeomagnetic secular variation and excursions from the western Equatorial Pacific Ocean (MIS2-4), Geophys. J. Int., 209, 587–596, doi:10.1093/gji/ggx029, 2017.

Mauz, B. and Lang, A.: Removal of the feldspar-derived luminescence component from polymineral fine silt samples for optical dating applications: evaluation of chemical treatment protocols and quality control procedures, Anc. TL, 22(1), 1–8 [online] Available from: http://www.aber.ac.uk/temp-ancient-tl/issue22_1/mauz_atl_22(1)_1-8.pdf, 2004.

McHargue, L. R., Damon, P. E. and Donahue, D. J.: Enhanced cosmic-ray production of 10 Be coincident with the Mono Lake and Laschamp Geomagnetic Excursions, Geophys. Res. Lett., 22(5), 659–662, doi:10.1029/95GL00169, 1995.

Mejdahl, V.: Thermoluminescence Dating: Beta-Dose Attenuation in Quartz Grains, Archaeometry, 21(1), 61–72, 1979.

Ménabréaz, L., Thouveny, N., Bourlès, D. L., Deschamps, P., Hamelin, B. and Demory, F.: The Laschamp geomagnetic dipole low expressed as a cosmogenic 10Be atmospheric overproduction at ~ 41 ka, Earth Planet. Sci. Lett., 312(3–4), 305–317, doi:10.1016/j.epsl.2011.10.037, 2011.

Mochizuki, N., Tsunakawa, H., Shibuya, H., Cassidy, J. and Smith, I. E. M.: Palaeointensities of the Auckland geomagnetic excursions by the LTD-DHT Shaw method, Phys. Earth Planet. Inter., 154(2), 168–179, doi:10.1016/j.pepi.2005.09.005, 2006.

Molloy, C., Shane, P. and Augustinus, P.: Eruption recurrence rates in a basaltic volcanic field based on tephralayers in maar sediments: Implications for hazards in the Auckland volcanic field, Bull. Geol. Soc. Am., 121(11–12), 1666–1677, doi:10.1130/B26447.1, 2009.

Muscheler, R., Beer, J., Kubik, P. W. and Synal, H.-A.: Geomagnetic field intensity during the last 60,000 years based on 10Be and 36Cl from the Summit ice cores and 14C, Quat. Sci. Rev., 24(16–17), 1849–1860, doi:10.1016/j.quascirev.2005.01.012, 2005.

Needham, A. J., Lindsay, J. M., Smith, I. E. M., Augustinus, P. and Shane, P. A.: Sequential eruption of alkaline and sub-alkaline magmas from a small monogenetic volcano in the Auckland Volcanic Field, New Zealand, J. Volcanol. Geotherm. Res., 201(1–4), 126–142, doi:10.1016/j.jvolgeores.2010.07.017, 2011.

Newnham, R., Lowe, D. J., Gehrels, M. and Augustinus, P.: Two-step human –environmental impact history for northern New Zealand linked to late-Holocene climate change, Holocene, 28(7), 1093–1106, doi:10.1177/0959683618761545, 2018.

NGRIP Members: High-resolution record of Northern Hemisphere climate extending into the last interglacial period, Nature, 431(7005), 147–151, 2004.

Nilsson, A., Muscheler, R., Snowball, I., Aldahan, A., Possnert, G., Augustinus, P., Atkin, D. and Stephens, T.: Multi-proxy identification of the Laschamp geomagnetic field excursion in Lake Pupuke, New Zealand, Earth Planet. Sci. Lett., 311(1–2), 155–164, doi:10.1016/j.epsl.2011.08.050, 2011.

Nishiizumi, K., Imamura, M., Caffee, M. W., Southon, J. R., Finkel, R. C. and Mcaninch, J.: Absolute calibration of 10Be AMS standards Kunihiko, Nucl. Instruments Methods Phys. Res. B, 258, 403–413, doi:10.1016/j.nimb.2007.01.297, 2007.

Nowaczyk, N. R. and Baumann, M.: Combined high-resolution magnetostratigraphy and nannofossil biostratigraphy for late Quaternary Arctic Ocean sediments, Deep Sea Res., 39, S567–S601, 1992.

Nowaczyk, N. R. and Frederichs, T. W.: Geomagnetic events and relative palaeointensity variations during the past 300 ka as recorded in Kolbeinsey Ridge sediments , Iceland Sea : indication for a strongly variable geomagnetic field, Int. J. Earth Sci.,

88, 116–131, 1999.

Nowaczyk, N. R., Frederichs, T. W., Eisenhauer, A. and Gard, G.: Magnetostratigraphic data from late Quaternary sediments from the Yermak Plateau , Arctic Ocean: evidence for four geomagnetic polarity events within the last 170Ka of the Brunhes Chron, Geophys. J. Int., 117, 453–471, 1994.

Nowaczyk, N. R., Antonow, M., Knies, J. and Spielhagen, R. F.: Further rock magnetic and chronostratigraphic results on reversal excursions during the last 50 ka as derived from northern high latitudes and discrepancies in precise AMS 14C dating, Geophys. J. Int., 155, 1065–1080, 2003.

Nowaczyk, N. R., Frank, U., Kind, J. and Arz, H. W.: A high-resolution paleointensity stack of the past 14 to 68 ka from Black Sea sediments, Earth Planet. Sci. Lett., 384, 1–16, doi:10.1016/j.epsl.2013.09.028, 2013.

Olley, J. M., Pietsch, T. and Roberts, R. G.: Optical dating of Holocene sediments from a variety of geomorphic settings using single grains of quartz, Geomorphology, 60(3–4), 337–358, doi:10.1016/j.geomorph.2003.09.020, 2004.

Osete, M.-L., Martin-Chivelet, J., Rossi, C., Edwards, R. L., Egli, R., Munoz-Garcia, M. B., Wang, X., Pavon-Carrasco, F. J. and Heller, F.: The Blake geomagnetic excursion recorded in a radiometrically dated speleothem, Earth Planet. Sci. Lett., 353–354, 173–181, doi:10.1016/j.epsl.2012.07.041, 2012.

Pepper, A. C., Shulmeister, J., Nobes, D. C. and Augustinus, P. A.: Possible ENSO signals prior to the Last Glacial Maximum, during the last deglaciation and the early Holocene, from New Zealand, Geophys. Res. Lett., 31(15), 1–4, doi:10.1029/2004GL020236, 2004.

Peters, C. and Thompson, R.: Magnetic identification of selected natural iron oxides and sulphides, J. Magn. Magn. Mater., 183, 365–374, 1998.

Peti, L. and Augustinus, P. C.: Stratigraphy and sedimentology of the Orakei maar lake sediment sequence (Auckland Volcanic Field , New Zealand), Sci. Drill., 25, 47–56, 2019.

Peti, L., Gadd, P. S., Hopkins, J. L. and Augustinus, P. C.: Itrax μ-XRF core scanning for rapid tephrostratigraphic analysis: a case study from the Auckland Volcanic Field maar lakes, J. Quat. Sci., 1–12, doi:10.1002/jqs.3133, 2019.

Philippsen, B.: The freshwater reservoir effect in radiocarbon dating, Herit. Sci., 1(24), 1–19, doi:10.1186/2050-7445-1-24, 2013.

Pickarski, N., Kwiecien, O., Djamali, M. and Litt, T.: Vegetation and environmental changes during the last interglacial in eastern Anatolia (Turkey): a new high-resolution pollen record from Lake Van, Palaeogeogr. Palaeoclimatol. Palaeoecol., 435, 145–158, doi:10.1016/j.palaeo.2015.06.015, 2015.

Prescott, J. R. and Hutton, J. T.: Cosmic ray contributions to dose rates for luminescence and ESR dating: Large depths and long-term time variations, Radiat. Meas., 23(2–3), 497–500, doi:10.1016/1350-4487(94)90086-8, 1994.

R Core Team: R: A Language and Environment for Statistical Computing. R Foundation for Statistical Computing, Vienna, Austria., [online] Available from: https://www.r-project.org, 2020.

Rasmussen, S. O., Bigler, M., Blockley, S. P., Blunier, T., Buchardt, S. L., Clausen, H. B., Cvijanovic, I., Dahl-Jensen, D., Johnsen, S. J., Fischer, H., Gkinis, V., Guillevic, M., Hoek, W. Z., Lowe, J. J., Pedro, J. B., Popp, T., Seierstad, I. K., Peder Steffensen, J., Svensson, A. M., Vallelonga, P., Vinther, B. M., Walker, M. J. C., Wheatley, J. J. and Winstrup, M.: A stratigraphic framework for abrupt climatic changes during the Last Glacial period based on three synchronized Greenland ice-core records: refining and extending the INTIMATE event stratigraphy, Quat. Sci. Rev., 106, 14–28, doi:10.1016/j.quascirev.2014.09.007, 2014.

Rees-Jones, J.: Optical dating of young sediments using fine-grain quartz, Anc. TL, 13(2), 9–14 [online] Available from: http://www.researchgate.net/publication/242076570_Assessing_the_error_on_equivalent_dose_estimates_derived_from_single_aliquot_regenerative_dose_measurements/file/60b7d52d0216f80b64.pdf, 1995.

Rees-Jones, J. and Tite, M. S.: Optical Dating Results for British Archaeological Sediments, Archaeometry, 39(1), 177–187, doi:10.1111/j.1475-4754.1997.tb00797.x, 1997.

Roperch, P., Bonhommet, N. and Levi, S.: Paleointensity of the earth's magnetic field during the Laschamp excursion and its geomagnetic implications, Earth Planet. Sci. Lett., 88, 209–219, 1988.

Seelos, K., Sirocko, F. and Dietrich, S.: A continuous high-resolution dust record for the reconstruction of wind systems in central Europe (Eifel , Western Germany) over the past 133 ka, Geophys. Res. Lett., 36, doi:10.1029/2009GL039716, 2009.

Shanahan, T. M., Overpeck, J. T., Anchukaitis, K. J., Beck, J. W., Cole, J. E., Dettman, D. L., Peck, J. A., Scholz, C. A. and King, J. W.: Atlantic Forcing of Persistent Drought in West Africa, Science (80-.)., 324(5925), 377–380, 2009.

Shane, P.: Tephrochronology:~a New Zealand case study, Earth-Science Rev., 49, 223–259, 2000.

Shane, P. and Sandiford, A.: Paleovegetation of marine isotope stages 4 and 3 in Northern New Zealand and the age of the widespread Rotoehu tephra, Quat. Res., 59(3), 420–429, doi:10.1016/S0033-5894(03)00044-9, 2003.

Simon, Q., St-Onge, G. and Hillaire-Marcel, C.: Late Quaternary chronostratigraphic framework of deep Baffin Bay glaciomarine sediments from high-resolution paleomagnetic data, Geochemistry, Geophys. Geosystems, 13(1), 1–24, doi:10.1029/2012GC004272, 2012.

Simon, Q., Bourlès, D. L., Bassinot, F., Nomade, S., Marino, M., Ciaranfi, N., Girone, A., Maiorano, P., Thouveny, N., Choy, S., Dewilde, F., Scao, V., Isguder, G. and Blamart, D.: Authigenic 10Be/9Be ratio signature of the Matuyama–Brunhes boundary in the Montalbano Jonico marine succession, Earth Planet. Sci. Lett., 460, 255–267, doi:10.1016/j.epsl.2016.11.052, 2016.

Simon, Q., Ledru, M.-P., Oliveira Sawakuchi, A., Favier, C., Mineli, T. D., Grohmann, C. H., Guedes, M., Bard, E., Thouveny, N., Garcia, M., Tachikawa, K., Rodríguez-Zorro, P. A. and Team, A.: Chronostratigraphy of a 1.5±0.1 Ma composite sedimentary record from Colônia basin (SE Brazil): Bayesian modeling based on paleomagnetic, authigenic 10Be/9Be, radiocarbon and luminescence dating, Quat. Geochronol., 58, 101081, doi:10.1016/j.quageo.2020.101081, 2020a.

Simon, Q., Thouveny, N., Bourlès, D. L. and Valet, J.: Cosmogenic 10 Be production records reveal dynamics of geomagnetic dipole moment (GDM) over the Laschamp excursion (20 – 60 ka), Earth Planet. Sci. Lett., 550, 116547, doi:10.1016/j.epsl.2020.116547, 2020b.

Smith, J. D. and Foster, J. H.: Geomagnetic Reversal in Brunhes Normal Polarity Epoch Published by : American Association for the Advancement of Science Stable URL : https://www.jstor.org/stable/1726285, , 163(3867), 565–567, 1969.

Stanley, D. J. and Hait, A. K.: Deltas, radiocarbon dating, and measurements of sediment storage and subsidence, Geology, 28(4), 295–298, 2000.

Stanton, T., Nilsson, A., Snowball, I. and Muscheler, R.: Assessing the reliability of Holocene relative palaeointensity estimates: a case study from Swedish varved lake sediments, Geophys. J. Int., 187, 1195–1214, doi:10.1111/j.1365-246X.2011.05049.x, 2011.

Stephens, T., Atkin, D., Cochran, U., Augustinus, P., Reid, M., Lorrey, A., Shane, P. and Street-Perrott, A.: A diatom-inferred record of reduced effective precipitation during the Last Glacial Coldest Phase (28.8-18.0 cal kyr BP) and increasing Holocene seasonality at Lake Pupuke, Auckland, New Zealand, J. Paleolimnol., 48(4), 801–817, doi:10.1007/s10933-012-9645-y, 2012.

Stockhecke, M., Kwiecien, O., Vigliotti, L., Anselmetti, F. S., Beer, J., Çağatay, M. N., Channell, J. E. T., Kipfer, R., Lachner, J., Litt, T., Pickarski, N. and Sturm, M.: Chronostratigraphy of the 600,000 year old continental record of Lake Van (Turkey), Quat. Sci. Rev., 104, 8–17, doi:10.1016/j.quascirev.2014.04.008, 2014.

Tauxe, L.: Sedimentary records of relative paleointensity of the geomagnetic field: Theory and practice, Rev. Geophys., 31(3), 319–354, 1993.

Thiel, C., Buylaert, J. P., Murray, A., Terhorst, B., Hofer, I., Tsukamoto, S. and Frechen, M.: Luminescence dating of the Stratzing loess profile (Austria) - Testing the potential of an elevated temperature post-IR IRSL protocol, Quat. Int., 234(1–2), 23–31, doi:10.1016/j.quaint.2010.05.018, 2011.

Thiel, C., Horváth, E. and Frechen, M.: Revisiting the loess/palaeosol sequence in Paks, Hungary: A post-IR IRSL based chronology for the "Young Loess Series," Quat. Int., 319, 88–98, doi:10.1016/j.quaint.2013.05.045, 2014.

Thompson, R. and Oldfield, F.: Environmental magnetism, 1st ed., Allen & Unwin, London., 1986.

Thouveny, N., Carcaillet, J., Moreno, E., Leduc, G. and Nérini, D.: Geomagnetic moment variation and paleomagnetic excursions since 400 kyr BP: a stacked record from sedimentary sequences of the Portuguese margin, Earth Planet. Sci. Lett., 219, 377–396, doi:10.1016/S0012-821X(03)00701-5, 2004.

Tric, E., Laj, C., Valet, J. P., Tucholka, P., Paterne, M. and Guichard, F.: The Blake geomagnetic event: transition geometry, dynamical characteristics and geomagnetic significance., Earth Planet. Sci. Lett., 102(1), 1–13, doi:10.1016/0012-821X(91)90013-8, 1991.

Valet, J.-P. and Meynadier, L.: A comparison of different techniques for relative paleointensity, Geophys. Res. Lett., 25(1), 89–92, 1998.

Vandergoes, M. J., Newnham, R. M., Preusser, F., Hendy, C. H., Lowell, T. V, Fitzsimons, S. J., Hogg, A. G., Kasper, H. U. and Schluchter, C.: Regional insolation forcing of late Quaternary climate change in the Southern Hemisphere, Nature, 436(7048), 242–245, doi:10.1038/nature03826, 2005.

Vandergoes, M. J., Hogg, A. G., Lowe, D. J., Newnham, R. M., Denton, G. H., Southon, J., Barrell, D. J. A., Wilson, C. J. N., McGlone, M. S., Allan, A. S. R., Almond, P. C., Petchey, F., Dabell, K., Dieffenbacher-Krall, A. C. and Blaauw, M.: A revised age for the Kawakawa/Oruanui tephra, a key marker for the Last Glacial Maximum in New Zealand, Quat. Sci. Rev., 74, 195–201, doi:10.1016/j.quascirev.2012.11.006, 2013.

Wagner, G., Masarik, J., Beer, J., Baumgartner, S., Imboden, D., Kubik, P. W., Synal, H.-A. and Suter, M.: Reconstruction of the geomagnetic field between 20 and 60 kyr BP from cosmogenic radionuclides in the GRIP ice core, Nucl. Instruments Methods Phys. Res. Sect. B Beam Interact. with Mater. Atoms, 172(1–4), 597–604, doi:10.1016/S0168-583X(00)00285-8, 2000.

White, D. A., Fink, D., Post, A. L., Simon, K., Galton-Fenzi, B., Foster, S., Fujioka, T., Jeromson, M. R., Blaxell, M. and Yokoyama, Y.: Beryllium isotope signatures of ice shelves and sub-ice shelf circulation, Earth Planet. Sci. Lett., 505, 86–95, 2019.

Wilcken, K. M., Fujioka, T., Fink, D., Fülöp, R. H., Codilean, A. T., Simon, K., Mifsud, C. and Kotevski, S.: SIRIUS Performance: 10Be, 26Al and 36Cl measurements at ANSTO, Nucl. Inst . Methods Phys. Res. B, 455(February), 300–304, doi:10.1016/j.nimb.2019.02.009, 2019.

Willenbring, J. K. and von Blanckenburg, F.: Meteoric cosmogenic Beryllium-10 adsorbed to river sediment and soil: Applications for Earth-surface dynamics, Earth-Science Rev., 98(1–2), 105–122, doi:10.1016/j.earscirev.2009.10.008, 2010.

Wittmann, H., Blanckenburg, F. Von, Bouchez, J., Dannhaus, N., Naumann, R., Christl, M. and Gaillardet, J.: The dependence of meteoric 10Be concentrations on particle size in Amazon River bed sediment and the extraction of reactive 10Be/9Be ratios, Chem. Geol., 318–319, 126–138, doi:10.1016/j.chemgeo.2012.04.031, 2012.

Wittmann, H., Blanckenburg, F., Dannhaus, N., Bouchez, J., Gaillardet, J., Guyot, J. L., Maurice, L., Roig, H., Filizola, N. and Christl, M.: A test of the cosmogenic 10Be(meteoric)/9Be proxy for simultaneously determining basin-wide erosion rates, denudation rates, and the degree of weathering in the Amazon basin, J. Geophys. Res. Earth Surf., 120, 2498–2528, doi:10.1002/2015JF003581.Received, 2015.

Xuan, C., Channell, J. E. T., Polyak, L. and Darby, D. A.: Paleomagnetism of Quaternary sediments from Lomonosov Ridge and Yermak Plateau: implications for age models in the Arctic Ocean, Quat. Sci. Rev., 32, 48–63, doi:10.1016/j.quascirev.2011.11.015, 2012.

Zhu, R. X., Zhou, L. P., Laj, C., Mazaud, A. and Ding, Z. L.: The Blake geomagnetic polarity episode recorded in Chinese loess, Geophys. Res. Lett., 21(8), 697–700, 1994.

Zolitschka, B., Anselmetti, F., Ariztegui, D., Corbella, H., Francus, P., Lücke, A., Maidana, N. I., Ohlendorf, C., Schäbitz, F. and Wastegård, S.: Environment and climate of the last 51,000years - new insights from the Potrok Aike maar lake Sediment Archive Drilling prOject (PASADO), Quat. Sci. Rev., 71, 1–12, doi:10.1016/j.quascirev.2012.11.024, 2013.